LIMIT LOAD ESTIMATION FOR STRUCTURES UNDER MECHANICAL LOADS

CENTRE FOR NEWFOUNDLAND STUDIES

TOTAL OF 10 PAGES ONLY
MAY BE XEROXED

(Without Author's Permission)

LI PAN

National Library
of Canada

Acquisitions and
Bibliographic Services

395 Wellington Street
Ottawa ON K1A 0N4
Canada

Bibliothèque nationale
du Canada

Acquisisitons et
services bibliographiques

395, rue Wellington
Ottawa ON K1A 0N4
Canada

Your file Votre référence
ISBN: 0-612-89698-6
Our file Notre référence
ISBN: 0-612-89698-6

The author has granted a non-exclusive licence allowing the National Library of Canada to reproduce, loan, distribute or sell copies of this thesis in microform, paper or electronic formats.

The author retains ownership of the copyright in this thesis. Neither the thesis nor substantial extracts from it may be printed or otherwise reproduced without the author's permission.

L'auteur a accordé une licence non exclusive permettant à la Bibliothèque nationale du Canada de reproduire, prêter, distribuer ou vendre des copies de cette thèse sous la forme de microfiche/film, de reproduction sur papier ou sur format électronique.

L'auteur conserve la propriété du droit d'auteur qui protège cette thèse. Ni la thèse ni des extraits substantiels de celle-ci ne doivent être imprimés ou aturement reproduits sans son autorisation.

In compliance with the Canadian Privacy Act some supporting forms may have been removed from this dissertation.

While these forms may be included in the document page count, their removal does not represent any loss of content from the dissertation.

Conformément à la loi canadienne sur la protection de la vie privée, quelques formulaires secondaires ont été enlevés de ce manuscrit.

Bien que ces formulaires aient inclus dans la pagination, il n'y aura aucun contenu manquant.

Canada

LIMIT LOAD ESTIMATION FOR STRUCTURES UNDER MECHANICAL LOADS

by

© Li Pan

A thesis submitted to the
School of Graduate Studies
in partial fulfillment of the
requirements for the degree of
Doctor of Philosophy

Faculty of Engineering and Applied Science
Memorial University of Newfoundland
St. John's, Newfoundland

January 2003

Abstract

Limit analysis is germane to the assessment and design of mechanical components and structures. Among the various methods for limit load estimation, robust methods based on linear elastic finite element analysis are appealing to analysts and designers due to the conceptual insight, economy of computational effort and wide applicability.

A robust limit load estimation scheme based on the extended Mura's variational principle that is used in conjunction with repeated elastic finite element analyses (FEA) is developed in this thesis. The secant modulus of individual elements in a finite element discretization scheme is prescribed to account for the plastic flow variation in a component or structure. The multipliers m^0 and m' obtained using this formulation converge rapidly to the exact value with the use of repeated elastic FEA. Using the notion of "leap-frogging to limit state," an improved lower-bound multiplier m_α can be obtained. This method is applied to several component geometric configurations made of isotropic materials.

The method is further extended to layered structures, cracked components and components made of anisotropic materials. For all these applications, the multipliers m^0, m' and m_α predicted by the proposed procedure are compared with those obtained by the lower bound estimation based on the elastic compensation method (ECM) and inelastic FEA. The results show that the robust method developed in this thesis can be applied to various components and structures leading to good limit load estimates.

Acknowledgments

I would like to express my deep gratitude to my supervisor Dr. R. Seshadri for his guidance, support and care during the entire course of my graduate program. He was readily available for discussion despite his heavy administrative duties as Dean of Engineering.

I would also like to thank Dr. Suresh Babu for his teaching and guidance in my second year of graduate study. Thanks are also directed to Dr. Wolf Reinhardt for his kind checking of this thesis and insightful suggestion.

Finally, the financial supports from the Faculty of Engineering and Applied Science and the School of Graduate Studies are gratefully acknowledged.

To my son Victor

To my wife Jian Yang for her continuous support and patience

To my parents and parents-in-law for their support and encouragement

Table of Contents

List of Tables

List of Figures

List of Abbreviations and Symbols

Abbreviations

2D	Two-dimensional
3D	Three-dimensional
APDL	ANSYS Parametric Design Language
ASME	The American Society of Mechanical Engineers
ASP	Method of Adjusted Secant for Piping
CPU	Central Processing Unit
ECM	Elastic Compensation Method
EMAP	Elastic Modulus Adjustment Procedures
FE	Finite Element
FEA	Finite Element Analysis
GLOSS	Generalized Local Stress and Strain
LB	Lower Bound
LEFEA	Linear Elastic Finite Element Analysis
MARS	Modulus Adjustment and Redistribution of Stress
R-Node	Redistribution Node

Symbols

a	Crack length
B	Thickness
B, n	Creep parameters for second stage power law creep
C_{ijkl}	Fourth order tensor of elastic constants
D	Plastic dissipation
$\dot{D}$	Increment of plastic dissipation per unit volume
E'	Modified Young's modulus

E_0	Original Young's modulus of material
E_{ij}	Young's moduli and shear moduli along the anisotropic principal axes or principal planes
E_{mod}	Modified Young's modulus
E_p	Slope of effective stress versus effective plastic strain curve
E_S	Secant modulus; modified Young's modulus
E_{Sx}	Secant modulus in the x-direction
E_x, E_y, E_z	Young's modulus in x, y and z directions
$f, f', f(s_{ij})$	Yield function
$F(v_i, s_{ij}, \sigma, R_i, m, \mu, \varphi)$	Functional associated with Mura's formulation
F_i	Surface traction
$G(\vec{x})$	Spatially varying shear modulus, where $\vec{x}$ represents the spatial variation.
G_{ij}	Shear modulus in the i-j plane
H	Height
I	Moment of inertia
J	J-integral
$\bar{J}$	Normalized J-integral
J_e	Elastic J-integral
k	Yield stress in pure shear
K_I	Opening mode stress intensity factor
L	Length
m	Exact multiplier or safety factor
m^0	Statically admissible upper bound multiplier
m'	Lower bound multiplier from Mura's formulation
m_α	Improved lower bound multiplier
m_k	Kinematically admissible multiplier
m_L	Classical lower bound multiplier

m_s	Statically admissible multiplier
m_U	Classical upper bound multiplier
M	Bending moment
M_{ij}, M_{ijkl}	Material strength tensor in anisotropic yield function, which describes the effect of orientation on yield stresses
M_p	Plastic moment
n_j	Unit outer normal vector on surface
N	Total number of elements in a finite element model
p	Internal pressure
P	Applied load
P_b	Primary bending stress
P_L	Limit load
P_m	Primary membrane stress
P_n	Nominal load set
q	Modulus adjustment index; uniformly distributed load for a beam
Q_e	Effective generalized stress
r	Radius
R_0	Normalized m^0 multiplier
R'	Normalized m' multiplier
R_α	Normalized m_α multiplier
R_B	Reaction at point B
R_i	Reaction at S_V where velocity is prescribed
R_L	Normalized m_L multiplier
R_U	Normalized m_U multiplier
s_{ij}	Deviatoric stress
s_{ij}^0	Statically admissible deviatoric stress field under applied load $m^0 T_i$
$\tilde{s}_{ij}^0$	Statically admissible deviatoric stress field under applied load T_i

SI	Stress Intensity
S_{ij}	Generalized deviatoric stress
S_m	ASME code allowable stress
S_T	Surface of the body where surface traction is prescribed
S_V	Surface of the body where velocity is prescribed
t_x	Traction vector along x axis
t_y	Traction vector along y axis
T_i	Surface traction
$\dot{u}$	Velocity field
U	Elastic strain energy of the body
v	Beam deflection
v_i	Velocity vector
v_i^*	Kinematically admissible velocity
V	Volume
V_R	Reference volume
V_T	Total volume
W	Strain energy density; width

Greek Symbols

α	Ratio of original modulus of elasticity between layers
α_{ij}	Dimensionless anisotropic parameters
β	Ratio of yield stress between layers
β_i	Parameters in anisotropic yield function, which describe the strength differential between tensile and compressive yield stresses
γ	Constant of proportionality
Γ	Any path surrounding the crack tip
δ	Deflection

δ_{ij}	Kronecker delta
ε	Strain
$\bar{\varepsilon}$	Equivalent strain
$\dot{\varepsilon}, \dot{\varepsilon}_{ij}$	Strain rate
ε_e	Effective strain
$d\varepsilon_{ij}^p$	Plastic strain increment
ε'_{ij}	Deviatoric strain
$\dot{\varepsilon}_{ij}^*$	Kinematically admissible strain rate
ε_n	R-node strain
$\bar{\varepsilon}_n$	Normalized r-node strain
$\bar{\varepsilon}_p$	Effective plastic strain
ε_y	R-node strain at collapse
ζ	Iteration variable
η	Scaling factor for surface traction F_i
θ	Follow-up angle
θ_A, θ_B	Angle of rotation at point A, B
$d\lambda$	Positive scalar of proportionality in the flow rule (incremental theory of plasticity)
μ	Positive scalar of proportionality in the flow rule (deformation theory of plasticity)
μ^0	Plastic flow parameter
ν	Poisson's ratio
ν_{ij}	Poisson's ratio for transverse strain induced in j-direction when loaded in the i-direction
σ	Stress; hydrostatic stress (Mura's formulation)
$\bar{\sigma}$	Equivalent or effective stress
$\bar{\sigma}_0$	Reference yield stress
σ_{0x}	Initial uniaxial yield stress along x direction

σ_{0xy}	Initial shear yield stress in *xy* plane
σ_{arb}	Arbitrary non-zero stress
σ_e, σ_{eq}	von Mises equivalent stress
σ_{ij}	Stress tensor
σ_{ij}^*	Statically admissible stress
$\sigma_{\max}$	Maximum equivalent stress
σ_M^0	Maximum equivalent stress in a body under traction T_i
σ_n	R-node peak stress (r-node method); nominal stress value (elastic compensation method)
$\overline{\sigma}_n$	Combined r-node effective stress
σ_y	Yield stress
φ	Point function defined in conjunction with yield criterion

Subscript

e	von Mises equivalent
i	Iteration number
i, j	Tensorial indices
k	Element number
L	Limit load; lower bound
r	Radial direction
θ	Circumferential direction

Superscript

0	Statically admissible quantities
I, II	Linear elastic analyses iteration No. 1 and 2
L	Lower bound
u	Upper bound

List of Appendices

Appendix A ANSYS Models for Major Components

Appendix B ANSYS Macros for Multiplier Evaluations

Chapter 1 Introduction

1.1 General Background

Design for safety, reliability and low cost are the main concerns for engineers. Designers should be cognizant of the possible failure modes involved during the service life of structures and components, and be able to devise failure-avoidance strategies while fulfilling the design objectives.

Among various failure modes, plastic collapse is important since it leads to excessive plastic deformation or ductile rupture of structures such as pressure vessel components. Therefore, it is necessary to estimate the load-carrying capacity (limit load) of a structure and thus prevent it from catastrophic failure due to a single application of load.

Limit load is defined as the load at which a structure reaches a state of uncontained plastic flow, characterized by an increase of deformation without limit. It is usually assumed that the structure is made of perfectly plastic material with a sharply defined yield point. Although perfect plasticity is only an idealization of material behavior it leads to the important concept of limit load which provides a meaningful measure for a design load of a component or structure.

Research on limit analysis is concerned with the development of simple and efficient methods that can enable engineers to estimate the limit load of a structure in a direct manner.

Limit analysis is an acceptable basis for design in the various Boiler and Pressure Vessel Codes. The ASME Boiler and Pressure Vessel Code, Section VIII, Division 2 (ASME, 1992), for instance, states that the design loadings on components must not exceed two-thirds of the lower bound limit load. A knowledge of the limit load enables engineers not only to ensure that the structure can operate safely under the working loads, but also to be economical in the use of material. Since the material strength of the structure beyond initial yield is taken into account, limit analysis has a cost-saving benefit especially for redundant structures.

Limit analysis is also important for the structural integrity assessment. To ensure safer, more reliable and lower cost operation, a service life assessment has to be made for equipment with flaws and defects, and limit analysis provides an important tool for serviceability evaluation. The related concept of reference stress is used extensively in the United Kingdom in elastic-plastic fracture evaluations and high-temperature assessment procedures.

1.2 Limit Load Determination and Robust Methods

The determination of limit load is by no means an easy task. There are several methods for the determination of limit load: analytical methods, inelastic finite element analysis, and simplified methods using linear elastic finite element analysis.

Computation of limit load by solving all the field equations is usually difficult and sometimes mathematically intractable. Other analytical methods are developed on the basis of two basic limit theorems of plasticity: the upper bound theorem and the lower bound theorem. They provide bounds on the collapse load, not its exact value. A statically admissible stress distribution or kinematically admissible collapse mechanism is postulated and by invoking the bounding theorems, lower or upper bound limit loads can be obtained. If the assumed distributions are close to the actual ones the calculated value of limit loads will be close to the exact value. Analytical methods provide direct estimation of limit loads for simple structures, but it is very difficult to apply them for complex structures and loadings.

With the rapid development of computer hardware and software, engineers are now able to perform complicated inelastic finite element analysis (FEA) using desktop computers, which was impossible even a decade ago. Finite element analysis is so versatile that the structure analyzed may have arbitrary shapes, supports and loads. The computation of limit load using inelastic FEA is usually considered very accurate when analytical solutions are not available.

The use of inelastic FEA for limit load estimation, on the other hand, is involved due to material nonlinearity. The inelastic FEA requires a great deal of computing resources, detailed constitutive relationships and necessary expertise to obtain accurate and reliable limit load values. Moreover, it should be noted that the inelastic formulation itself is based on a number of postulates and assumptions.

Since performing inelastic FEA is complex, and since analytical methods apply only to simple geometries, simplified methods using linear elastic finite element analysis have been developed and are of interest to practicing engineers.

There are two categories of simplified methods: mathematical programming techniques using the finite element method, and robust methods using linear elastic finite element analysis. The former limit analysis technique is based on solving an optimization problem in conjunction with the finite element method and the bounding theorems. It requires more computing resources compared with the latter and has not been easily incorporated into commercial finite element packages. Robust methods using elastic finite element analysis, on the other hand, do not have such problems.

Robustness in the context of limit analysis is the ability of a method to provide acceptable results on the basis of less than ideal input, combined with conceptual insight and economy of computational effort (Seshadri and Marriott, 1992). Robust methods do not require exact inelastic flow rules and normally make use of linear elastic constitutive relationships, and the amount of computing resources is greatly reduced. Their robust nature enables them to be applied to various components and structures under different loading conditions. In robust methods, the effect of plastic flow on stress distribution of the structure is simulated by changing the elastic modulus of elements using modulus adjustment techniques.

Robust methods are especially appropriate for the preliminary design of components and for related feasibility studies. They can also be used for screening critical segments in

large complex systems. Furthermore, robust methods can be used to independently verify or benchmark the detailed inelastic FEA results.

1.3 Objective and Organization of The Thesis

Among the several robust methods used for limit analysis, the m_α - multiplier method is the focus of current research. It provides an improved estimate of limit load, and is based on extended Mura's variational principles in conjunction with repeated linear elastic finite element analyses.

The objectives of the thesis are:

1. to improve the existing m_α - multiplier method formulation to account for variable plastic flow rates within an isotropic component,

2. to extend the above formulation to multiply connected or layered structures,

3. to apply the above formulation to cracked components, and to make use of the calculated limit load for estimating fracture parameters,

4. and to extend the above formulation to components and structures made of anisotropic materials.

The thesis is organized as follows:

Chapter 2 gives a brief account of the literature on limit analysis. First, classical bounding theorems are described. Then the inelastic finite element method and simplified methods using linear elastic finite element analysis are discussed.

Chapter 3 provides a detailed explanation and finite element implementation of robust methods, namely, the r-node method, the elastic compensation method and the m_α - multiplier method.

In Chapter 4, the concept and the evaluation of the plastic flow parameter μ^0 are introduced and consequent modifications to the m_α - method are discussed. The modified formulation is applied to a number of component configurations in order to compare its accuracy with the existing m_α - multiplier method, the lower bound elastic compensation method and the inelastic FEA. There is also a discussion of the bounds on multipliers of the m_α - multiplier formulation.

The modified m_α - formulation is further extended to layered structures in Chapter 5. The derivation is based on the extended Mura's variational principles. The formulation is then applied to some practical examples: two-layered cylinders and beams, and three-layered cylinders and beams.

In Chapter 6, the modified m_α - formulation is applied to several cracked components, and the fracture parameters are then calculated by using the estimated limit load.

Chapter 7 presents the extension of the modified m_α - method to anisotropic materials. The estimation of the plastic flow parameter for the anisotropic components is described with reference to the theories of anisotropic elasticity and plasticity. A modulus adjustment technique is proposed with an adopted method of modified initial elastic properties. The formulation is then applied to two anisotropic components.

An overall evaluation of the modified m_α - multiplier method is given in Chapter 8, followed by the recommendation of areas for future research.

ANSYS input files for the models of various component configurations analyzed are documented in Appendix A. The ANSYS macros for the modified m_α - formulation for isotropic, anisotropic and layered structures are listed in Appendix B.

1.4 Original Contributions of Research

The novel contributions of the current research are as follows:

1. The concept of the plastic flow parameter μ^0 is introduced into the existing m_α - multiplier formulation. Numerically, μ^0 is determined from the secant modulus of elements in conjunction with repeated linear elastic FEA. The introduction of the plastic flow parameter has circumvented the previously required reference volume determination (Seshadri and Mangalaramanan, 1997) and improved the convergence of the various multipliers. A number of components made of isotropic material are investigated using this modified formulation.

2. The modified m_α - formulation for layered structures is developed by making use of the extended Mura's variational principle. Modified initial elastic properties are proposed to ensure flow parameter continuity at the layer interface. The formulation is applied to several typical layered components.

3. Several cracked components are examined by the modified m_α - formulation. The estimated limit loads are used to calculate the fracture parameters of these components.

4. The extension of the modified m_α - formulation to components made of anisotropic materials is proposed. The secant modulus of the discretized finite elements in the reference direction in successive elastic iterations is used to estimate the plastic flow parameter for the anisotropic material. The modified initial elastic properties are adopted to ensure the "elastic" stress fields satisfy the anisotropic yield surface. The analyses of two anisotropic components by this formulation yield satisfactory results.

In general, the current research not only significantly improves the existing m_α - multiplier method by the introduction of plastic flow parameter, but also makes the method "full-fledged" so that it can be applied to a wide range of structures and materials. The modified m_α - multiplier method provides engineers with a practical limit load estimation scheme for the assessment and design of mechanical components and structures.

Chapter 2 Literature Review

2.1 Introduction

The theoretical background and the relevant literature related to limit analysis are covered briefly in this chapter. Various methods of limit load estimation are discussed and the advantages and disadvantages of these methods are presented.

Limit analysis is based on two basic assumptions. The first assumption is that the structure is made of a perfectly plastic ductile material. This material must be able to absorb large deformation beyond the elastic limit without the danger of fracture. Secondly the deflections of a structure under loading are assumed small such that the effect of this upon the overall geometry can be ignored. These assumptions simplify the analysis and are reasonable for a wide range of structures made of ductile materials, and they apply to the theories and analyses in this thesis.

2.2 Limit State and Classical Theorems of Limit Analysis

2.2.1 Limit State

Consider a perfectly plastic structure that is in equilibrium under surface traction F_i on S_T, and constraint $v_i = 0$ on S_V. It is assumed that the surface traction is applied in proportional loading, that is, the external traction is assumed to be ηF_i where η is a

monotonically increasing parameter. When the value of η is sufficiently small, the structure behaves elastically. As η increases, a point in the body reaches the plastic state. When η increases further, the plastic region spreads gradually, while the remaining part of the structure may still be in the elastic state. If the value of η continues to increase, a state of impending plastic collapse will be reached in such a way that an increase of plastic strain under constant surface tractions becomes possible for the first time during the loading process. Then the set of loads corresponding to the impending plastic collapse is called the collapse load of the structure, and the safety factor m of this system is determined from the condition that the system collapses under the load mF_i. It is observed that at the collapse load the elastic strain rates and stress rates are identically zero and the body behaves as if it was made from rigid-plastic material.

At the state of the impending plastic collapse, the following conditions are satisfied:

$$\sigma_{ij,j} = 0 \tag{2.1}$$

$$s_{ij}s_{ij} = 2k^2 \tag{2.2}$$

$$\dot{\varepsilon}_{ij} = \mu s_{ij} \text{ where } s_{ij}s_{ij} = 2k^2 \tag{2.3}$$

$$\dot{\varepsilon}_{ij} = 0 \text{ where } s_{ij}s_{ij} < 2k^2 \tag{2.4}$$

$$\dot{\varepsilon}_{ij} = \frac{1}{2}(v_{i,j} + v_{j,i}) \tag{2.5}$$

$$\dot{\varepsilon}_{ii} = 0 \tag{2.6}$$

$$\sigma_{ij} n_j = m F_i \text{ on } S_T \tag{2.7}$$

$$v_i = 0 \text{ on } S_V \tag{2.8}$$

In Eq. (2.2), $s_{ij} = \sigma_{ij} - \delta_{ij}\sigma$, $\sigma = \frac{1}{3}\sigma_{kk}$, and k is the yield stress in pure shear.

The above equations are the equilibrium equations, constitutive relations, compatibility equations and boundary conditions of the analyzed structure. The computation of the safety factor m by solving all these governing equations at the limit state is usually difficult or even impossible. Therefore, recourse must be made to lower and upper bound solutions which bracket the safety factor. Satisfying part of the governing equations, these solutions are provided by the lower and upper bound theorems of limit analysis derived from extremum principles of variational methods.

2.2.2 Lower and Upper Bound Theorems

The stress field which satisfies the equations of equilibrium and the stress boundary conditions, and nowhere violates the yield criterion is termed a statically admissible stress field. That is,

$$\sigma^*_{ij,j} = 0 \tag{2.9}$$

$$s^*_{ij} s^*_{ij} \le 2k^2 \tag{2.10}$$

$$\sigma_{ij}^{*} n_j = m_s F_i \text{ on } S_T \tag{2.11}$$

where m_s is a scalar called statically admissible multiplier, and the superscript * of σ denotes the statically admissible stress field.

On the other hand, an assumed deformation mode that satisfies velocity boundary conditions and strain rate and velocity compatibility conditions is termed a kinematically admissible velocity field. That is,

$$\dot{\varepsilon}_{ij}^{*} = \frac{1}{2}(v_{i,j}^{*} + v_{j,i}^{*}) \tag{2.12}$$

$$\dot{\varepsilon}_{ii}^{*} = 0 \tag{2.13}$$

$$v_i^{*} = 0 \text{ on } S_V \tag{2.14}$$

$$\int_{S_T} F_i v_i^{*} ds > 0 \tag{2.15}$$

where the superscript * of $\dot{\varepsilon}$ denotes the kinematically admissible velocity field.

A scalar defined by the equation (Mura and Koya, 1992)

$$m_k = \sqrt{2}k \frac{\iiint_V \sqrt{\dot{\varepsilon}_{ij}^{*} \dot{\varepsilon}_{ij}^{*}}\, dv}{\int_{S_T} F_i v_i^{*} ds} \tag{2.16}$$

is called kinematically admissible multiplier.

The lower bound theorem can be stated as follows (Calladine, 1969): If any stress distribution throughout the structure can be found which is everywhere in equilibrium internally, balances the external loads and at the same time does not violate the yield criterion, those loads will be carried safely by the structure.

The upper bound theorem can be stated by Calladine, 1969: If an estimate of the plastic collapse load of a body is made by equating internal rate of dissipation of energy to the rate at which external forces do work in any postulated mechanism of deformation of the body, the estimate will be either high, or correct.

The limit theorems in terms of multipliers can be expressed as

$$m_s \leq m \leq m_k \tag{2.17}$$

The proof of the limit theorems can be found in many places in the literatures (Calladine, 1969; Chen and Han, 1988; Mura and Koya, 1992).

Lower bound theorem is considered as the "equilibrium" approach, in which only the equilibrium equations and yield conditions are satisfied while the deformation mode is not considered at all. The collapse load predicted by the "equilibrium" approach is always lower than or equal to the exact collapse load. Therefore, it provides safe estimate and is desirable from the viewpoint of structural design.

The upper bound theorem is considered as the "geometry" approach, in which only deformation mode and energy dissipation are considered while the stress distribution

need not be in equilibrium. The "geometry" approach always overestimates the collapse load, and is useful in the work load estimation of metal forming and cutting.

With the proper choice of stress and deformation fields, the limit theorems enable one to bracket the collapse load in a direct manner. The objective of research is to make the bounds as close as necessary for problems under consideration.

2.3 Classical Analytical Methods

The limit theorems have been applied successfully in the analysis of beams, plane frames, and simple plane stress and plane strain problems. By assuming a proper stress resultant (such as bending moment) distribution or collapse mechanism (strain resultant distribution), the limit theorems can provide good bounding values with the aid of ordinary mechanics of materials.

The following is an example showing how the bound values are calculated for the collapse of a beam under uniformly distributed load. The beam is clamped at one end and simply-supported at the other. It is subjected to a uniformly distributed load of q (Figure 2.1).

The beam is an indeterminate structure. To obtain the reaction at B, R_B, when the beam is elastic, the deflection at B of the cantilever beam under load q only is matched with the deflection under tip load R_B only. Using elasticity theory, the deflection at B, v_B, is

$$v_B = \frac{R_B L^3}{3E_0 I} - \frac{qL^4}{8E_0 I} = 0 \qquad (2.18)$$

Therefore, the reaction at B is $R_B = \frac{3}{8}qL$.

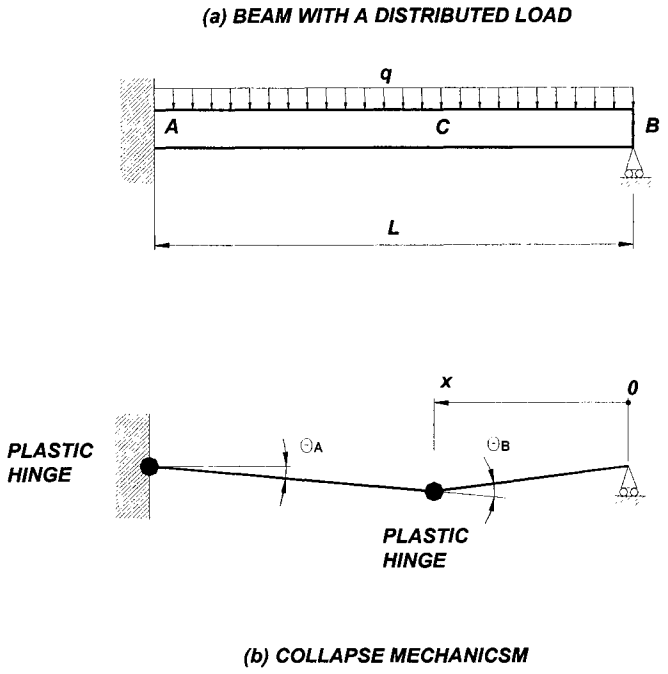

Figure 2.1 Indeterminate beam under uniformly distributed load

The elastic moment distribution along the beam is found to be

$$M(x) = R_B x - \frac{qx^2}{2} = \frac{qx}{2}(\frac{3}{4}L - x) \qquad (2.19)$$

The maximum moment occurs at $x = L$, and it can be made equal to the plastic moment M_p;

$$\frac{qL^2}{8} = M_p \qquad (2.20)$$

Therefore, the elastic solution for moment distribution is scaled using the lower bound theorem. A lower bound limit load is then obtained by assuming that the beam collapse when the first plastic hinge forms

$$q_L^{(-)} = \frac{8M_p}{L^2} \qquad (2.21)$$

For the upper bound estimates, it is assumed that plastic hinges occur at the center of beam C and the left end A, and the beam becomes a collapse mechanism. This assumption may not be the actual failure mechanism but it is kinematically admissible. The deflection of C is δ_C.

The external work done by the uniform load q is

$$External \quad Work = \frac{qL}{2}\frac{\delta_C}{2} + \frac{qL}{2}\frac{\delta_C}{2} = \frac{qL\delta_C}{2} \qquad (2.22)$$

The internal dissipation is

$$Internal \quad Dissipation = M_p(2\theta_A + \theta_B) = \frac{6M_p\delta_C}{L} \qquad (2.23)$$

By equating external work with the internal dissipation, the upper bound limit load is

$$q_L^{(+)} = \frac{12M_p}{L^2} \tag{2.24}$$

Therefore, the bounding values of limit load can be expressed as

$$\frac{8M_p}{L^2} \le q_L \le \frac{12M_p}{L^2} \tag{2.25}$$

The exact value of limit load is (Mendelson, 1968)

$$q_{exact} = \frac{11.657M_p}{L^2} \tag{2.26}$$

It can be found in the above examples that the classical analytical methods are simple and direct in the estimation of the bounds for limit load of beams and plane structures. But it is very difficult to apply them for more complex structures and loadings.

2.4 Inelastic Finite Element Analysis

2.4.1 Advantages of Inelastic FEA

The finite element method was initially developed mostly by engineers using physical insight rather than by mathematicians using abstract methods. It was applied to stress analysis problems before being used to solve other problems of continua. The basic concept is that a body is divided into smaller elements of finite dimensions and simple shapes called "finite elements." The original body is then considered as an assemblage of these elements connected at a finite number of joints called "nodes." Using "shape functions," a field quantity is interpolated over the element from the known field values

at the nodes. By connecting elements together at the nodes, the field quantity becomes interpolated over the entire body in a piecewise fashion. The "best" values of the field variable at the nodes are those that minimize some functional such as the total energy. The minimization process generates a set of simultaneous algebraic equations for values of the field quantity at the nodes. Having the field quantity solved at the nodes, other field quantities, such as stresses and strains, can be evaluated.

The important advantages of the finite element method are its generality and its versatility. There are few restrictions on the shape of the structure or the manner of loading. The problem may be static or dynamic. The analysis may be linear or nonlinear. Moreover, the method is not limited to stress analysis.

For structures involving plastic deformation, analytical solutions are difficult to obtain due to the nonlinear nature of the plastic constitutive relations. At present, only very few exact solutions of simple elastic-plastic problems are available, and it seems practically impossible to solve more complicated cases, such as three-dimensional problems. With the rapid development of high-speed computers and modern numerical techniques, on the other hand, incremental inelastic finite element analysis now can solve virtually any nonlinear structural problem.

Therefore, inelastic finite element analysis (or incremental elastic-plastic FEA) is the most important alternative method apart from limit analysis techniques for the determination of limit load. The material is assumed to be elastic perfectly-plastic and the complete solution for a monotonically increasing loading state is determined. The load at

which uncontained plastic flow happens is the limit load. Inelastic FEA provides considerably more information about the behavior of the structure than the limit analysis techniques.

2.4.2 Drawbacks of Inelastic FEA

In addition to the above-mentioned advantages, performing inelastic finite element analysis has its inherent drawbacks. It is more demanding than linear analysis in terms of computer resources, constitutive model and the analyst's time and expertise.

Firstly, the inelastic FEA is complex because of the irreversibility of plastic deformation, its dependence on loading history, and more importantly, the necessity of carrying out the analysis in an iterative and incremental manner. A great amount of computing resources and time are needed for performing the iterations and the storage of intermediate results.

Secondly, inelastic FEA requires the availability of material properties under all loading conditions and an exact inelastic flow rule. Material constitutive relationships need to be described completely and precisely before the analysis. This may not be the case especially in the initial design stages.

Thirdly, conducting the analysis and interpreting the results of inelastic FEA require experience and relatively deep knowledge of nonlinear analysis techniques. The nonlinear results should be closely examined to check their accuracy and reliability.

A variety of factors may affect the inelastic result greatly, such as the appropriate elements, the mesh layout, solution algorithms, load step control and convergence tolerance. A change in these variables may on occasion produce a significant difference in the final solution. There are some guidelines for their proper choice, but the analyst's experience and expertise play an important part.

Achieving convergence is a problem in inelastic analysis. A large load step may produce convergence failure and cause an abrupt change in the load-deflection curve. As the analysis approaches the limit load, the solution becomes more and more difficult to obtain as the plastic regions spread. Especially when the plastic regions first meet and merge together, the plastic-elastic boundary starts to spread rapidly and further development of the solution becomes extremely difficult. In many cases, convergence failures occur before an uncontained plastic flow happens due to the limitation of iteration number or limit value of degrees of freedom. However, these kinds of convergence problems tend to give safe lower bound estimates of the collapse load. Insufficiently fine meshing or the use of improper elements, on the other hand, may lead to overly high estimates.

Therefore, inelastic FEA is involved, costly and somewhat subjective, which has provided enough motivation for researchers to develop simpler and more general techniques using the linear elastic finite element method or mathematical programming techniques combined with finite element method.

2.5 Simplified Methods using Finite Element Analysis

2.5.1 Introduction

To avoid the complexities of inelastic FEA, many simplified methods have been developed. They are based on finite element technique, which enables their application to analyze complicated structures. They use limit theorems for the direct estimation of limit load, bypassing the contained plastic flow analysis so that the iterations involved are greatly reduced compared with inelastic FEA. Although the information so obtained is just a part of the total solution, these simple and direct methods are of great value to practicing engineers. The methods can be divided into two categories: mathematical programming techniques and robust methods using linear elastic analysis.

2.5.2 Mathematical Programming Techniques

By combining mathematical programming techniques and the finite element method, simplified analytical methods were developed to compute lower and upper bound limit load using limit theorems (Maier et al, 1977). More recent work can be found in some papers that show the application to plane and axisymmetric structures (Berak and Gerdeen, 1990; Zhang and Lu, 1995) and relatively simple three-dimensional structures (Chen and Shu, 1999 and 2000).

This class of methods can be divided into two groups depending on the mathematical technique used. One approach is to treat the limit analysis problem as a linear programming problem with the use of a linearized yield condition (Maier et al, 1977). Another more popular approach is nonlinear programming, which uses the nonlinear

yield criteria and higher order approximations to the stress and velocity fields. There are different solution algorithms for the lower and upper bound problems in the latter approach.

These nonlinear programming techniques consist of some form of optimization program and a search algorithm on a goal function. Direct iterative algorithms are usually employed to determine the lower and upper bound multipliers. Some of these techniques can be applied to structures under multi-loading systems.

However, most of these methods are costly and time-consuming. Berak and Gerdeen (1990) at the time added that, "Both of the finite element analysis procedures, however, are ideally suited for parallel processing on super computers." Even then, the computational effort is especially a problem for the lower bound analysis, since it demands large computer memory and expensive CPU time due to the huge number of constraint equations and degrees of freedom introduced by constructing a statically admissible stress field. This is one of the main reasons for the inapplicability of these methods to complex three-dimensional problems.

Moreover, because of the nonlinearity and non-smoothness of the goal function in the upper bound procedure and the strong physical nonlinearity and unidirectionality of the constraints in lower bound analysis, many of the existing techniques can not be used.

Although Zhang and Liu (1995), Chen and Shu (1999 and 2000) overcame some of the difficulties of physical nonlinearity and reduced the computational dimensions of the problems to a certain degree, these methods have only been applied to two-dimensional

structures and relatively simple three-dimensional structures. The convergence rate of their estimations is not encouraging even for simple structures. Further work is required to show general applicability, performance and accuracy of the solution, especially for complex three-dimensional structures. Furthermore, these methods seem to be not easily incorporated into commercially available finite element packages.

2.5.3 Robust Methods using Linear Elastic Analysis

Robust methods here refer to simplified methods that use linear elastic finite element analysis, and they are often termed as elastic modulus adjustment procedures (EMAP). In EMAP, the effect of plastic flow on the stiffness of the structure is simulated by changing the elastic modulus using a modulus adjustment technique.

Jones and Dhalla (1981) first used the EMAP to classify clamp-induced, deformation-controlled stress in thin-walled straight pipes, where the inelastic effects in a piping system are simulated by an adjusted secant modulus of the material. The method is termed "method of Adjusted Secant for Piping" (ASP). The main purpose of the ASP method is to discern trends in the simulated inelastic response near structural discontinuities, so that the discontinuity stresses can be appropriately classified to satisfy the intent of the ASME code (Dhalla, 1991).

Marriott (1988) modified the ASP method to categorize stresses in pressure components and estimate the lower bound limit load. Using a modulus adjustment technique, elastic finite element analysis generates statically admissible stress fields so that the limit load could be estimated with the lower bound theorem. In this procedure, the first analysis

starts with the uniform original Young's modulus E_0 of the material. Then for all elements in which the stress intensity, SI, exceeds the code allowable S_m, the moduli are modified according to the equation

$$E_{\text{mod}} = \frac{S_m}{SI} E_0 \qquad (2.27)$$

The analysis is rerun with the modified properties. The process is repeated until the maximum stress intensity is reduced to less than S_m, or converges to some value greater than S_m. The lower bound limit load can be obtained for each iteration as:

$$P_L = P \frac{\sigma_y}{\sigma_{\max}} \qquad (2.28)$$

where P is the applied load, σ_y is the yield stress and σ_{max} is the maximum equivalent stress in the component.

Actually, Marriott's procedure is primarily intended for finding the stress distribution with the least maximum stress for a certain load, rather than the determination of limit load. Partial softening of the structure does not entirely characterize the actual stress redistribution that would occur during plastic collapse, and it does not assure the converged value of stress would always be less than the code allowable.

The importance of Marriott's finding is pointed out in his paper as follows, "The obvious advantage of performing the iteration manually is that it is possible to obtain inelastic solutions using a linear elastic code. This opens up a wide range of possibilities for doing

fairly complex analyses on microcomputers." The advent of EMAP enabled engineers to simulate inelastic effects for realistic problems with limited computing resources. This is one of the main reasons that EMAP have attracted interest from researchers and engineers. Up to now, a number of EMAP have been developed which fall into the following groups:

- Stress Classification: This includes the ASP method by Jones and Dhalla (1981) and Marriott's procedures, which are intended wholly or partly for stress classification.

- Local Inelastic Analysis: It deals with local plasticity, such as the estimation of stress and strain at notches (stress raisers). The related EMAP include the generalized local stress and strain (GLOSS) method by Seshadri et al (Seshadri, 1991; Seshadri and Kizhatil, 1993; Seshadri and Babu, 2000), and the modulus adjustment and redistribution of stress (MARS) method by Babu and Iyer (1998, 1999). In these methods, after the first linear analysis, the moduli of those elements whose equivalent stresses are above yield stress are adjusted systematically. With one or more iterations, the local inelastic strains are estimated.

- Limit Analysis: The EMAP for limit analysis include the GLOSS R-node method, the elastic compensation method and the variational m_α - multiplier method. Both the r-node method and elastic compensation method are recommended for pressure vessel design in the ASME task group report on

primary stress (Pastor and Hechmer, 1997). Investigation of the theoretical aspects of EMAP of limit analysis was performed by Ponter et al (Ponter and Carter, 1997a; Ponter et al, 2000).

- Shakedown and Ratchet Analysis: The relevant EMAP include methods to assess the elastic shakedown by Mackenzie et al (Mackenzie and Boyle, 1993b; Mackenzie et al, 1995), and Ponter and Carter (1997b). Further development of EMAP to evaluate shakedown limit and ratchet limit is made available by Ponter et al (Ponter and Engelhardt, 2000; Ponter and Chen, 2001; Chen and Ponter, 2001).

Since limit analysis is the area of interest in this thesis, all three major methods for the determination of limit load are discussed briefly as follows:

1. R-Node Method

Rather than using the lower bound theorem to evaluate limit load, Seshadri et al (Seshadri, 1991; Seshadri and Fernando, 1992) suggested the concept of r-nodes, adapting the skeletal point concept from the reference stress method in creep design. The r-node method is based on two linear elastic analyses. After the first elastic analysis, all the elements in the structure will have their moduli modified individually using the equation

$$E_s = \left[\frac{(\sigma_e)_j}{(\sigma_e)}\right] E_0 \qquad (2.29)$$

where E_s is the modified modulus, E_0 is the original modulus, $(\sigma_e)_j$ is the equivalent stress at a chosen location j within the component and σ_e is the element equivalent stress. After the second analysis, those elements whose equivalent stresses are unchanged during the two analyses are designated as r-nodes. It is considered that these locations are load-controlled and statically determinate. Then the r-node stresses are treated as reference stresses and related to the limit load of the component with the following equation

$$P_L = \frac{\sigma_y}{(\sigma_e)_{r-node}} P \qquad (2.30)$$

where P is the applied load.

It is argued (Seshadri and Marriott, 1992; Seshadri, 1996 and 1997) that the r-nodes can relate the concepts of reference stress, limit load and ASME stress classification. The r-node method has been applied to the estimation of fracture parameters (Seshadri and Kizhatil, 1995), minimum weight design (Mangalaramanan and Seshadri, 1997), limit load for orthotropic structures (Mangalaramanan et al, 1999) and ship type structures (Ralph, 2000). In r-node procedures, there exist some difficulties for combined loads and general three-dimensional structures.

2. Elastic Compensation Method

Using repeated elastic analyses similarly as Marriott and adapting Seshadri's modulus modification technique in the r-node method, Mackenzie et al proposed the elastic

compensation method (ECM) to obtain for every iteration lower and upper bound limit loads utilizing the limit theorems (Mackenzie and Boyle, 1993a; Nadarajah et al, 1993; Shi et al, 1993; Mackenzie et al, 1993).

The purpose of the elastic compensation method is to construct a stress field and strain field suitable for substitution into the lower and upper bound theorems by systematically modifying the element elastic modulus in a finite element model so that the stress can be redistributed. First, a conventional elastic analysis is carried out. In a series of elastic iterations following the first, the elastic modulus of each element is modified according to

$$E_i = E_{(i-1)} \frac{\sigma_n}{\sigma_{(i-1)}} \qquad (2.31)$$

where i is the iteration number, σ_n is a nominal stress value and $\sigma_{(i-1)}$ is the maximum unaveraged nodal equivalent stress for the element in the previous iteration. ECM makes use of iterative analyses in order to obtain convergence.

ECM has been applied to structures modeled in solid, shell (Boyle et al, 1997) or beam elements. The method was used to analyze various structures, such as a branch pipe tee connection (Plancq and Berton, 1998), anisotropic tubesheet design (Reinhardt and Mangalaramanan, 1999 and 2000) and nozzle-sphere intersections (Mohamed, 1999). A study of the effect of finite element modeling parameters on the result of ECM was performed by Mackenzie et al (1994). Mackenzie et al (2000) recently published a

detailed review of this method and recommended the element level formulation of EMAP for future work.

The theoretical aspects of ECM were investigated by Ponter and Carter (1997a). One of their findings is that the exact limit solution for a von Mises yield condition may be exactly simulated by an incompressible linear elastic solution with a spatial variation in the shear modulus $G(\vec{x})$ ($\vec{x}$ represents the spatial variation). Secondly, the iterative process results in a monotonically reducing upper bound which converges to the exact solution, if the elastic solutions are evaluated exactly. Thirdly, ECM can be interpreted as a special nonlinear mathematical programming technique, but no search algorithm on a global functional is required. Finally, in the finite element displacement approach, the ECM upper bound solutions reduce monotonically to a least upper bound, and the ECM lower bounds are pseudo-lower bounds due to the finite element approximation of the stress field.

3. m_α - Multiplier Method

To remove the difficulties with the r-node method for complex structures and to provide better lower bound limit loads than ECM, Seshadri and Mangalaramanan (1997) proposed the m_α - multiplier method using the extended variational theorems in limit analysis of Mura et al (1965). In limit theorems, a statically admissible stress field cannot lie outside the yield surface. Mura et al have eased this restriction by introducing the concept of "integral mean of yield" into the variational formulation so that pseudo-elastic

distributions of stresses that exceed yield can be utilized for the determination of upper and lower bound limit loads. The "integral mean of yield" criterion can be expressed as

$$\int_V \mu^0 [f(s_{ij}^0) + (\varphi^0)^2] dV = 0 \qquad (2.32)$$

where s_{ij}^0 is the deviatoric tensor associated with a statically admissible stress field close to an impending plastic collapse state and $\mu^0 \geq 0$. Satisfying the integral mean of yield criterion and using variational principles, an upper bound multiplier m^0 and a lower bound multiplier m' can be calculated on the basis of two linear elastic FEA using the modulus adjustment scheme of the r-node method. With the idea of "leap-frogging" to the limit state, an improved lower bound multiplier m_α can be obtained by solving a simple quadratic equation (Seshadri and Mangalaramanan, 1997). The new concept of "reference volume," based on the theorem of nesting surfaces (Calladine and Drucker, 1962; Boyle, 1982), is used to derive the limit load. The purpose of the relatively involved determination of the reference volume is to narrow the upper and lower bound spread for localised plastic collapse. The m_α method is robust and applicable to symmetric and non-symmetric components and structures. The m_α method was applied to simple cracked components by Fowler (1998) and ship type structure by Ralph (2000).

The m_α - multiplier method can also be carried out on the basis of successive elastic iterations (Seshadri, 2000), and the estimates become better as the number of iterations is increased. The convergence rate of m_α is faster than that of the lower bound multiplier by ECM. The evaluation of m_α is direct since all the evaluations can be completed within

the macros of finite element software package. Further work is needed for the application of the m_α - multiplier method to layered, anisotropic and cracked components and structures.

2.6 Closure

The EMAP for limit analysis are simple, direct and applicable to complex components and structures, compared with classical analytical methods that are only useful for simple plane structures and with the costly and laborious inelastic FEA. Among the EMAP for limit analysis, the m_α - multiplier method provides better lower bound performance than ECM and simpler procedures than the r-node method. Therefore, there are enough incentives for the further development of the m_α - method, not only to extend its application to other structures and materials, but also to improve the basic formulation of the method.

The following chapter provides a detailed theoretical background of the three major EMAP for limit analysis: the r-node method, elastic compensation method and the m_α - multiplier method.

Chapter 3 Elastic Modulus Adjustment Procedures for Limit Analysis

3.1 Introduction

The detailed theoretical background for three major elastic modulus adjustment procedures of limit analysis is discussed in this chapter: the r-node method, the elastic compensation method and the m_α - multiplier method. The advantages and limitations of these methods are also presented.

All these three methods use a similar modulus adjustment scheme with elastic finite element analysis. The difference lies in the way of interpreting the result based in each respective theory. The r-node method tries to find the load-controlled locations in the structure within two elastic finite element analyses and relates their stresses with the limit load. Both the elastic compensation method and the m_α - multiplier method use repeated elastic finite element analyses to generate statically admissible stress fields and kinematically admissible strain fields. The elastic compensation method substitutes these fields into the upper and lower bound theorems to obtain limit loads, while the m_α - multiplier method substitutes them into Mura's variational principle and uses the idea of "leap-frogging" to estimate limit load values.

3.2 R-Node Method

3.2.1 Redistribution Nodes and Plastic Collapse

Schulte (1960) discovered that in the creep solution of beams there were points in the cross section at which the stress did not change as the solution progressed from initial elastic stage to the final stationary stage, and Marriott and Leckie (1964) later termed such locations "skeletal points." Despite the common belief that there is no special significance attached to such points, Seshadri and Marriott (1992) showed that they are quite important in unifying the apparently disconnected concepts of reference stress, limit load and ASME stress classification.

Skeletal points can be thought of as "nodes of redistribution of stresses." The r-node stresses are considered load-controlled. Load controlled stresses are statically determinate in that they are induced in order to preserve equilibrium with externally applied forces and moments and are proportional to these. When inelastic action occurs, involving the entire cross-sections of a component, the statically indeterminate stresses undergo a redistribution throughout the component except at the r-nodes.

Consider a beam of rectangular cross section subjected to a bending moment M. If the constitutive relationship of the material is given by $\varepsilon = B\sigma^n$, where B and n are material parameters, $n = 1$ corresponds to elastic behavior and $n \to \infty$ corresponds to perfect plasticity. Stationary stress distributions across the beam for various values of n are shown in Figure 3.1. The intersection of stress distributions for $n = 1$ and $n \to \infty$ is designated as r-nodes, and the stress distribution for all other n's is assumed to pass

through r-nodes. The r-node can be represented by a uniaxial bar of a prescribed material behavior.

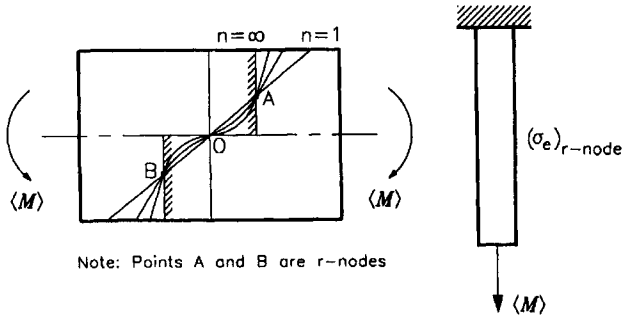

Figure 3.1 R-nodes in a beam subjected to bending

Since the stresses at r-nodes are considered to be load-controlled, they should be linearly proportional to the external loads, i.e.,

$$(\sigma_e)_{r-node} = \gamma P \tag{3.1}$$

where γ is a constant of proportionality that depends on the geometry and loading. Plastic collapse occurs when the r-node stress reaches yield, i.e.,

$$\sigma_y = \gamma P_L \tag{3.2}$$

Therefore, the plastic collapse load can be expressed as

$$P_L = P\frac{\sigma_y}{(\sigma_e)_{r-node}} \tag{3.3}$$

For components or structures that require multiple plastic hinges (or plastic hinge contours) to form a collapse mechanism, a multi-bar model can be used to represent the collapse process. It enables "transfer of loads" to appropriate bars until collapse occurs. The combined r-node effective stress, $\bar{\sigma}_n$, can be obtained as

$$\bar{\sigma}_n = \frac{\sum_{j=1}^{N} \sigma_{nj}}{N} \tag{3.4}$$

where σ_{nj} 's are the r-node peak stresses and N is the number of r-node peaks, plastic hinges or plastic hinge contours. The limit load is given by

$$P_L = \frac{\sigma_y}{\bar{\sigma}_n} P \tag{3.5}$$

3.2.2 Determination of Limit Loads Using R-Nodes

The r-node method can be implemented in the following manner (Mangalaramanan and Seshadri, 1997):

- A linear elastic finite element analysis for a given mechanical component or structure is performed for prescribed isothermal loadings.
- The elastic moduli of all the element in the model are modified using the following equation

$$E_s = \frac{\sigma_{arb}}{\sigma_{ei}} E_0 \qquad (3.6)$$

where σ_{arb} is an arbitrary non-zero stress value and σ_{ei} is the effective stress of element i. A second linear elastic analysis is carried out with the model of all modified properties.

- On the basis of two linear elastic analyses, the follow up angle θ on the GLOSS diagram (Figure 3.2) can be determined for each element. The location for which $\theta = 90$ degree can be identified as the r-node location through interpolation.

- A given structure can be visualized to be made of a finite number of sections across the thickness, throughout its length. Each section may contain r-node and is a potential plastic hinge location. A plot of these r-node stresses along the structure will show peaks which will form plastic hinges. For a structure having M peaks, these peak r-node stresses can be arranged in descending order and denoted by σ_{n1}, σ_{n2}, ..., σ_{nM}.

- As the external load increases, plastic hinges form at the peak location of σ_{n1} and then at σ_{n2} and so on until a collapse mechanism can be identified in the structure. The effective r-node stress is given by Eq. (3.4) and the limit load of the structure is then given by Eq. (3.5).

3.2.3 Features Relating to the R-Node Method

The r-nodes are basically locations in a cross section of a mechanical component or structure that are load-controlled. Therefore, r-node stresses are basically load-controlled quantities that can be used to evaluate collapse loads, and would be insensitive to the constitutive relationship of the material of the component. In this sense it serves as the reference stress. Limiting the r-node effective stress below allowable stress essentially stipulates the ASME's P_m and $P_m + P_b$ stress limits. The concepts of r-nodes, reference stress, limit loads and the requirements of primary membrane and primary membrane plus bending stress limits are therefore related (Seshadri and Fernando, 1992).

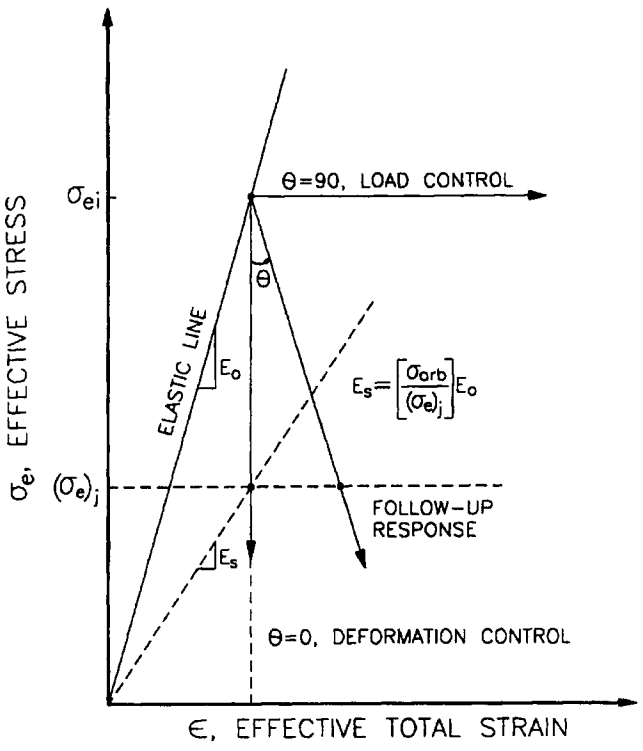

Figure 3.2 Follow-up angle (θ) on the GLOSS diagram

The limit load estimates obtained using the r-node method are usually lower than those obtained from inelastic finite element analysis since the formulation is based on equilibrium considerations alone. This conservative feature of lower bound limit loads is significant from the standpoint of engineering design. The "theorem of nesting surfaces," first introduced by Calladine and Drucker (1962), can be used to ensure the conservativeness of r-node method estimation (Seshadri, 1997). This theorem is briefly explained in Section 3.4.2.

3.2.4 Discussions of the R-Node Method

Although Mangalaramanan (1997) has developed conceptual models for r-nodes, the concept of the skeletal point in creep design and its extension to the r-node for inelastic analysis is not fully understood. Further work is needed for the theoretical justification of lower bound estimation though the r-node method.

R-node identification is trivial for simple structures like a cylinder or a single beam. For more complex structures such as general three-dimensional components, it becomes difficult, although guidelines for the identifying procedures have been given (Seshadri, 1997). The analysts have to rely on practical experience to identify r-node locations, extract stress values for them and average these values. This makes the determination of the limit load indirect and undermines the robustness of this method.

It is suggested that, for general three-dimensional components, when the identification of r-node peaks become very difficult, the maximum r-node effective stress can be used for

calculating limit load (Seshadri, 1997). This could lead to an over-conservative estimate of the limit load, since other plastic hinges or hinge contours may exist.

3.3 Elastic Compensation Method

3.3.1 Elastic Compensation Procedures

Mackenzie et al (1993) proposed the elastic compensation method utilizing the limit theorems to calculate the lower and upper bound limit loads. In the ECM procedure, a series of statically admissible stress fields and kinematically admissible strain fields are obtained by performing a series of elastic analyses in which the elastic modulus of each element is systematically modified by a scheme similar as in the r-node method. This causes the stress to redistribute between analyses.

First, an elastic analysis with the original isotropic homogeneous material property is carried out for a nominal load set P_n. A series of linear elastic analyses are then performed in which the elastic modulus of each element is modified by the equation

$$E_{i+1} = \frac{\sigma_n}{\sigma_i} E_i \qquad (3.7)$$

where E_i is the current value of Young's modulus in the element, E_{i+1} is the value for the next analysis, σ_n is the nominal value of stress and σ_i is the maximum unaveraged nodal equivalent stress for the element in the current solution. The value of σ_n is arbitrary, usually taken to be of the order of the nominal yield stress of the material. Over a number of iterations, this procedure causes the stress in highly loaded elements to decrease while

elements with initially low stress take more load. The evaluation procedures of upper and lower bound limit load using ECM are discussed next. They can be implemented in commercial finite element programs by using external routines to automate the procedures.

3.3.2 Lower Bound Limit Load

The lower bound theorem requires an acceptable statically admissible stress field which is limited to the yield stress in order to define a lower bound limit load. The elastic compensation procedures generate a series of equilibrium stress fields. These stress fields can be substituted into the lower bound theorem to establish lower bound limit loads for the structure. Since the solution is linear, the maximum unaveraged nodal equivalent stress for solution i, σ_{maxi}, is proportional to the applied nominal load set P_n; the lower bound limit load for iteration i, P_{Li}, is obtained from proportionality

$$P_{Li} = P_n \frac{\sigma_y}{\sigma_{\max i}} \qquad (3.8)$$

The best estimate of lower bound limit load in the series of iterations is

$$P_L^L = \max(P_{Li}) \qquad (3.9)$$

It is found that the calculated limit load is always lower than the exact solution, when the ECM is applied to a finite element model (Mackenzie et al, 1994). Because the stiffness is discretely modified at individual element levels, the step changes in elastic modulus

between adjacent elements lead to a jagged discontinuous stress field. Typically, finer meshes and higher order element formulations enhance the calculated limit load.

3.3.3 Upper Bound Limit Load

Using the principle of virtual work, the upper bound theorem may be expressed as

$$\sum P\dot{u} \leq \int_V \dot{D}dV \qquad (3.10)$$

where $\dot{D}$ is the increment of plastic dissipation per unit volume, which for the von Mises yield criterion equals

$$\dot{D} = \sigma_y \int_V \sqrt{\frac{2}{3}(\dot{\varepsilon}_1^2 + \dot{\varepsilon}_2^2 + \dot{\varepsilon}_3^2)}dV \qquad (3.11)$$

To apply the upper bound theorem, a kinematically admissible mode of deformation is required. The ECM procedure automatically generates such a deformation mode by modulus adjustment. Therefore, an upper bound limit load can be obtained by substituting the elastic compensation displacement increment and strain rate fields into Eq. (3.10).

The calculation of the work term can be solved by invoking the linear elastic nature of the solution in the ECM procedure. Since the work done is equal to the elastic strain energy calculated in the FEA, Eq. (3.10) may be rewritten as

$$U = \int_V \sigma \dot{\varepsilon} dV \leq \int_V \dot{D} dV = D \qquad (3.12)$$

where U is the elastic strain energy of the body and D is the plastic dissipation. The upper bound limit load can be obtained from Eq. (3.12) by performing a series of elastic analyses under the nominal load set P_n.

In iteration i, the strain energy and energy dissipation are denoted as U_{ni} and D_{ni} respectively. As illustrated in Figure 3.3 for a one-degree of freedom system, the strain energy of the elastic solution varies with the square of the applied load while energy dissipation varies linearly with the applied load. The load is an upper bound limit load when the curves in Figure 3.3 intersect. In general, the upper bound limit load may be expressed as

$$P_{Li}^u = \frac{D_{ni}}{U_{ni}} P_n \qquad (3.13)$$

The best estimate of the upper bound limit load in a series of ECM iterations is

$$P_L^u = \min(P_{Li}^u) \qquad (3.14)$$

It is found that the upper bound estimation of ECM is usually very close to the exact solution, and the upper bound limit load given by ECM is more accurate than the lower bound limit load. In the upper bound procedure, the energy dissipations are usually evaluated at the centroid or Gauss points of the element, where the results are more

accurate than the nodal values. While in the lower bound procedure, the maximum stress is the unaveraged nodal stress, which could be too high due to extrapolation.

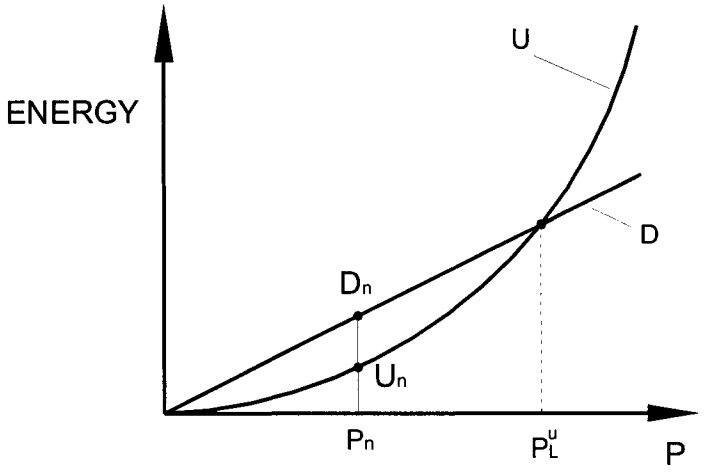

Figure 3.3 Variation of strain energy U and energy dissipation D versus applied load

3.3.4 Theoretical Justification and Discussion

Ponter and Carter (1997) provided the theoretical justification of the ECM procedure, and they identified two characteristics of the limit analysis using ECM. First, the exact limit load solution for a von Mises yield criterion may be exactly simulated by an incompressible linear elastic solution with a spatial variation in the shear modulus $G(\vec{x})$. The iterative process simulates the distribution of $G(\vec{x})$ at limit state except for an arbitrary scaling factor. Secondly, they proved that the iterative process results in a monotonically reducing upper bound which converges to the exact solution, if the elastic

solutions are continuous. But a proof that the lower bounds monotonically increase is lacking, and probably does not exist.

Ponter and Carter discussed the numerical inaccuracies of ECM due to the finite element displacement method. They demonstrated the effect by using a simple double edge cracked plate. The upper bound solutions reduce monotonically to a least upper bound, and the lower bound solutions (where the maximum stress is evaluated at the Gauss points) are more correctly called pseudo-lower bounds: lower bounds to the "exact" upper bounds. Because of the approximate nature of the finite element method, especially the displacement method, the stress fields are in equilibrium only in an averaged sense either within elements or across element boundaries.

The problems associated with ECM are its inherent degree of over-conservatism (when the unaveraged nodal stress is used for maximum stress) in the lower bound solutions and the problem dependence for the convergence rate. Further investigation is needed to close the gap between the lower and upper bounds, to provide a measure for appropriate finite element discretization and to extend the limit analysis procedure to cracked structures.

3.4 m_α - Multiplier Method

3.4.1 Introduction

The theory behind this method uses a different starting point than the r-node method and ECM. The m_α method is based on Mura's extended variational principle in conjunction

with repeated elastic finite element analyses. By using the idea of "leap-frogging to limit state," an improved estimate of limit load can be obtained. The concept of "reference volume" is introduced in conjunction with the theorem of nesting surfaces to obtain good lower and upper bound limit loads. This method can be applied to symmetric and non-symmetric structures.

3.4.2 Theorem of Nesting Surfaces

In the steady state creep analysis, the constitutive equation is given by

$$\frac{d\varepsilon}{dt} = B\sigma^n \qquad (3.15)$$

By the means of elastic analogy (Hoff, 1954), the creep problem can be replaced by a problem in non-linear elasticity with the stress-strain law

$$\varepsilon = B\sigma^n \qquad (3.16)$$

The value of exponent $n = 1$ is analogous to linear elasticity, while $n \to \infty$ resembles perfect plasticity.

The "effective generalized stress" is

$$Q_e = \left[\frac{1}{V}\int_V \sigma_e^{n+1} dV\right]^{1/(n+1)} \qquad (3.17)$$

Calladine and Drucker (1962) extended the work of Hoff and suggested the theorem of nesting surfaces. The theorem can be stated as follows: If a hypersurface $Q_e(\sigma_{ij}) =$

constant in stress space is considered, then for increasing exponent n the corresponding surfaces must "nest" inside each other; i.e., they are enveloped on the outside by surface $n = 1$, analogous to linear elasticity, and on the inside by the limit surface $n \to \infty$, which is a yield surface in generalized forces construed on the assumption that the condition of plasticity is given by Q_e = constant. Incidentally, Q_e is also the reference stress. A plot of nesting surfaces for a two-bar pin jointed structure under combined load Q_1 and Q_2 is shown in Figure 3.4. The bars have equal length L and cross section area A.

For a linear elastic material $n = 1$, the reference stress is expressed as

$$Q_e = \left[\frac{1}{V} \int_V \sigma_e^2 dV \right]^{1/2} \tag{3.18}$$

For a finite element discretization scheme

$$Q_e = \left[\frac{1}{V} \left(\sum_{k=1}^{N} \sigma_{ek}^2 \Delta V_k \right) \right]^{1/2} \tag{3.19}$$

where N is the number of elements and V is the volume of the component or structure.

3.4.3 Mura's Extended Variational Principle

Mura and Lee (1963) showed by means of variational principles that the safety factor, the kinematically admissible multiplier and the statically admissible multiplier for a body made of perfectly plastic material and subjected to a given surface traction are actually extremum values of the same functional under different constraint conditions.

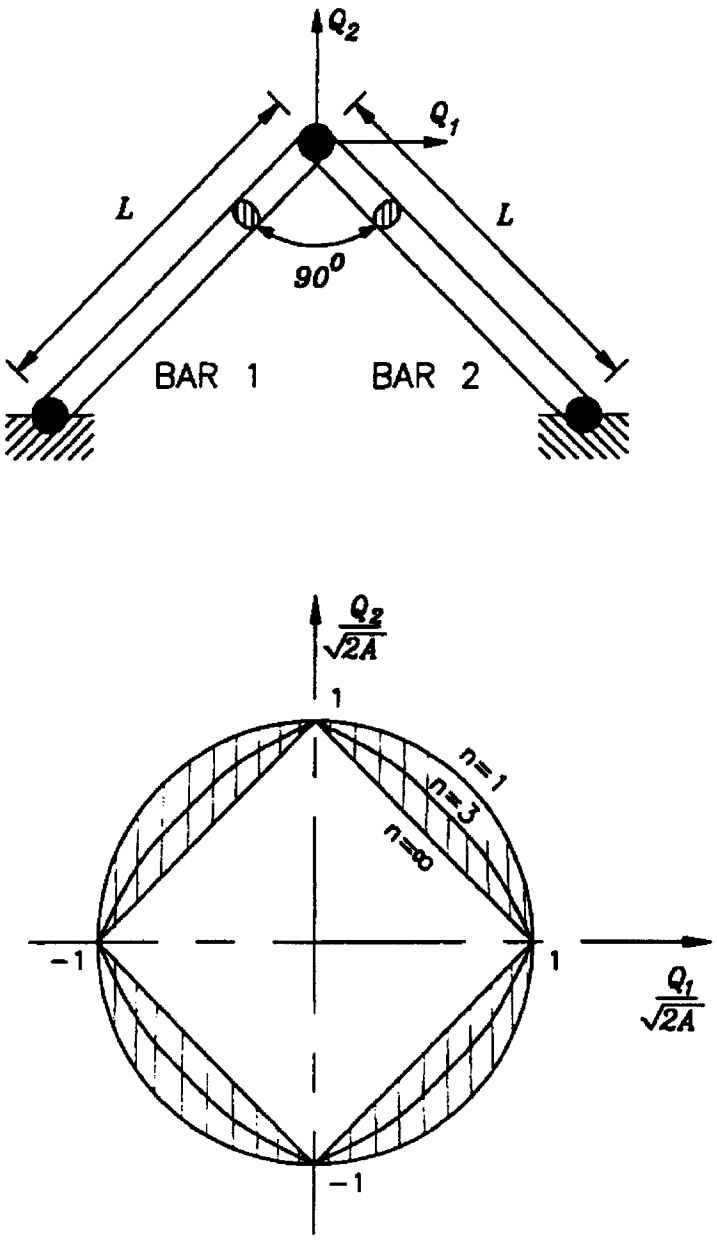

Figure 3.4 Nesting surfaces for a two-bar structure

Mura et al (1965) further introduced the integral mean of the yield criterion so that a pseudo-elastic distributions of stresses can be utilized for the determination of upper and lower bound limit loads. The following is the proof.

A state of impending plastic flow renders the following functional stationary, the safety factor m being the stationary value of the functional (Mura and Lee, 1963).

$$F[v_i, s_{ij}, \sigma, R_i, m, \mu, \varphi] = \int_V s_{ij} \frac{1}{2}(v_{i,j} + v_{j,i})dV + \int_V \sigma \delta_{ij} v_{i,j} dV$$

$$- \int_{S_V} R_i v_i dS - m(\int_{S_T} T_i v_i dS - 1) - \int_V \mu[f(s_{ij}) + \varphi^2]dV \qquad (3.20)$$

with constraint condition

$$\mu \geq 0 \qquad (3.21)$$

The arguments of F are the independent variables: velocity v_i, deviatoric stress s_{ij}, mean stress σ, reaction R_i on S_V where the velocity vector is zero, positive scalar of proportionality μ relating the strain rate and the deviatoric stress, surface traction T_i on S_T and a point function φ which takes into account the inequality of the yield condition. The variables σ, R_i, m and μ are Lagrangian multipliers. The yield function is given by

$$f(s_{ij}) = \frac{1}{2} s_{ij} s_{ij} - k^2 \qquad (3.22)$$

Setting the variation of Eq. (3.20) equal to zero generates the following conditions:

$$\frac{1}{2}(v_{i,j} + v_{j,i}) = \mu \frac{\partial f}{\partial s_{ij}} \quad \text{in } V \text{ with } \mu \geq 0 \qquad (3.23)$$

$$(s_{ij} + \delta_{ij}\sigma)_{,j} = 0 \qquad \text{in } V \qquad (3.24)$$

$$(s_{ij} + \delta_{ij}\sigma)n_j = mT_i \qquad \text{on } S_T \qquad (3.25)$$

$$(s_{ij} + \delta_{ij}\sigma)n_j = R_i \qquad \text{on } S_V \qquad (3.26)$$

$$f(s_{ij}) + \varphi^2 = 0 \qquad \text{in } V \qquad (3.27)$$

$$\mu\varphi = 0 \qquad \text{in } V \qquad (3.28)$$

$$\delta_{ij}v_{i,j} = 0 \qquad \text{in } V \qquad (3.29)$$

$$v_i = 0 \qquad \text{on } S_V \qquad (3.30)$$

$$\int_{S_T} T_i v_i dS = 1 \qquad (3.31)$$

Equations (3.23) to (3.31) are the conditions for incipient plastic flow, and the variables in these equations correspond to a state of impending plastic flow.

Consider the arbitrary arguments, which correspond to a state deviating from the state of impending plastic flow denoted with the superscript '*0*'

$$v_i^0 = v_i + \delta v_i,\ s_{ij}^0 = s_{ij} + \delta s_{ij},\ \ldots\ldots, \qquad (3.32)$$

in which v_i, s_{ij}, ... denote the stationary set of arguments of Eq.(3.20) and δv_i, δs_{ij}, ... are the variations. Substituting Eqs. (3.32) into the arguments of Eq.(3.20) and considering Eqs. (3.23) to (3.31), F can be written as

$$F[v_i^0, s_{ij}^0, \sigma^0, R_i^0, m^0, \mu^0, \varphi^0] = m + \int_V \delta s_{ij} \frac{1}{2}(\delta v_{i,j} + \delta v_{j,i}) dV$$

$$+ \int_V \delta\sigma \delta_{ij} \delta v_{i,j} dV - \int_{S_V} \delta R_i \delta v_i dS - \delta m \int_{S_T} T_i \delta v_i dS$$

$$- \int_V \mu \{\frac{1}{2} \delta s_{ij} \delta s_{ij} + (\delta\varphi)^2\} dV - \int_V \delta\mu \{f(s_{ij}^0) + (\varphi^0)^2\} dV \qquad (3.33)$$

Utilizing the equilibrium equations and boundary conditions of Eqs. (3.24), (3.25) and (3.26) for the impending collapse state, and also the same statically admissible requirement for the new state, viz.,

$$(s_{ij}^0 + \delta_{ij}\sigma^0)_{,j} = 0 \quad \text{in } V \qquad (3.34)$$

$$(s_{ij}^0 + \delta_{ij}\sigma^0) n_j = m^0 T_i \quad \text{on } S_T \qquad (3.35)$$

$$(s_{ij}^0 + \delta_{ij}\sigma^0) n_j = R_i^0 \quad \text{on } S_V \qquad (3.36)$$

Equation (3.33) can be transformed into

$$F = m - \int_V \mu \{\frac{1}{2} \delta s_{ij} \delta s_{ij} + (\delta\varphi)^2\} dV - \int_V \delta\mu \{f(s_{ij}^0) + (\varphi^0)^2\} dV \qquad (3.37)$$

Also, integrating Eq. (3.20) with arbitrary arguments v_i^0, s_{ij}^0, σ^0, R_i^0, m^0, μ^0, and φ^0 and constraint conditions Eqs. (3.34), (3.35) and (3.36) gives

$$F = m^0 - \int_V \mu^0 \{f(s_{ij}^0) + (\varphi^0)^2\} dV \qquad (3.38)$$

Combining Eqs. (3.37) and (3.38), and imposing the integral mean of yield criterion,

$$\int_V \mu^0 \{f(s_{ij}^0) + (\varphi^0)^2\} dV = 0 \qquad (3.39)$$

where

$$\mu^0 \geq 0 \qquad (3.40)$$

the following inequality can be found

$$m^0 \leq m - \int_V \delta\mu \{f(s_{ij}^0) + (\varphi^0)^2\} dV \qquad (3.41)$$

because the second term of the right hand side of Eq. (3.37) is positive definite. The integral mean of yield also gives

$$-\int_V \delta\mu \{f(s_{ij}^0) + (\varphi^0)^2\} dV = \int_V \mu \{f(s_{ij}^0) + (\varphi^0)^2\} dV \qquad (3.42)$$

since $\mu^0 = \mu + \delta\mu$. Substituting (3.42) into (3.41) and taking the maximum value of the integrand, we have

$$m^0 \leq m + \max\{f(s_{ij}^0) + (\varphi^0)^2\} \int_V \mu dV \qquad (3.43)$$

where max $\{f(s_{ij}^0)+(\varphi^0)^2\} \geq 0$ because of conditions (3.39) and (3.40).

Since

$$m = m\int_{S_T} T_i v_i dS = \int_S (s_{ij} + \delta_{ij}\sigma) n_j v_i dS \qquad (3.44)$$

$$= \int_V (s_{ij} + \delta_{ij}\sigma) v_{j,i} dV + \int_V (s_{ij} + \delta_{ij}\sigma) v_{i,j} dV$$

$$= \int_V s_{ij} \frac{1}{2}(v_{i,j} + v_{j,i}) dV = \int_V s_{ij} \mu s_{ij} dV = 2k^2 \int_V \mu dV$$

rearranging yields

$$\int_V \mu dV = m/(2k^2) \qquad (3.45)$$

From (3.43) and (3.45), a new low bound multiplier m' for the safety factor m can be obtained as

$$m' = \frac{m^0}{1 + \max\{f(s_{ij}^0) + (\varphi^0)^2\}/2k^2} \le m \qquad (3.46)$$

which holds for a broader class of stress fields than the statically admissible stress field by taking the integral mean of yield criterion.

Equation (3.46) includes the classical definition of the lower bound, wherein max $\{f(s_{ij}{}^0)+(\varphi^0)^2\} = 0$, and Eq. (3.46) reduces to

$$m^0 \le m \qquad (3.47)$$

Mura and co-workers have shown that m^0, μ^0, and φ^0 can be determined by rendering the functional F stationary in

$$F = m^0 - \int_V \mu^0 [f(s_{ij}^0) + (\varphi^0)^2] dV \qquad (3.48)$$

leading to the set of equations

$$\frac{\partial F}{\partial m^0} = 0; \quad \frac{\partial F}{\partial \mu^0} = 0; \quad \frac{\partial F}{\partial \varphi^0} = 0 \qquad (3.49)$$

3.4.4 Finite Element Implementation of Mura's Principle and Elastic Iterations

Since s_{ij}^0 is the stress state close to impending plastic flow, $s_{ij}^0 = m^0 \tilde{s}_{ij}^0$, where $\tilde{s}_{ij}^0$ corresponds to the applied traction T_i. Therefore, Equation (3.48) can be rewritten as

$$F = m^0 - \int_V \mu^0 [\frac{1}{2}(m^0)^2 \tilde{s}_{ij}^0 \tilde{s}_{ij}^0 - k^2 + (\varphi^0)^2] dV \qquad (3.50)$$

In terms of effective stress and yield stress, the above equation can be further rewritten as

$$F = m^0 - \int_V \frac{\mu^0}{3} [(m^0 \sigma_e)^2 - \sigma_y^2 + 3(\varphi^0)^2] dV \qquad (3.51)$$

Setting $\delta F = 0$ yields (Seshadri and Mangalaramanan, 1997)

$$m^0 = \frac{\sigma_y \sqrt{V}}{\sqrt{\sum_{k=1}^{N} (\sigma_{ek})^2 \Delta V_k}} \qquad (3.52)$$

$$\varphi^0 = 0 \qquad (3.53)$$

where N is the total number of elements, σ_{ek} and ΔV_k are the effective stress and volume of element k, and V is the total volume of the component or structure.

Combining Eqs. (3.18) and (3.52), we get

$$m^0 = \frac{\sigma_y}{Q_e} \qquad (3.54)$$

Therefore, m^0 is related to the reference stress Q_e, and Mura's formulation is related to the theorem of nesting surfaces.

On the other hand, using Eq. (3.46), the lower bound multiplier can be expressed as

$$m' = \frac{2m^0 \sigma_y^2}{\sigma_y^2 + (m^0)^2 (\sigma_M^0)^2} \qquad (3.55)$$

where $\sigma_M{}^0$ is the maximum equivalent stress in a component or structure for a prescribed set of loads.

The multiplier, m^0, is an upper bound for all stress states that are statically admissible. Therefore, the exact multiplier m is bounded by m^0 and m'. For any structure analyzed by finite element analysis, m^0 and m' can be readily obtained by Eqs. (3.52) and (3.55).

Using a modulus adjustment scheme similar as the r-node method, statically admissible stress fields and kinematically strain fields can be obtained from a linear elastic finite element analysis. The first linear analysis is a conventional elastic analysis, while the second analysis involves modification of all the elements using the equation

$$E_s = \left(\frac{\sigma_{arb}}{\sigma_e} \right)^q E_0 \qquad (3.56)$$

where q is a modulus adjustment parameter which in nominally taken as one. The iterations can be repeated any number of times until convergence is obtained, although it must be assured that the theorem of nesting surfaces is satisfied.

On the basis of successive elastic iterations, where the elastic modulus adjustments are made according to Eq. (3.56), the values of m_1^0, m_2^0, ... , m_p^0, can be readily obtained. The theorem of nesting surfaces can be stated as

$$m_1^0 \geq m_2^0 \geq m_3^0 \geq \cdots \geq m_p^0 \geq m \qquad (3.57)$$

where m_1^0, m_2^0, ... , m_p^0 represent a series of average surfaces of dissipation.

An iteration variable ζ is now introduced in such a manner that infinitesimal changes to the elastic modulus of various elements in successive elastic analysis would induce a corresponding change $\Delta\zeta$. As ζ increases with the iterations, m^0 and m' should ideally converge uniformly to the exact value of the safety factor, m. A schematic of the ideal variation of m^0 and m' with ζ is shown in Figure 3.5.

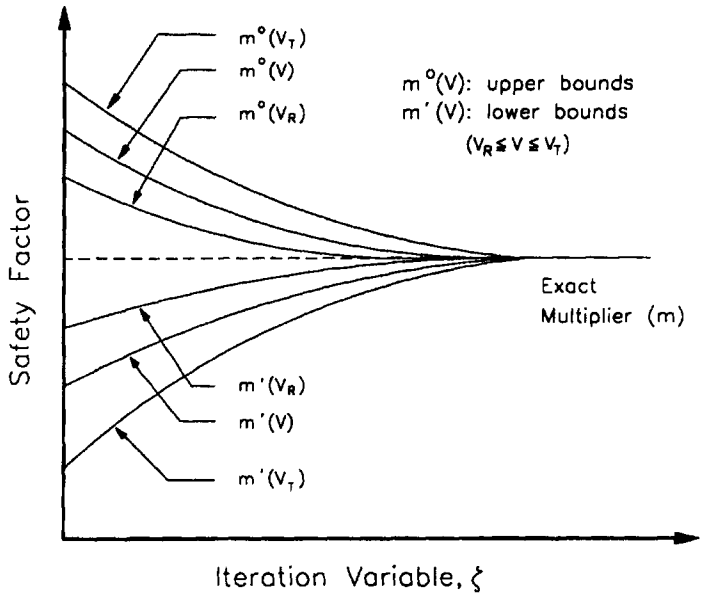

Figure 3.5 m^0 and m' versus iteration variable ζ

3.4.5 Reference Volume - Local Plastic Collapse

When plastic collapse occurs over a localized region of a component or structure, the value of m^0 will be overestimated if it is calculated on the basis of the total volume, V, as in Eq. (3.52). Furthermore, the corresponding m' will be underestimated.

The reference volume concept is introduced to identify the "kinematically active" portion of the structure that participates in the plastic actions. If V_R is the reference volume, such that $V_R \leq V$, then

$$m^0(V_R) = \frac{\sigma_y \sqrt{V_R}}{\sqrt{\sum_{k=1}^{\alpha} (\sigma_{ek})^2 \Delta V_k}} \qquad (3.58)$$

where $V_R = \sum_{k=1}^{\alpha} (\Delta V_k)$, and $\alpha < N$.

The elements are arranged in the descending order of energy dissipation

$$(\sigma_{e1}^0)^2 \Delta V_1 > (\sigma_{e2}^0)^2 \Delta V_2 > \cdots > (\sigma_{eN}^0)^2 \Delta V_N \qquad (3.59)$$

As k is increased from 1 to N, the value of m^0 will increase for any given linear elastic iteration. The variation of m_1^0 and m_2^0 with volume corresponding to the first and second linear elastic FEA is shown in Figure 3.6. When $m_1^0(V_R) = m_2^0(V_R)$ the two curves intersect. It can be seen that for $V \geq V_R$, the theorem of nesting surfaces would be valid since $m_1^0 > m_2^0$. The phrase "m_α - method" refers to the use of α elements in the finite element discretization scheme that pertains to the identification of an appropriate reference volume (Seshadri and Mangalaramanan, 1997).

The introduction of the reference volume enables the narrowing of the spread between upper and lower bounds m^0 and m'.

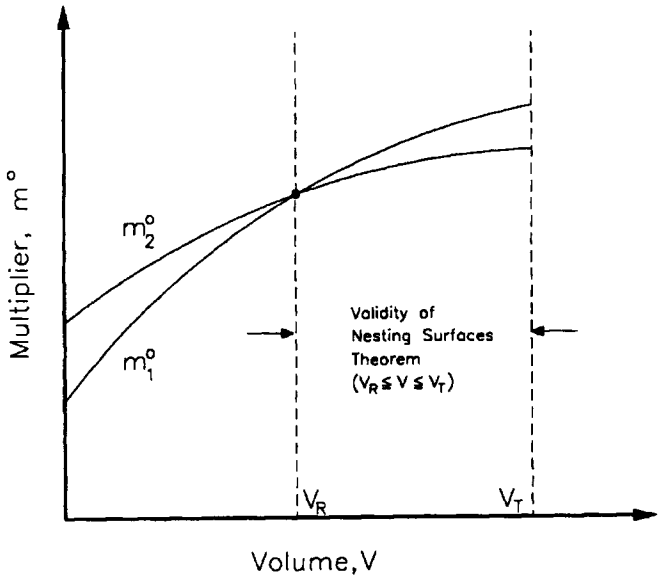

Figure 3.6 Identification of the reference volume, V_R.

3.4.6 Improved Lower Bound Limit Loads: The m_α - Method

In terms of iteration variable ζ, Mura's lower bound multiplier can be expressed as

$$m'(\zeta) = \frac{2m^0(\zeta)\ \sigma_y^2}{\sigma_y^2 + [m^0(\zeta)]^2 \cdot [\sigma_M^0(\zeta)]^2} \tag{3.60}$$

where $\sigma_M{}^0(\zeta)$ is the maximum equivalent stress.

In terms of finite-differences, we have

$$\Delta m' = \left.\frac{\partial m'}{\partial m^0}\right|_{\zeta_i} \cdot (\Delta m^0) + \left.\frac{\partial m'}{\partial \sigma_M^0}\right|_{\zeta_i} \cdot (\Delta \sigma_M^0) \tag{3.61}$$

where $\zeta = \zeta_i$ corresponds to the i-th iteration.

For a limit-type state (ζ_∞), we define

$$\left.\begin{aligned} \Delta m' &= m_\alpha - m_i' \\ \Delta m^0 &= m_\alpha - m_i^0 \\ and \quad \Delta\sigma_M^0 &= \frac{\sigma_y}{m_\alpha} - \sigma_{Mi}^0 \end{aligned}\right\} \qquad (3.62)$$

m_α is the value to which m' and m^0 are conjectured to converge to. The idea of "leap-frogging" of iterations is shown in Figure 3.7.

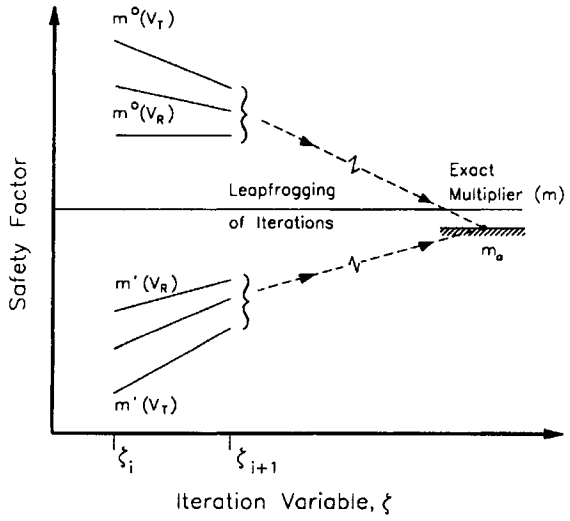

Figure 3.7 Leapfrogging to the limit state

Combining Eqs. (3.61) and (3.62), and carrying out the necessary algebraic manipulations, the following quadratic equation can be obtained:

$$Am_\alpha^2 + Bm_\alpha + C = 0 \qquad (3.63)$$

where $A = (m_i^0 \bar{\sigma}_{Mi}^0)^4 + 4(m_i^0 \bar{\sigma}_{Mi}^0)^2 - 1$

$$B = -8m_i^0 (m_i^0 \bar{\sigma}_{Mi}^0)^2$$

$$C = 4(m_i^0)^3 \bar{\sigma}_{Mi}^0$$

and $\bar{\sigma}_{Mi}^0 = \dfrac{\sigma_{Mi}^0}{\sigma_y}$.

Coefficients A, B, C and finally m_α can be evaluated from the results of any linear elastic FEA iteration. Although the m_α - method was intended for two iterations at first, increasing iterations would give better estimations provided certain conditions are satisfied (Seshadri and Mangalaramanan, 1997).

To ensure that the roots of Eq. (3.63) are not imaginary, as could be the case during early iterations in structures and components containing sharp notches or cracks,

$$m_i^0 \bar{\sigma}_{Mi}^0 \le 1 + \sqrt{2} \qquad (3.64)$$

3.4.7 Discussions

Although the derivation for the m_α - method is involved, the implementation of the method is simple and can be automated using the external routine of the commercial finite element codes. This method is robust and applicable to a wide range of geometric configurations and complex loading combinations.

The main drawback of the m_α - method is the wide spread of the upper and lower bound multipliers for structures experiencing local collapse. A procedure of identifying the reference volume is introduced to solve this problem, but the procedure itself is problematic:

1. The procedure is more like a technique than a method with solid theoretical basis.

2. The procedure of the identification of the reference volume is somewhat involved.

3. The performance can not be guaranteed for successive iterations. The identification of reference volume could become difficult as the stress distribution gets smoother for later iterations.

4. The sequence arrangement of the internal dissipation could be better if the density of internal dissipation is used. The variable representing degree of plastic deformation is better to be the equivalent strain than the equivalent stress.

5. If the reference volume has been chosen inappropriately, m^0 and m' may not be bounds any more.

Therefore, it is necessary to find a concept for the recognition of greater contribution of plastic active region to the m^0 multiplier.

Since the m_α - method was first introduced for two linear elastic finite element analyses, its performance for successive iterations needs to be investigated.

Finally, the m_α - method needs to be extended to layered, anisotropic and cracked components and structures.

3.5 Closure

The m_α - method is discussed in more detail in this chapter than the r-node method and the elastic compensation method, not only because the theories behind it are more complex, but also because the m_α - method has more advantages than the others. The following chapters will describe the author's work for the improvement and the further extension of the m_α - method.

Chapter 4 Collapse Load Estimation for Components and Structures Made of Isotropic Materials

4.1 Introduction

After explaining the basic concepts of the m_α - multiplier method, the further developments of this method for isotropic materials are discussed in this chapter. The concept of the plastic flow parameter μ^0 is introduced into the basic m_α formulation to improve the estimation of the multipliers. The modified approach is applied to several components and structures and the results are compared with those obtained from the basic m_α formulation, lower bound elastic compensation method and inelastic FEA.

A study of the bounds on m^0, m' and m_α (Reinhardt and Seshadri, 2003) is also presented in this chapter. The quality of estimates of these multipliers is assessed.

4.2 Plastic Flow Parameter

4.2.1 Distributed Plastic Flow

In Mura's variational formulation, the "integral mean of yield" criterion is expressed as

$$\int_V \mu^0 \{f(s_{ij}^0) + (\varphi^0)^2\} dV = 0 \qquad (4.1)$$

Letting $\varphi^0 = 0$ (see Section 3.4.4), Eq. (4.1) can be expressed in terms of m^0 and the equivalent stress σ_{eq} as

$$\int_V \frac{\mu^0}{3}[(m^0\sigma_{eq})^2 - \sigma_y^2]dV = 0 \qquad (4.2)$$

Based on Mura's variational principle and Eq. (4.2), Seshadri and Mangalaramanan (1997) defined m^0 as

$$m^0 = \frac{\sigma_y\sqrt{V}}{\int_V \sigma_{eq}^2 dV} = \frac{\sigma_y\sqrt{V}}{\sqrt{\sum_{k=1}^{N}(\sigma_{ek})^2\Delta V_k}} \qquad (4.3)$$

If one examines the derivation from Eq. (4.2), the above definition of m^0 implies that the parameter μ^0 is constant throughout the structure. This means all the elements possess an equal weight in Eq. (4.2) no matter what degree of plastic deformation they have.

It has been found that, when plastic collapse occurs over a localized region of the structure, Eq. (4.3) could significantly overestimate m^0 and in turn underestimate m'. To overcome this problem, Seshadri and Mangalaramanan (1997) introduced the concept of reference volume to identify the "kinematically-active" portion of the structure. However, the procedure to determine the reference volume for the m^0 estimation is empirical, and cannot at present be programmed.

When a component is at a state of collapse, the degree of plastic flow varies from point to point. The plastic flow parameter μ^0 should be a distributed parameter that characterizes

the degree of plastic flow at a given location. If it can be evaluated in a region such that more plasticity means higher value of μ^0 (higher weighting in Eq. (4.2)), the estimation of m^0 and other multipliers will be improved.

4.2.2 Deformation Theory of Plasticity

On the basis of the deformation theory of plasticity, the stress-strain relationship is

$$\varepsilon'_{ij} = \mu s_{ij} \qquad (4.4)$$

where μ is a positive scalar, and s_{ij} and ε_{ij}' are the stress and strain deviators. Therefore, μ must be defined as

$$\mu = \frac{3\bar{\varepsilon}}{2\bar{\sigma}} = \frac{3}{2E_S} \qquad (4.5)$$

where $\bar{\sigma} = \sqrt{\frac{3}{2} s_{ij} s_{ij}}$ is the equivalent stress, $\bar{\varepsilon} = \sqrt{\frac{2}{3} \varepsilon'_{ij} \varepsilon'_{ij}}$ is the equivalent strain, and E_S is the secant modulus of a point in a component or structure.

4.2.3 Plastic Flow Parameter

Elastic modulus adjustment procedures are known to produce stress distributions close to the limit type stress distribution. Hence, EMAP are able to generate a secant modulus distribution close to the limit type secant modulus distribution.

For each elastic iteration, one can postulate that the plastic flow parameter μ^0 can be considered as a function of the secant modulus (E_S) of every element in a given elastic FEA scheme, i.e.,

$$\mu^0 = \frac{C}{E_S} \tag{4.6}$$

where C is a constant whose value depends on the arbitrary stress, specific geometric configuration and loading pattern. As the stress distribution approaches the limit type distribution with successive elastic FEA iterations, the distribution of the plastic flow parameter μ^0 within the structure will also be closer to the distribution of the actual flow parameter μ at the state of impending collapse. As the amount of plasticity at a point increases, the secant modulus E_S drops and the parameter μ^0 assigns a higher weight to this location.

4.2.4 An Example

To compare the distribution of μ at plastic collapse with the distribution of μ^0 during elastic iterations, an incompressible thick cylinder of axial plane strain condition under internal pressure is analyzed.

The compatibility equation for an axisymmetric structure is given as follows:

$$r\frac{d\varepsilon_\theta}{dr} = \varepsilon_r - \varepsilon_\theta \tag{4.7}$$

The incompressibility and axial plane strain conditions can be expressed as

$$\varepsilon_\theta + \varepsilon_r + \varepsilon_z = 0 \text{ and } \varepsilon_z = 0 \qquad (4.8)$$

Equations (4.8) yield

$$\varepsilon_r = -\varepsilon_\theta \qquad (4.9)$$

Substituting Eq. (4.9) into Eq. (4.7) and integrating, the strains can be found as

$$\varepsilon_r = -\varepsilon_\theta = \frac{C_1}{r^2} \qquad (4.10)$$

where C_1 is a constant.

The equivalent strain can then be written as (Kraus, 1980)

$$\bar{\varepsilon} = \frac{2C_1}{\sqrt{3}r^2} \qquad (4.11)$$

Since the derivation of Eq. (4.11) involves only geometry, it can be used for the cylinder at the plastic collapse state. The constant C_1 can be evaluated using $\bar{\varepsilon} = \sigma_y / E_0$ at $r = r_o$ as

$$C_1 = \frac{\sqrt{3}\sigma_y r_0^2}{2E_0} \qquad (4.12)$$

where E_0 is the Young's modulus, σ_y is the yield stress and r_o is the outer radius of the cylinder.

Therefore, the distribution of the secant modulus for cylinder at the collapse state can be expressed as

$$E_S = \frac{\bar{\sigma}}{\bar{\varepsilon}} = \frac{\sigma_y \sqrt{3} r^2}{2C_1} = \frac{E_0}{r_0^2} r^2 \qquad (4.13)$$

To obtain the secant modulus distribution for the linear elastic analyses, we introduce the definition of von Mises equivalent stress as

$$\bar{\sigma} = \frac{1}{\sqrt{2}} \left[(\sigma_r - \sigma_\theta)^2 + (\sigma_\theta - \sigma_z)^2 + (\sigma_z - \sigma_r) \right]^{\frac{1}{2}} \qquad (4.14)$$

The axial plane strain and incompressibility conditions give

$$\sigma_z = \nu(\sigma_r + \sigma_\theta) = 0.5(\sigma_r + \sigma_\theta) \qquad (4.15)$$

Substituting Eq. (4.15) into Eq. (4.14) gives the simplified form of equivalent stress

$$\bar{\sigma} = \frac{\sqrt{3}}{2} (\sigma_\theta - \sigma_r) \qquad (4.16)$$

For the first linear elastic analysis, Lame's solution (Chen and Han, 1988) for the stresses is

$$\begin{cases} \sigma_r = \dfrac{p r_i^2 (r^2 - r_o^2)}{r^2 (r_o^2 - r_i^2)} \\ \sigma_\theta = \dfrac{p r_i^2 (r^2 + r_o^2)}{r^2 (r_o^2 - r_i^2)} \end{cases} \qquad (4.17)$$

where p is the internal pressure and r_i is the inner radius.

Hence, the equivalent stress for the first elastic analysis is given by

$$\bar{\sigma}^{I} = \frac{\sqrt{3}p}{r^2}\frac{r_i^2 r_o^2}{r_o^2 - r_i^2} \tag{4.18}$$

The equivalent stress-strain relationship for the second linear elastic analysis is

$$\bar{\sigma}^{II} = E_S^{II}\bar{\varepsilon}^{II} \tag{4.19}$$

where E_S^{II} is the secant modulus for the second analysis. Using the modulus adjustment scheme, the secant modulus can be expressed as (Mangalaramanan and Reinhardt, 2001)

$$E_S^{II} = E_0\frac{\sigma_{arb}}{\bar{\sigma}^{I}} = \frac{E_0\sigma_{arb}(r_o^2 - r_i^2)}{\sqrt{3}pr_i^2 r_o^2}r^2 = Kr^2 \tag{4.20}$$

where σ_{arb} is the arbitrary stress and K is a constant for this given problem.

Using Eq. (4.11) and Eq. (4.20), Eq. (4.19) can be written as

$$\bar{\sigma}^{II} = \frac{2C_1K}{\sqrt{3}} \tag{4.21}$$

The equilibrium equation for an axisymmetric structure is

$$r\frac{d\sigma_r}{dr} = \sigma_\theta - \sigma_r \tag{4.22}$$

Substituting Eq. (4.16) and Eq. (4.21) into the equilibrium equation leads to the differential equation for the radial stress

$$\frac{d\sigma_r}{dr} = \frac{4C_1 K}{3r} \qquad (4.23)$$

Integrating the above equation and using the stress boundary condition at the inner radius, the constant C_1 can be evaluated as

$$C_1 = \frac{3p}{4K\ln(r_0 / r_i)} \qquad (4.24)$$

Therefore, the equivalent stress for the second elastic analysis is (Mangalaramanan and Reinhardt, 2001)

$$\bar{\sigma}^{II} = \frac{\sqrt{3}p}{2\ln(r_o / r_i)} \qquad (4.25)$$

Equation (4.25) shows that the equivalent stress in the cylinder is constant for the second analysis and it pertains to the stress distribution of limit type.

From Eq. (4.20) and Eq. (4.13), it can be seen that the secant modulus distributions of the second linear elastic analysis and the collapse state are both quadratic. If we equate these two equations, the constant C in Eq. (4.6) is found to be

$$C = \frac{3E_S^{II}}{2E_S} = \frac{3kr^2}{2E_0 r^2 / r_o^2} = \frac{\sqrt{3}\sigma_{arb}(r_o^2 - r_i^2)}{2pr_i^2} \qquad (4.26)$$

The above equation suggests that the ratio between the plastic flow parameters μ^0 and μ at the collapse state is a constant for a given problem. The value of the constant depends on the arbitrary stress, load and component geometry.

4.3 Formulations

4.3.1 m^0, m′ and m_α

The evaluation of the plastic flow parameter μ^0 enables us to estimate m^0 more accurately.

Mura's variational principle (Section 3.4.3) states that $\varphi = 0$ for plastic region and $\varphi > 0$ for elastic region. In the current investigation, the distribution of φ^0 is assumed to be 0 throughout the structure. The reason is that, in the "integral mean of yield" criterion, the contribution from the elastic region is negligible due to its low plastic flow parameter value. Hence, φ^0 does not need to be accurately evaluated in the elastic region.

Therefore, rearranging "the integral mean of yield" criterion and specifying $\varphi^0 = 0$, m^0 can be expressed as

$$m^0 = \sigma_y \left[\frac{\int_V \mu^0 dV}{\int_V \mu^0 \sigma_{eq}^2 dV} \right]^{1/2} \qquad (4.27)$$

Substituting Eq. (4.6) into the above equation, m^0 can be rewritten as

$$m^0 = \sigma_y \left[\frac{\int_V \frac{1}{E_S} dV}{\int_V \frac{\sigma_{eq}^2}{E_S} dV} \right]^{1/2} = \sigma_y \left[\frac{\sum_{k=1}^{N} \Delta V_k / E_{Sk}}{\sum_{k=1}^{N} \sigma_{ek}^2 \Delta V_k / E_{Sk}} \right]^{1/2} \qquad (4.28)$$

where N is the total number of finite elements of the structure; σ_{ek}, ΔV_k, E_{Sk} are the equivalent stress, element volume and secant modulus of element k, respectively. The constant C cancels out during the algebraic manipulations.

The evaluation procedure for m' and m_α is the same as for the basic m_α - formulation.

It will be shown in the numerical examples that the modified expression for m^0 leads to accelerated convergence to the exact value when compared with the basic m_α formulation. It can also be seen that m' converges more rapidly to the exact value, m.

4.3.2 Modulus Adjustment Scheme

The following equation is used to modify the modulus in the repeated elastic FEA

$$E_{k(i)} = \left[\frac{\sigma_{arb}}{\sigma_{ek(i-1)}} \right]^q E_{k(i-1)} \qquad (4.29)$$

where σ_{arb} is the arbitrary stress; i is the iteration number; q is a modulus adjustment index which is normally taken as one; k is the element number in the discretized component or structure; σ_{ek} is the averaged equivalent stress for element k.

Poisson's ratio is usually taken as a value near 0.5 (0.47 in the current investigation) to simulate the incompressibility of the material at plastic collapse but at the same time avoid volumetric locking which occurs if the analysis uses a value very close to 0.5. It is also found that for certain cases in which the plastic collapse occurs throughout the component, as for a cylinder under internal pressure, a Poisson's ratio near 0.5 leads to faster convergence of multipliers than the elastic value.

Although it was pointed out by Ponter et al (2000) that, theoretically, Poisson's ratio should be 0.5 to ensure convergence to limit type deformation, the current investigation shows that a value of 0.47 can provide very good accuracy without using special finite elements and longer computer runtime. Furthermore, Poisson's ratio of 0.47 can reduce the possibility of imaginary roots for m_α estimation compared with a value of 0.49.

4.4 Applications

4.4.1 Numerical Examples

In this section, the m_α - multiplier method based on the plastic flow parameter is applied to several general type components and pressure vessel configurations, including

- thick cylinder under internal pressure,
- indeterminate beam under uniformly distributed load,
- non-symmetric rectangular plate,
- torispherical head,
- sphere-nozzle junction,
- pressure vessel support skirt.

All these components are analyzed using the ANSYS finite element code (ANSYS,1998). Four-noded isoparametric quadrilateral elements PLANE42 are used for 2D models and eight-noded isoparametric brick elements SOLID45 are used for 3D models. The mesh density is considered to be moderate, such as at least four elements for thin-shell structures. Further details of the discretization can be found in the ANSYS input files in Appendix A. The stress values are extracted from the centroid of the element. m^0, m', and m_α values are calculated automatically by macros programmed in ANSYS APDL language without any manual post processing or calculation.

The limit load multipliers predicted by various methods are plotted against iterations in the subsequent figures. In the legends, "m^0," "m'," "m_α" stand for the multipliers obtained from the distributed plastic flow parameter formulation. "m^0 basic" and "m' basic" represent the multipliers obtained from the basic m_α formulation. "ECM-LB" is the multiplier from the lower bound estimation of the elastic compensation method, while "m" stands for the multiplier from inelastic FEA or classical methods.

4.4.1.1 Thick Cylinder Under Internal Pressure

A thick cylinder under internal pressure of 275.8 MPa (40,000 psi) is modeled axisymmetrically with axial plane strain condition (Figure 4.1). The inner radius R_i is 76.2 mm (3 inch) and the outer radius R_o is 228.6 mm (9 inch). The material is elastic perfectly-plastic, with Young's modulus E_0 = 206.85 GPa (30×10^6 psi) and yield stress σ_y = 206.85 MPa (30,000 psi). A modified Poisson's ratio of 0.47 is used as the initial

properties rather than the actual elastic value of 0.3. The variation of multipliers predicted by various methods versus iteration is plotted in Figure 4.2.

The exact multiplier obtained by inelastic FEA is 0.9512, which is very close to the analytical solution of 0.9514 from the following equation (Chen and Han, 1988)

$$P_{\lim it} = \frac{2}{\sqrt{3}} \sigma_y \ln \frac{R_o}{R_i} \qquad (4.30)$$

As shown in Figure 4.2, the difference between the existing and the modified method of calculating m^0 and m' is small in this case because the entire volume is plastic at collapse. All the multipliers rapidly converge to the inelastic FEA value in the second and third iterations.

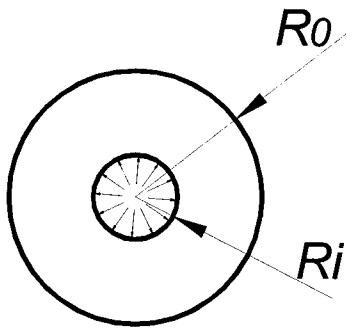

Figure 4.1 Thick cylinder under internal pressure

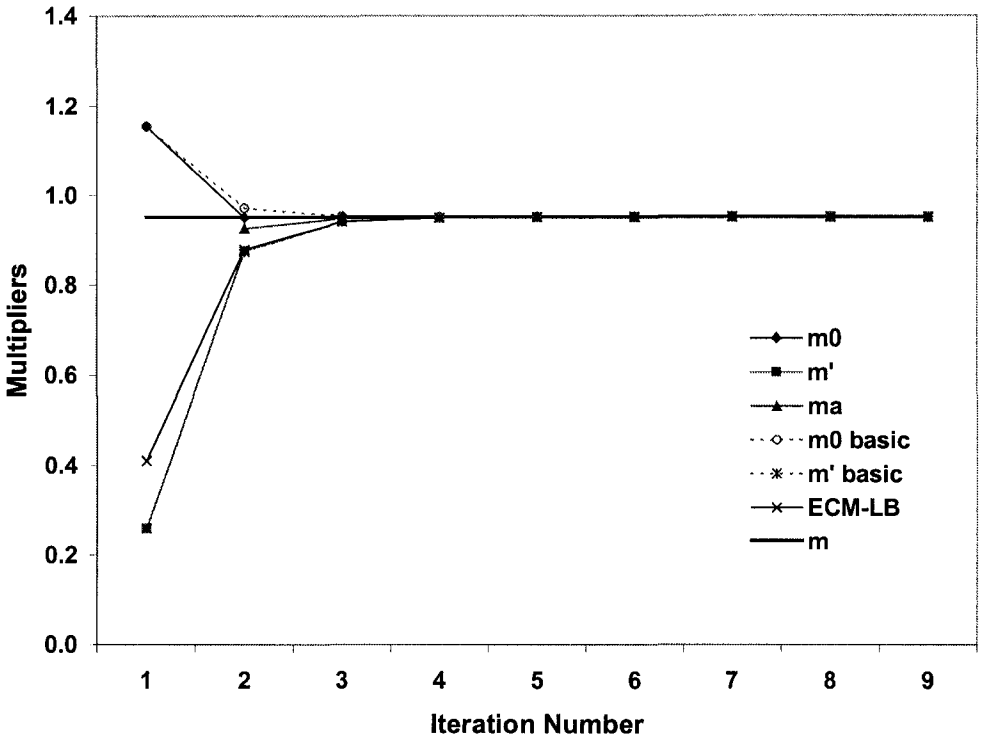

Figure 4.2 Multiplier estimations versus iteration for thick cylinder

4.4.1.2 Indeterminate Beam

An indeterminate beam with one end simply-supported and the other clamped is analyzed under plane stress condition (Figure 4.3). The beam span L is 508 mm (20 inch) and the height H is 25.4 mm (1 inch). A uniform distributed load 2.07 MPa (300 psi) is applied. The material is the same as that of the previous cylinder. The multipliers predicted by various methods versus iteration are plotted in Figure 4.4.

The exact multiplier m obtained by inelastic FEA is 0.7203, compared to a value of 0.7286 from analytical method using the following equation (Mendelson, 1968)

$$q_{exact} = \frac{11.657 M_p}{L^2} \qquad (4.31)$$

In Figure 4.4, the difference between the existing and the modified method of calculating m^0 and m' is large since the structure is experiencing local collapse. Excellent m_α value is obtained in the fourth iteration. As the iteration proceeds, the m_α multiplier goes over the inelastic result slightly.

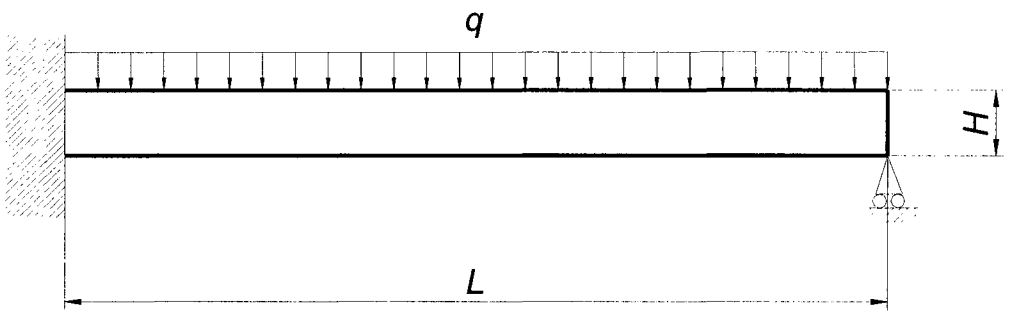

Figure 4.3 Indeterminate beam under uniformly distributed load

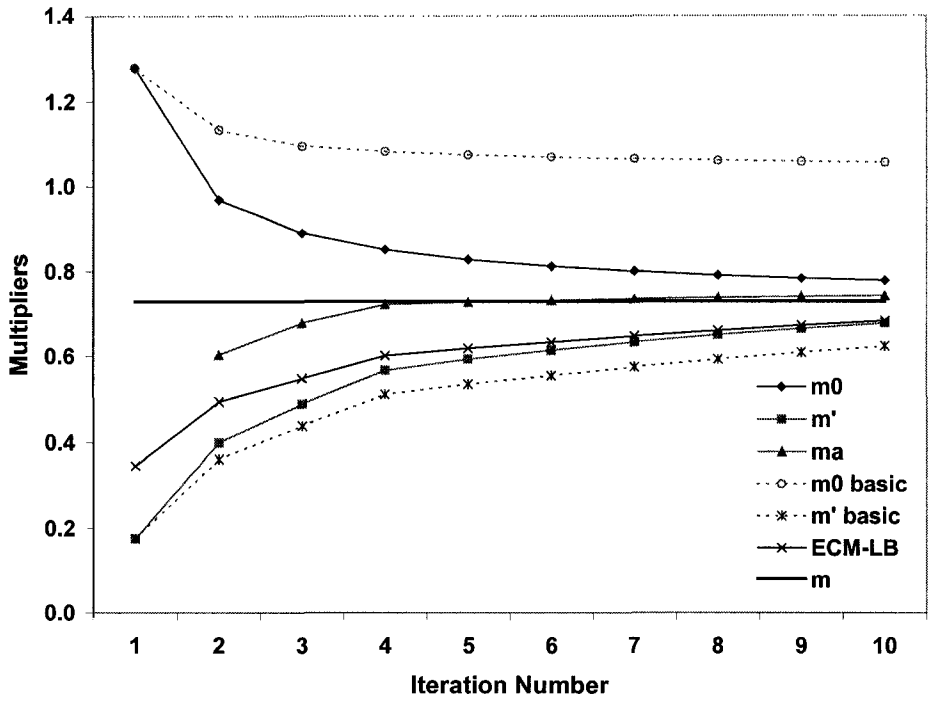

Figure 4.4 Multiplier estimations versus iteration for indeterminate beam

4.4.1.3 Non-Symmetric Rectangular Plate

A rectangular plate with non-symmetric complex boundary conditions (Figure 4.5) is investigated three-dimensionally using SOLID45 element (four elements through the thickness). The plate is partially fixed or simply-supported on its edges, and is under a uniform pressure of 6.895 MPa (1000 psi). The plate has a length (L) of 381 mm (15 inch), a width (W) of 254 mm (10 inch) and a uniform thickness of 12.7 mm (0.5 inch). The material properties are the same as those of the previous cylinder. Figure 4.6 shows the variation of multipliers estimated by various methods versus iteration, where the exact m value is obtained using nonlinear FEA.

All the multipliers show good convergence with the m_α value being the best lower bound in Figure 4.6. The difference between the existing and the modified method of calculating m^0 and m' is small. This implies that most of the plate is plastically deformed when it collapses.

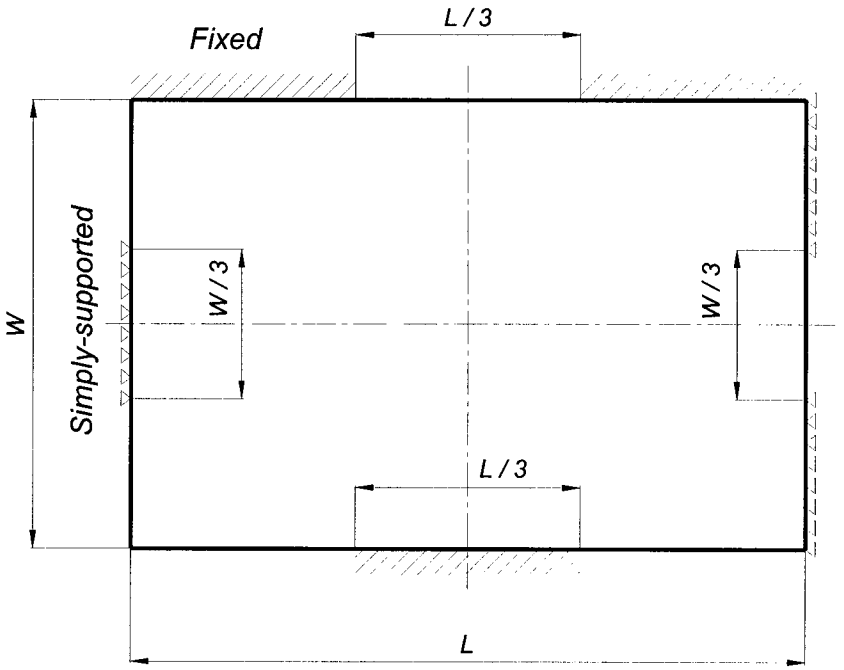

Figure 4.5 Non-symmetric rectangular plate

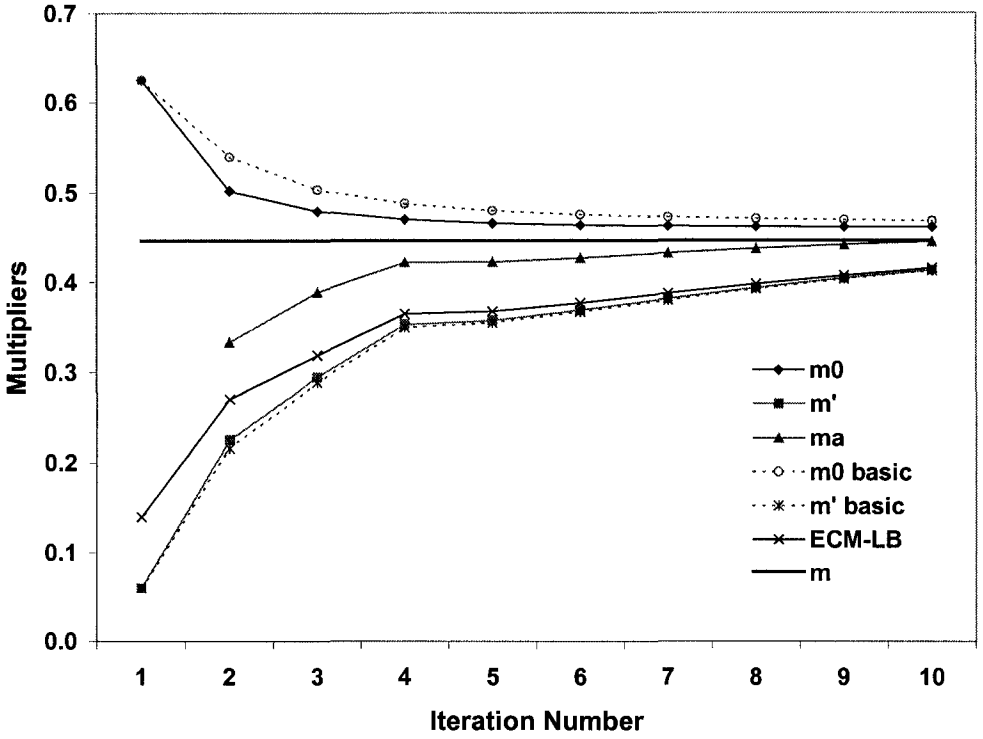

Figure 4.6 Multiplier estimations versus iteration for non-symmetric rectangular plate

4.4.1.4 Torispherical Head

A torispherical head of uniform thickness T = 25.4 mm (Figure 4.7) is examined axisymmetrically using PLANE42 elements with six elements through the thickness. The ratio of the average diameter D of the torispherical head to the thickness is 300. The ratios for spherical cap radius R_s and knuckle radius R_k over D are 0.8 and 0.12 respectively. The length of the cylindrical part (H) is modeled as $6\sqrt{DT/2}$ to avoid the discontinuity effect at the boundary. An internal pressure of 1 MPa is applied. The material is also the same as that of the previous cylinder. A modulus adjustment index q = 0.5 is used to ensure a relatively smooth variation of lower bound multipliers. The

variation of multipliers predicted by various methods versus iteration is presented in Figure 4.8.

In Figure 4.8, excellent result of m_α is obtained in the fourth iteration. The large difference between the existing and the modified method of calculating m^0 indicates that the structure is under local collapse.

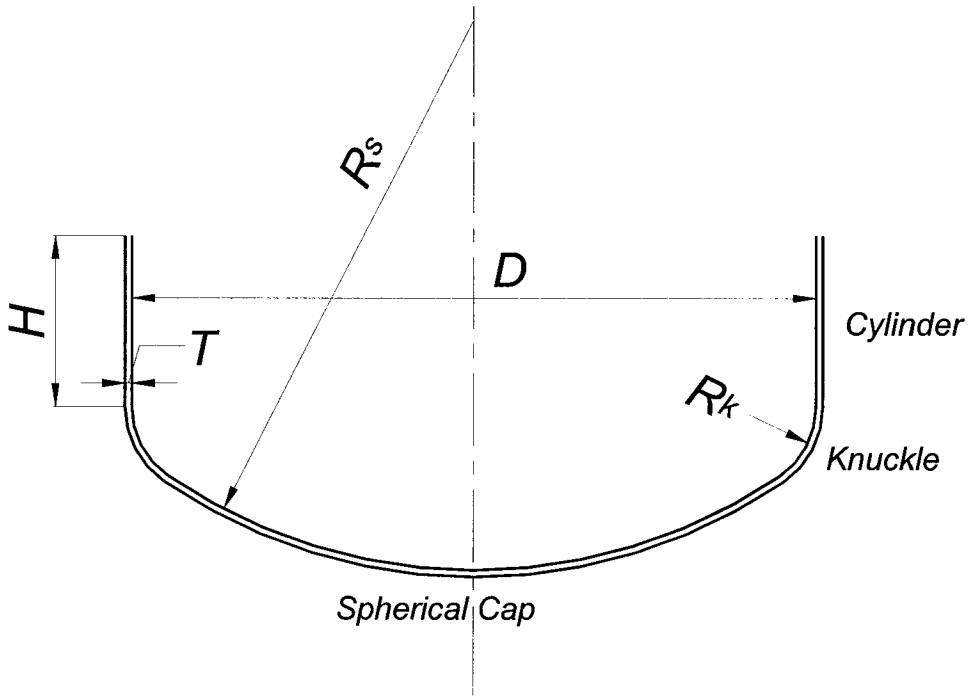

Figure 4.7 Dimensions of torispherical head

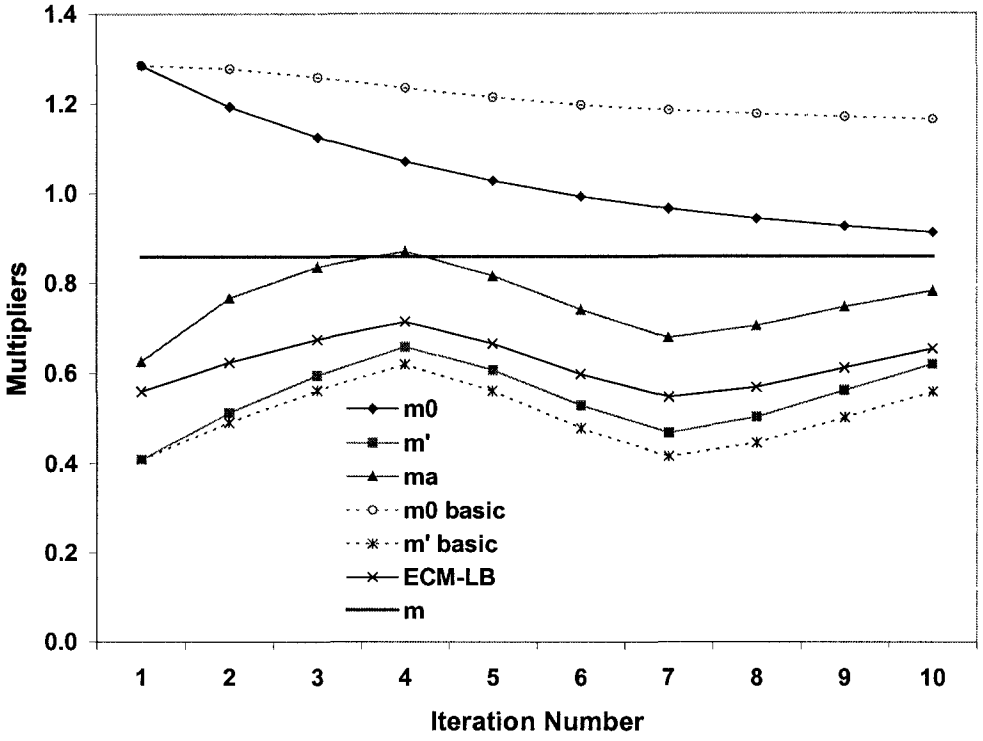

Figure 4.8 Multiplier estimations versus iteration for torispherical head

4.4.1.5 Sphere-Nozzle Junction

An axisymmetric model is used for the analysis of a sphere-nozzle junction under internal pressure (Figure 4.9). The sphere-nozzle geometry parameters are: sphere inner radius R = 1 m, sphere shell thickness T = 0.25 m and nozzle internal radius r = 0.20 m. The nozzle shell thickness t is determined based on the equivalence of the hoop stresses of the nozzle and the sphere by the equation

$$t = \frac{2Tr}{R} \qquad (4.32)$$

The length of the nozzle is $6\sqrt{rt}$ in order to eliminate the discontinuity effect. A fillet radius of $t/2$ is used to remove the stress singularity at the corner of sphere-nozzle juncture. The material is elastic perfectly-plastic with Young's modulus of 200 GPa and yield stress of 300 MPa. An internal pressure of 150 MPa is applied. The estimated multipliers versus iteration are shown in Figure 4.10.

The second iteration gives good m_α estimate and the estimate improves with more iteration in Figure 4.10. Again, the small difference between the existing and the modified method of calculating m^0 means that the structure is under gross plastic deformation. In the eighth to tenth iteration, m_α value goes over the inelastic result slightly.

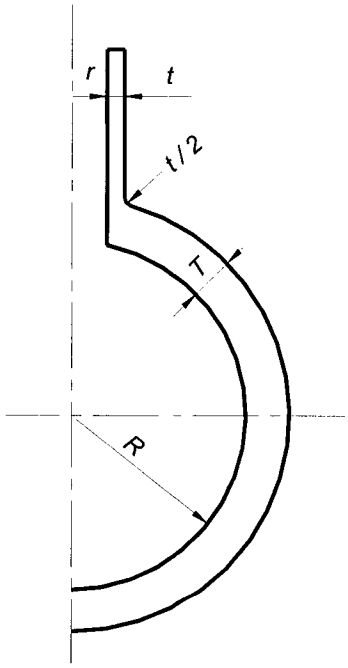

Figure 4.9 Dimensions of sphere-nozzle junction

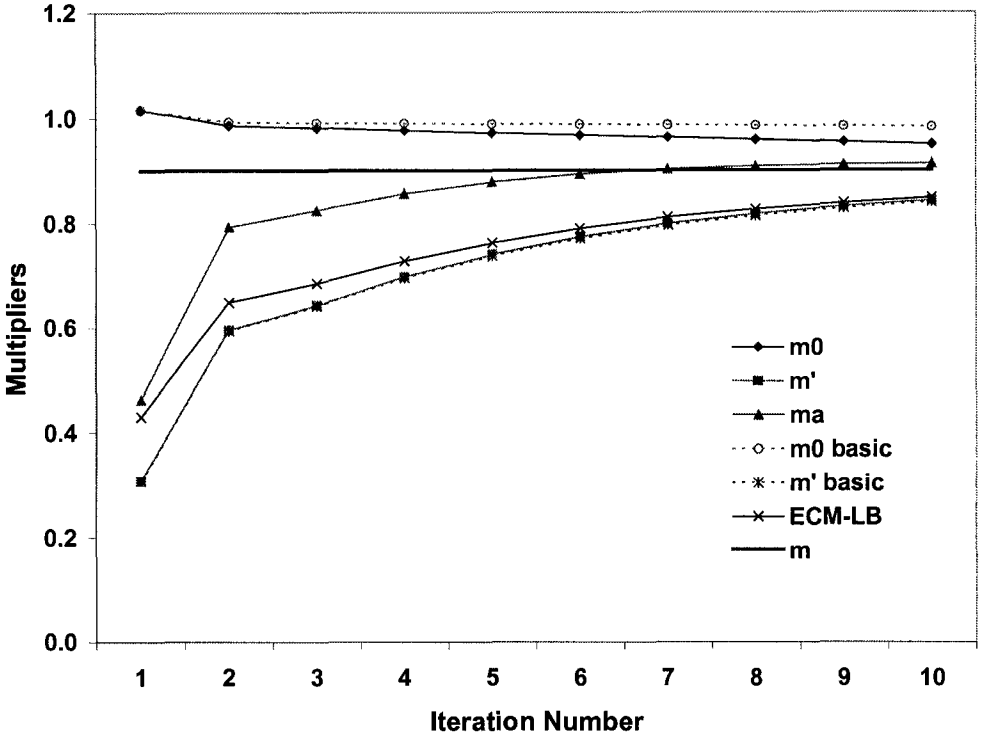

Figure 4.10 Multiplier estimations versus iteration for sphere-nozzle junction

4.4.1.6 Pressure Vessel Support Skirt

Figure 4.11 illustrates a pressure vessel support skirt, which is a cylinder with an attached cone. The thickness of the skirt shell is 50.8 mm (2 inch), and all the other dimensions are shown in the figure. The top end of the cone is fixed to a rigid foundation. The lower end of the cylinder is free to deflect and rotate, and is under a uniform axial pressure of 275.8 MPa (40,000 psi). The material is elastic perfectly-plastic, with Young's modulus E_0 = 206.85 GPa (30 × 10^6 psi) and yield stress σ_y = 275.79 MPa (40,000 psi). The multiplier estimates are presented in Figure 4.12.

In Figure 4.12, the best m_α estimate is obtained in the fourth iteration. Worse m_α values at later iteration show that local instability occurs as the maximum stress becomes higher.

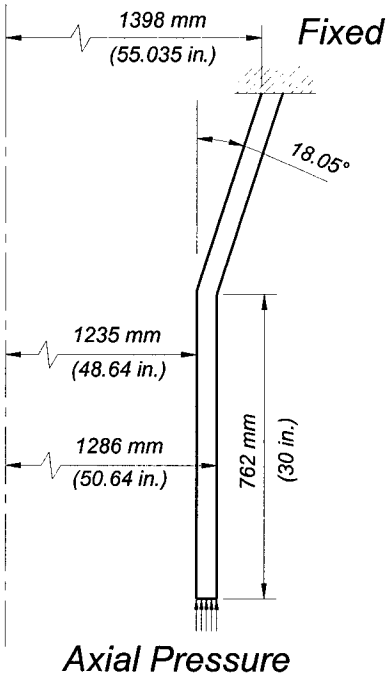

Figure 4.11 Pressure vessel support skirt

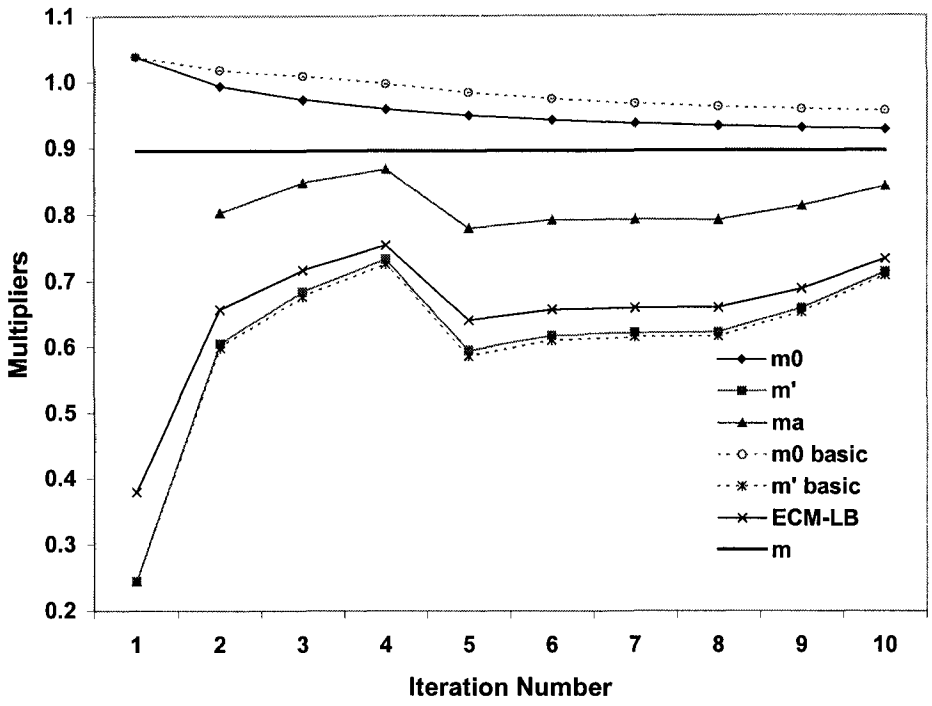

Figure 4.12 Multiplier estimations versus iteration for pressure vessel support skirt

4.4.2 Conclusions

From the multiplier plots for these six components, it can be seen that the m_α predictions under the modified formulation are closer to the value obtained by inelastic FEA than other lower bound estimates. The multipliers m^0 and m' obtained under the modified formulation, especially m^0, are closer to the inelastic FEA value as compared to m^0 and m' obtained from the basic m_α formulation. The improvement is more significant for structures having local collapse, such as the indeterminate beam and the torispherical head.

It can be concluded that the modified m_α formulation is applicable to a wide range of symmetric and non-symmetric components and structures. The m_α predictions are close to the inelastic FEA value and are usually a lower bound.

It is observed that the m_α values fluctuate as iterations continue for thin-shell structures. This is due to the fluctuation of the maximum stress. For those components, during iterations, the general deformation pattern approaches the limit state, but locally the maximum stress element may jump around as the load redistributes. Although the maximum stress oscillates between iterations, it decreases in the general sense.

In some cases, the m_α estimates go slightly over the inelastic FEA results, as for indeterminate beam and the sphere-nozzle junction when the iteration approaches to the exact value. This will be discussed in the following section.

4.5 Bounds on Multipliers

A study on multipliers m^0, m' and m_α has been carried out by Reinhardt and Seshadri (2003), in which the bounds and the quality of estimates of these multipliers are investigated.

4.5.1 Bounds on m′ and m^0

Mura's lower bound multiplier, m', can be shown to be equivalent to

$$m' = \frac{2m^0}{1+\left(\frac{m^0}{m_L}\right)^2} \leq m \qquad (4.33)$$

where m_L is the classical lower bound multiplier.

By using the true collapse multiplier m, the following normalised variables can be defined:

$$R_L = \frac{m_L}{m},\ R_U = \frac{m_U}{m},\ R' = \frac{m'}{m}\ \ and\ \ R_0 = \frac{m^0}{m} \qquad (4.34)$$

where m_U is the classical upper bound multiplier.

By virtue of Eq. (4.34), Eq. (4.33) can be written as

$$R' = \frac{2R_0}{1+\left(\frac{R_0}{R_L}\right)^2} \leq 1 \qquad (4.35)$$

It is now easily shown, in the following hypothesis, that R' is, in fact, not only a lower bound, but even that it is smaller than R_L.

$$\frac{2R_0}{1+\left(\frac{R_0}{R_L}\right)^2} \leq R_L \quad \Leftrightarrow \quad 2\frac{R_0}{R_L} \leq 1+\left(\frac{R_0}{R_L}\right)^2 \Leftrightarrow \quad 0 \leq 1-2\frac{R_0}{R_L}+\left(\frac{R_0}{R_L}\right)^2 = \left(1-\frac{R_0}{R_L}\right)^2 \qquad (4.36)$$

For the m^0 multipliers, bounds can be derived as well. The multiplier m_1^0, defined in Eq. (4.3), is shown to be greater than m_L by

$$m_1^0 = \frac{\sigma_y \sqrt{V_T}}{\sqrt{\int_{V_T} (\sigma_{eq})^2 \, dV}} = \frac{\frac{\sigma_y}{\sigma_{\max}} \sqrt{V_T}}{\sqrt{\int_{V_T} \left(\frac{\sigma_{eq}}{\sigma_{\max}} \right)^2 dV}} = m_L \sqrt{\frac{\int_{V_T} 1^2 \, dV}{\int_{V_T} \left(\frac{\sigma_{eq}}{\sigma_{\max}} \right)^2 dV}} \geq m_L \qquad (4.37)$$

The relationship (4.37) holds because everywhere $\sigma_{eq} \leq \sigma_{max} = max(\sigma_{eq})$. The multiplier m_1^0 may not converge to the limit multiplier m, meaning $R_1^0 \geq 1$ at the exact limit state. From Eq. (4.34), it is clear that $R_1^0 = 1$ can occur only if $\sigma_{eq} = \sigma_{max}$ everywhere in the volume V_T. If localized plastic hinges form in the structure, that condition is generally not satisfied. This property of m_1^0 can present a potential difficulty in some applications. As a remedy, the idea of the reference volume was introduced by Seshadri and Mangalaramanan (1997), which however complicates the application of the multiplier m_1^0.

For a restricted class of materials, namely those of the linear elastic type with homogenous properties throughout V_T, m_1^0 can be shown to be an upper bound. The proof makes use of the Schwarz inequality, according to which the inner product of linear operators of a fairly general class satisfies

$$(x, y) \leq \|x\| \, \|y\| \qquad (4.38)$$

where (x,y) is the inner product of x and y, and $\|x\|$ is the norm of x. Integrals for which the integrand is bounded are operators suitable for the application of the Schwarz

inequality, and $(x,y) = \int x\, y\, dz$, $\|x\| = \sqrt{\int x^2 dz}$. Therefore, the following relationship can be derived

$$\sqrt{\int_{V_T} \sigma_{eq}^2\, dV}\ \sqrt{\int_{V_T} 1^2\, dV} \geq \int_{V_T} \sigma_{eq} \cdot 1\, dV \quad \Leftrightarrow \quad \sqrt{V_T} \geq \frac{\int_{V_T} \sigma_{eq}\, dV}{\sqrt{\int_{V_T} \sigma_{eq}^2\, dV}} \tag{4.39}$$

By substituting the right expression in Eq. (4.39) into Eq. (4.3), it follows that

$$m_1^0 = \frac{\sigma_y \sqrt{V_T}}{\sqrt{\int_{V_T} \sigma_{eq}^2\, dV}} \geq \frac{\sigma_y \int_{V_T} \sigma_{eq}\, dV}{\int_{V_T} \sigma_{eq}^2\, dV} = \frac{\sigma_y \int_{V_T} E\varepsilon_{eq}\, dV}{\int_{V_T} E\sigma_{eq}\varepsilon_{eq}\, dV} \tag{4.40}$$

If the material is homogenous, the elastic modulus in the rightmost expression is constant and can be cancelled. Furthermore, for an isotropic-elastic material, the principal axes of stress and strain are coincident, and $\sigma_{eq}\, \varepsilon_{eq} = \sigma_{ij}\, \varepsilon_{ij}$. By virtue of classical upper bound theorem, the rightmost expression of Eq. (4.40) equals m_U, and hence it follows that $m_1^0 \geq m_U$, meaning that it is guaranteed to be an upper bound for a homogeneous, isotropic-elastic material.

A more general upper bound property can be derived for the multiplier m_2^0, defined by Eq. (4.28). The proof uses again the Schwarz inequality, this time with the linear operator $\int_{V_T} \frac{1}{E_s} \ldots dV$, with the requirement $0 < \frac{1}{E_S} < \infty$, which is always satisfied in practical numerical applications. The Schwarz inequality becomes

$$\sqrt{\int_{V_T}\frac{1}{E_S}\sigma_{eq}^2\,dV}\sqrt{\int_{V_T}\frac{1}{E_S}1^2\,dV}\geq\int_{V_T}\frac{1}{E_S}\sigma_{eq}\cdot 1\,dV\quad\Leftrightarrow\quad\sqrt{\int_{V_T}\frac{1}{E_S}1^2\,dV}\geq\frac{\int_{V_T}\frac{1}{E_S}\sigma_{eq}\,dV}{\sqrt{\int_{V_T}\frac{1}{E_S}\sigma_{eq}^2\,dV}} \qquad (4.41)$$

Again, substituting the right expression in Eq. (4.41) into Eq. (4.28) gives

$$m_2^0=\frac{\sigma_y\sqrt{\int_{V_T}\frac{1}{E_S}\,dV}}{\sqrt{\int_{V_T}\frac{1}{E_S}\sigma_{eq}^2\,dV}}\geq\frac{\sigma_y\int_{V_T}\frac{1}{E_S}\sigma_{eq}\,dV}{\int_{V_T}\frac{1}{E_S}\sigma_{eq}^2\,dV}=\frac{\sigma_y\int_{V_T}\varepsilon_{eq}\,dV}{\int_{V_T}\sigma_{eq}\varepsilon_{eq}\,dV} \qquad (4.42)$$

In this inequality, the possibility of an inhomogeneous material has been considered (that is, E_S can be a function of the location in the material). Therefore, assuming isotropic-elastic behaviour, Eq. (4.42) gives rise to the inequality $m_2^0\geq m_U$, meaning that m_2^0 is guaranteed to be an upper bound for any inhomogeneous, isotropic-elastic material.

4.5.2 Estimation of Bounds on m_α

m_α can be written in terms of m^0 and m_L as

$$m_\alpha=2m^0\frac{2\left(\frac{m^0}{m_L}\right)^2+\sqrt{\frac{m^0}{m_L}\left(\frac{m^0}{m_L}-1\right)^2\left(1+\sqrt{2}-\frac{m^0}{m_L}\right)\left(\frac{m^0}{m_L}-1+\sqrt{2}\right)}}{\left(\left(\frac{m^0}{m_L}\right)^2+2-\sqrt{5}\right)\left(\left(\frac{m^0}{m_L}\right)^2+2+\sqrt{5}\right)} \qquad (4.43)$$

For the following considerations, it is convenient to rewrite the solution for m_α in terms of the normalized multipliers that were introduced earlier, i.e., with $R_\alpha = \frac{m_\alpha}{m}$

$$R_\alpha = 2R_0 \frac{2\left(\frac{R_0}{R_L}\right)^2 + \sqrt{\frac{R_0}{R_L}\left(\frac{R_0}{R_L}-1\right)^2\left(1+\sqrt{2}-\frac{R_0}{R_L}\right)\left(\frac{R_0}{R_L}-1+\sqrt{2}\right)}}{\left(\left(\frac{R_0}{R_L}\right)^2+2-\sqrt{5}\right)\left(\left(\frac{R_0}{R_L}\right)^2+2+\sqrt{5}\right)} \qquad (4.44)$$

Due to the normalization, it is clear that $R_\alpha < 1$ means that m_α is effectively a lower bound, whereas $R_\alpha > 1$ denotes an upper bound. The above equation describes R_α as a function of two variables, and it is therefore possible to represent the boundary between the upper and lower bound regions as a line in two-dimensional space. This is done in Figure 4.13, which represents a section through the R_α surface at $R_\alpha = 1$ as a function of R_0 and R_0 / R_L. In the region below the line $R_\alpha = 1$, m_α is a lower bound, and above it is not. Since the normalizing factor m is unknown, a known combination of m^0 and m_L is a vertical line in R_0 versus R_0 / R_L space that connects the point where $R_0 = 1$ ($m = m^0$) to the point where $R_0 = R_0 / R_L$ ($m = m_L$). In other words, the line denotes the allowed range of m, which is between the upper bound m^0 and the lower bound m_L. The lower part of this line lies in the region where $R_\alpha \leq 1$ and the rest in the region where $R_\alpha > 1$. The length of the respective segments is a measure of the likelihood of whether or not R_α is a lower bound. Note that the m_α multiplier is guaranteed to be above the lower bound multiplier m_L.

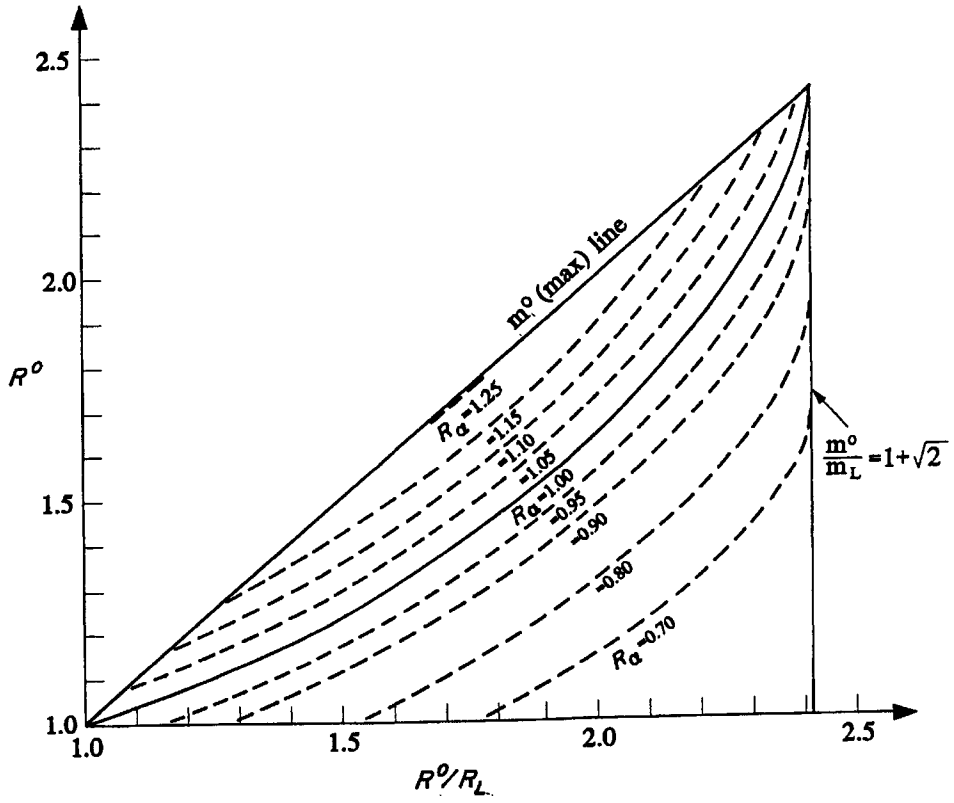

Figure 4.13 Region of lower and upper boundedness of m_α

The use of the diagram is envisioned as follows:

- From the FE model that gives the stress and strain distributions in the body, get the ratio R_0 / R_L (which equals the ratio m^0/m_L).

- Plot a vertical line in Figure 4.13 at the given R_0 / R_L.

- Since m is unknown, R_0 could theoretically have any value between 1 and R_0 / R_L as indicated by the length of the vertical line. Generally, the 45-degree line in Figure 4.13 indicates the maximum value of R_0. The admissible region (domain) for R_0 thus lies between the horizontal axis and the 45-degree line.

- The portion of the vertical line that lies below the line $R_\alpha = 1$ is the range of possible values R_0 for which m_α is a lower bound. It can be seen that this region is large when the ratio R_0 / R_L is high. This is desirable in the sense that the probability that m_α is a lower bound is high, but at the same time indicates that the true value m is likely underestimated by m_α. When R_0 / R_L is close to 1, the likelihood of overestimating m with m_α is relatively high, but the amount by which it may be overestimated is low because the bounds are good. Figure 4.13 shows a curve ($R_\alpha = 1.05$) for which m_α could be 5% on the upper bound side, which may be considered as acceptable within engineering accuracy. Another interpretation would be that $\frac{m_\alpha}{1.05} \leq m$. If this line is adopted as the limit, it is seen that the region in which m_α gives acceptable estimates of the limit load is quite large.

In practice, the m_α estimate for the initial iterations turns out to be a lower bound in the great majority of cases. Lower bound solutions are obtained if the quality of the upper and lower bounds entering Eq. (4.43) is roughly the same. Lower bound m_α estimates may not be obtained if a lower bound multiplier of very good quality is obtained while the upper bound multiplier is not so close to m. Clearly, the mesh sizes should be such that peak stresses are predicted accurately so that m_L and, therefore m_α is estimated properly. Coarse meshes tend to underestimate the peak stress and overestimate m_α.

4.5.3 Examples

Figure 4.14 is a plot of R_0 versus R_0 / R_L (i.e. m^0 / m_L) for some practical examples, shown as an iteration-by-iteration "trajectory". For the examples the limit multiplier m is known analytically or from an inelastic analysis, so that the normalized multiplier $R_0 = m_2^0 / m$ can be calculated.

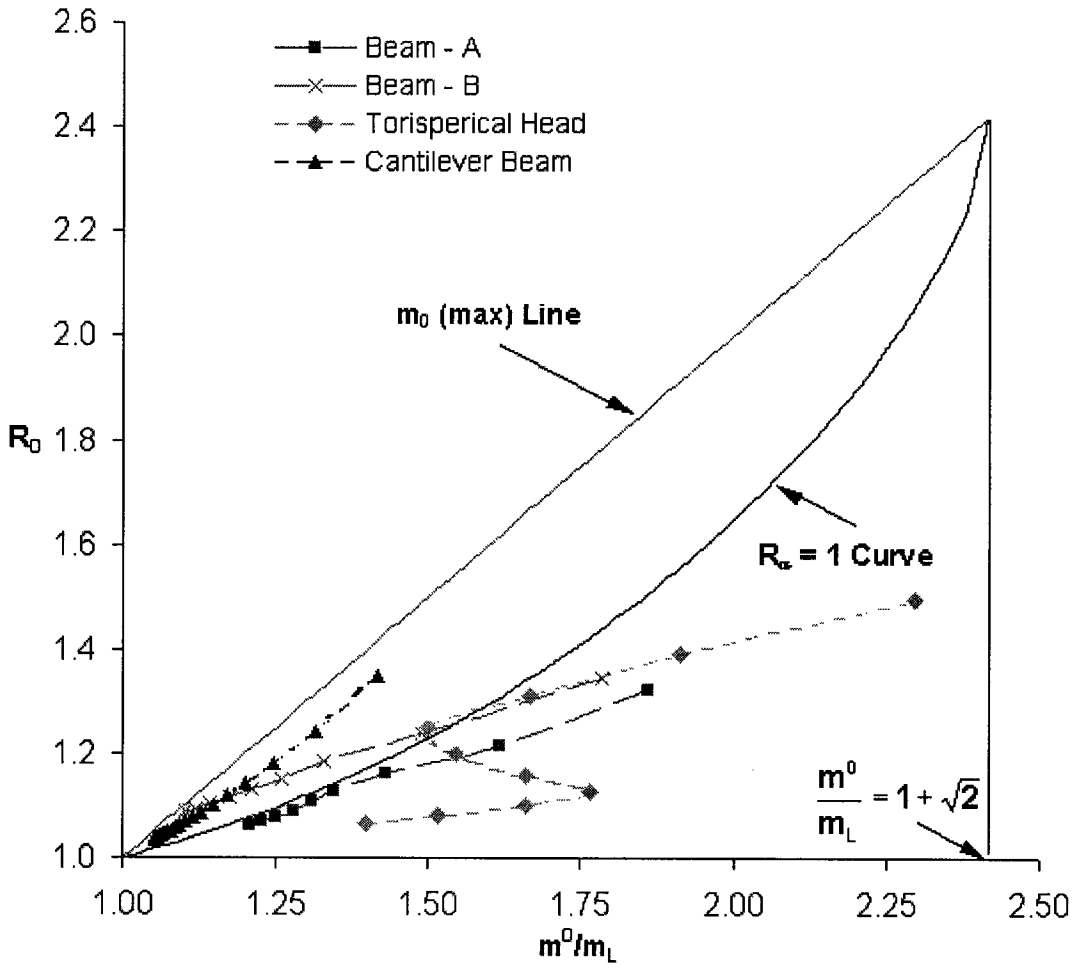

Figure 4.14 m_α trajectory for a simply supported beam, cantilever beam and a torispherical head

The first example is a beam that is built-in on one end and simply supported at the other, and subject to a uniformly distributed shear load (Figure 4.3). The length-to-height ratio of the beam is 20:1, and plane stress is assumed (unit width). Beam A is meshed with a FE mesh of 14 divisions through the thickness and 200 divisions along the length, while beam B has only 8 divisions through the thickness and 100 divisions along the length. It can be seen that the R_α trajectory for beam B crosses into the upper bound region for smaller R_0 / R_L ending up at $R_\alpha = 1.05$. However, the R_α trajectory of beam A is always in the lower bound region. In practical situations, one assigns a mesh size a priori not knowing the inelastic results. Clearly, coarse mesh sizes will overestimate m_α.

The second example is the torispherical head on a cylindrical shell (Figure 4.7) loaded by a uniform internal pressure. The R_α trajectory for the torispherical head is also plotted in Figure 4.14. The trajectory essentially remains in the lower bound region.

Finally, a cantilever beam under uniform load is examined. The length-to-height ratio of the beam is again 20:1, and plane stress is assumed (unit width). Figure 4.14 shows that the R_α trajectory starts at slightly less than 15% above the limit multiplier and remains in the upper bound region at all time. The reason for this behaviour is that the lower bound improves sharply after the first iteration, while the upper bound improves more gradually. Theoretically, the lower bound would be exact because the modulus adjustment formula transforms the linear bending stress distribution into the corresponding limit stress distribution after one iteration. The upper bound depends on the complete stress distribution in the structure and thus requires more time to converge.

This case represents the most severe test for the usefulness of m_α as an estimate of the limit load multiplier. But the problem can be spotted immediately by comparing the convergence of the upper and lower bounds with increasing iterations, even if the exact limit multiplier is not known (as it is the case in real-world problems).

4.5.4 Conclusions

The bounds on the multipliers m^0, m' and m_α have been discussed. It is found that m^0, Eq. (4.28), is greater than the classical upper bound multiplier and m' is lower than the classical lower bound multiplier. m_α multiplier tends to underestimate the limit load, i.e. it is usually on the safe side. The maximum theoretical amount by which the limit load could be overestimated is 25%. The worst actual overestimation in a specially constructed example was found to be below 15%. The indicator for such high estimates is a very rapidly converging lower bound in conjunction with an upper bound that is still improving. This scenario is easily detected, and is typically avoided in more complicated "real-world" structures, for which m_α generally results in lower bound estimates. For example, the value of R_0 / R_L is high for components with cracks, sharp notches or sudden geometric transitions for which the probability of lower bound is therefore very high.

In all limit load estimations, whether inelastic, repeated elastic or using bounds, proper mesh refinement is very important. Finite element meshes that are too coarse can yield "lower bound" estimates that are significantly above the true limit load. In cases of doubt, a mesh refinement study is highly recommended.

Chapter 5 Collapse Load Estimation for Layered Structures

5.1 Introduction

Layered structures are well known for their superior performance, such as the strength-to-weight and strength-to-cost characteristics, and have found widespread use in industry. The knowledge of limit load for these structures is often germane to the design process. As a result, there is a need to extend the robust methods to these structures to deal with the inhomogeneity.

In this chapter, the m_α - multiplier method modified by the introduction of the "plastic flow parameter" μ^0, is extended to layered structures. Suitable initial elastic properties are suggested; a systematic modulus adjustment scheme is proposed; and the derivations of the multipliers are presented. The procedure is applied to several layered cylinders and beams, and the estimations are compared with those obtained by the elastic compensation method and analytical methods.

5.2 Theory and Formulation

5.2.1 Modulus Adjustment Scheme

In the current investigation, it is assumed that each layer is homogeneous, isotropic and elastic perfectly-plastic. The modulus adjustment scheme is specified as:

$$E_i' = \left(\frac{\sigma_{yi}}{\sigma_{ei}}\right) E_i \qquad (5.1)$$

where E_i' is the modified modulus for element in i-th layer, E_i is the modulus for element in i-th layer in the prior iteration, σ_{yi} is the yield stress of i-th layer, σ_{ei} is the equivalent stress for a element in i-th layer. The use of yield stress as arbitrary stress in the numerator of Eq. (5.1) is to ensure that the moduli of elements within the respective layer are adjusted according to their load-carrying capacities at the limit state.

5.2.2 Modified Initial Elastic Parameters for Repeated Linear Elastic FEA

5.2.2.1 Modulus of Elasticity

For layered structures, the stiffness difference at the layer interface determines the load transfer between layers. At the interface between two plastically deformed layers, the stiffness ratio between the layers should become the ratio of the yield stress to correctly represent the stress state at collapse. This can be explained by considering two neighboring elements at different sides of the layer interface (Figure 5.1). Element 1 is in layer 1 and element 2 is in layer 2. Making use of effective stress-strain relationship, we have

$$\varepsilon_{e1} = \frac{\sigma_{e1}}{E_{S1}} \qquad \varepsilon_{e2} = \frac{\sigma_{e2}}{E_{S2}} \tag{5.2}$$

where σ_e is effective stress, ε_e is effective strain and E_S is secant modulus. Since the two elements are small and adjacent, it is reasonable to have

$$\varepsilon_{e1} = \varepsilon_{e2} \tag{5.3}$$

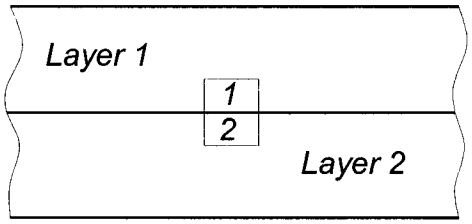

Figure 5.1 Two adjacent elements at the layer interface

At the limit state, both elements are yielded

$$\frac{\sigma_{e1}}{\sigma_{e2}} = \frac{\sigma_{y1}}{\sigma_{y2}} \tag{5.4}$$

Therefore, we have

$$\frac{E_{S1}}{E_{S2}} = \frac{\sigma_{y1}}{\sigma_{y2}} \tag{5.5}$$

In the above equation, the ratio of secant modulus is equal to the ratio of yield stress.

Taking a two-layered structure for example, the following ratios can be defined, i.e.,

$$\alpha = \frac{E_1}{E_2}, \qquad \beta = \frac{\sigma_{y1}}{\sigma_{y2}} \tag{5.6}$$

where α is the ratio of original modulus of elasticity and β is the ratio of yield stress between layers. Depending on original material properties, sometimes α is close to β, and sometimes α is far from β (such as $\alpha = 3$ and $\beta = 0.333$). If we start the repeated linear elastic analyses with an α value far from β, it may take many iterations to reach the limit state, or the iteration may reach certain states other than limit state, since the analysis starts with an unrealistic load-sharing situation.

Therefore, we suggest use the value of β for α in the first iteration. That is, $E_1 = K\sigma_{y1}$ for all elements in layer 1, and $E_2 = K\sigma_{y2}$ for all elements in layer 2, where K is a constant, such as 1000. Then the load transfer at the layer interface will easily converge to limit type.

The above-mentioned scheme can also be explained in another fashion. The limit state is essentially load-controlled, implying satisfaction of equilibrium with externally applied tractions. As such the ratio of yield stresses reflect the relative load carrying capacities of the respective layers. Since the ratio of modulus of elasticity is used in the algorithm, represented by α, then $\alpha = \beta$ constitutes a valid choice for the purpose of load carrying capacity assessments. This should rapidly lead to a realistic limit state load carrying capacity for each layer.

5.2.2.2 Poisson's Ratio

For layered structures at the point of plastic collapse, the material interfaces are locations where significant plastic deformation can occur. Therefore, Poisson's ratios close to 0.5 (such as 0.47) are specified as initial elastic properties in order to simulate the actual interaction between the layers at the limit state. It is found that the modulus adjustment scheme of Eq. (5.1) and a choice of Poisson's ratio close to 0.5 lead to stress distributions close to limit distribution after some number of iterations. In some cases, however, as many as ten iterations are required in order to approach the limit state closely.

5.2.3 Determination of m^0 Using the Plastic Flow Parameter

The concept of plastic flow parameter, introduced in the previous chapter, is used for the determination of m^0 multiplier for layered structures. In each linear elastic finite element analysis (LEFEA) iteration, it is postulated that the plastic flow parameter μ^0 can be considered as a function of the secant modulus of every element in a LEFEA scheme, i.e.

$$\mu^0 = \frac{C}{E_S} \qquad (5.7)$$

where C is a constant, and E_S is secant modulus of an element within the layered structure. The μ^0 evaluation makes the determination of multipliers for layered structures possible.

For two-layered structure, for example, the "integral mean of yield" criterion can be expressed as:

$$\int_{V1} \mu_1{}^0 [f_1(s_{ij}^0) + (\varphi_1{}^0)^2] dV + \int_{V2} \mu_2{}^0 [f_2(s_{ij}^0) + (\varphi_2{}^0)^2] dV = 0 \qquad (5.8)$$

Substituting the yield function into Eq. (5.8) and recognizing that $s_{ij}^0 = m^0 \tilde{s}_{ij}$, we get

$$\int_{V1} \mu_1{}^0 [\frac{1}{2}(m^0)^2 \tilde{s}_{ij}^0 \tilde{s}_{ij}^0 - k_1{}^2 + (\varphi_1{}^0)^2] dV + \int_{V2} \mu_2{}^0 [\frac{1}{2}(m^0)^2 \tilde{s}_{ij}^0 \tilde{s}_{ij}^0 - k_2{}^2 + (\varphi_2{}^0)^2] dV = 0 \qquad (5.9)$$

Expressing Eq. (5.9) in terms of effective stresses and yield stresses, we get

$$\int_{V1} \frac{\mu_1^0}{3} [\{(m^0)^2 (\sigma_e^0)^2 - \sigma_{y1}^2\} + 3(\varphi_1{}^0)^2] dV$$

$$+ \int_{V2} \frac{\mu_2^0}{3} [\{(m^0)^2 (\sigma_e^0)^2 - \sigma_{y2}^2\} + 3(\varphi_2{}^0)^2] dV = 0 \qquad (5.10)$$

Rearranging Eq. (5.10) and specifying $\varphi_1{}^0 = 0$ and $\varphi_2{}^0 = 0$ (See Section 4.3.1), the multiplier m^0 is found to be

$$m^0 = \left[\frac{\sigma_{y1}^2 \int_{V1} \mu_1^0 dV + \sigma_{y2}^2 \int_{V2} \mu_2^0 dV}{\int_{V1} \mu_1^0 (\sigma_e^0)^2 dV + \int_{V2} \mu_2^0 (\sigma_e^0)^2 dV} \right]^{1/2} \qquad (5.11)$$

where $\mu_1{}^0$ and $\mu_2{}^0$ can be calculated using Eq. (5.7) within respective layers. The constant C can be eliminated during the algebraic manipulations.

For an N-layered structure, the expression becomes

$$m^0 = \left[\frac{\sum_{i=1}^{N} \sigma_{yi}^2 \int_{Vi} \mu_i^0 dV}{\sum_{i=1}^{N} \int_{Vi} \mu_i^0 \left(\sigma_e^0\right)^2 dV} \right]^{1/2} \qquad (5.12)$$

5.2.4 Evaluation of m' and m_α

For two-layered structures, the inequality involving m^0 and m can be expressed as

$$m^0 \le m + \frac{\max[f_1(s_{ij}^0) + (\varphi_1{}^0)^2]}{2k_1^2} 2k_1^2 \int_{V1} \mu_1 dV + \frac{\max[f_2(s_{ij}^0) + (\varphi_2{}^0)^2]}{2k_2^2} 2k_2^2 \int_{V2} \mu_2 dV$$

$$\text{or} \qquad m^0 \le m + \alpha_1 \left(2k_1^2 \int_{V1} \mu_1 dV \right) + \alpha_2 \left(2k_2^2 \int_{V2} \mu_2 dV \right) \qquad (5.13)$$

where $\alpha_i = \dfrac{\max[f_i(s_{ij}^0) + (\varphi_i^0)^2]}{2k_i^2}$ for $i = 1,2$.

Stipulating α_{max} as the larger of α_1 and α_2, the following inequality holds:

$$m^0 \le m + \alpha_{\max} \left(2k_1^2 \int_{V1} \mu_1 dV + 2k_2^2 \int_{V2} \mu_2 dV \right) \qquad (5.14)$$

For the two layered structures, we also have

$$m = 2k_1^2 \int_{V1} \mu_1 dV + 2k_2^2 \int_{V2} \mu_2 dV \qquad (5.15)$$

Extending the concept to N-layered structures, Eqs. (5.14) and (5.15) can be generalized as

$$m^0 \le m + \alpha_{\max}\left(\sum_{i=1}^{N} 2k_i^2 \int_{Vi} \mu_i dV\right) \tag{5.16}$$

$$\text{and} \quad m = \sum_{i=1}^{N}\left(2k_i^2 \int_{Vi} \mu_i dV\right) \tag{5.17}$$

Substituting Eq. (5.17) into Eq (5.16), the lower bound multiplier is found to be

$$m' = \frac{m^0}{1+\alpha_{\max}} = \frac{2m^0}{1+(m^0)^2(\bar{\sigma}_M^0)^2} \le m \tag{5.18}$$

where $\bar{\sigma}_M^{\,0} = (\sigma_e)_{max}/\sigma_y$ is chosen as the largest value of $\bar{\sigma}_{Mi}^{\,0}$ from all layers, and $\bar{\sigma}_{Mi}^{\,0}$ $= (\sigma_e)_{i\text{-}max}/\sigma_{yi}$, where i refers to the layer number.

Equation (5.18) has the same form for a structure made from single isotropic material, Eq. (3.55). Therefore, the m_α evaluation for the layered structures becomes similar to that for single material structures.

5.3 Applications

The aforementioned procedure is applied to two types of configurations: two-layered structures and three-layered structures. All the components are analyzed using the ANSYS finite element program (ANSYS, 1998) with four-noded isoparametric quadrilateral elements. Multipliers m^0, m', and m_α are calculated automatically with macros written in ANSYS APDL language.

The multipliers predicted by various methods versus iteration are plotted in the subsequent figures. In the legends, the words "m^0," "m'," "m_α" stand for the multipliers obtained from the modified m_α - formulation. "ECM-LB" is the lower bound multiplier from elastic compensation method, while "m" stands for the exact multiplier obtained from analytical methods.

5.3.1 Two-Layered Structures

In the current investigation, the two-layered structures include two-layered cylinders under internal pressure and two-layered beams under uniformly distributed load (Figure 5.2). The multipliers calculated by various methods are plotted in Figure 5.3 to Figure 5.10 for the two-layered cylinders, and in Figure 5.12 to Figure 5.19 for the two-layered beams.

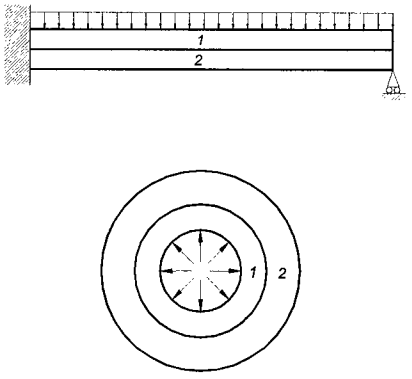

Figure 5.2 Two-layered beam and two-layered cylinder

5.3.1.1 Two-Layered Cylinders under Internal Pressure

The two-layered cylinder is modeled under axial plane strain condition with a uniform pressure applied at the inside surface. To test the applicability of the m_α procedure, two geometric configurations and four material combinations are used. Therefore, a total of eight cases have been analyzed.

In the first geometric configuration, the inner radius of the cylinder is 80 mm and the outer radius is 230 mm, with the interface radius at 130 mm. In the second geometric configuration, the inner radius of the cylinder is 100 mm and the outer radius is 300 mm, with the interface radius at 200 mm.

For the four material combinations, four yield stress ratios of β = 1/3, 3, 1/6, 6 are used, with material 1 for inside layer and material 2 for outside layer. The yield stress combinations are 70 MPa with 210 MPa, and 70 MPa with 420 MPa. The initial Young's modulus combinations are 70 GPa with 210 GPa, and 70 GPa with 420 GPa.

Poisson's ratios for both layers are 0.3, but a modified value of 0.47 is used for as the initial property. An internal pressure of 500 MPa is applied for all cases. The variation of multipliers predicted by various methods versus iteration for all the cases are plotted in Figure 5.3 to Figure 5.10.

The exact multiplier m is evaluated analytically as follows:

Equilibrium equation for plane axisymmetric problem is

$$\frac{d\sigma_r}{dr} + \frac{\sigma_r - \sigma_\theta}{r} = 0 \qquad (5.19)$$

The conditions of plane strain and Poisson's ratio of 0.5 give

$$\sigma_z = 0.5(\sigma_r + \sigma_\theta) \qquad (5.20)$$

Substituting Eq. (5.20) into von-Mises yield criterion yields

$$\sigma_\theta - \sigma_r = \frac{2}{\sqrt{3}}\sigma_y \qquad (5.21)$$

Substituting Eq. (5.21) back into equilibrium equation, we get

$$\frac{d\sigma_r}{dr} = \frac{2}{\sqrt{3}}\sigma_y \qquad (5.22)$$

Integrating Eq. (5.22), we have

$$\sigma_r = \frac{2}{\sqrt{3}}\sigma_y \ln r + C \qquad (5.23)$$

Applying boundary conditions of each layer to Eq. (5.23) and simplifying, the limit pressure is found to be

$$P_L = \frac{2}{\sqrt{3}}(\sigma_{y1} \ln\frac{r_{\text{int}}}{r_i} + \sigma_{y2} \ln\frac{r_0}{r_{\text{int}}}) \qquad (5.24)$$

where r_i is the inner radius, r_o is the outer radius and r_{int} is the radius of the interface.

For the first geometric configuration of r_i = 80 mm, r_o = 230 mm, r_{int} = 130 mm, with σ_{y1} = 70 MPa and σ_{y2} = 210 MPa, the limit pressure is

$$P_L = \frac{2}{\sqrt{3}}(70\ln\frac{130}{80} + 210\ln\frac{230}{130}) = 177.9MPa \qquad (5.25)$$

The exact multiplier m is

$$m = \frac{177.9MPa}{500MPa} = 0.356 \qquad (5.26)$$

The exact multipliers for the other cases are evaluated in the same fashion.

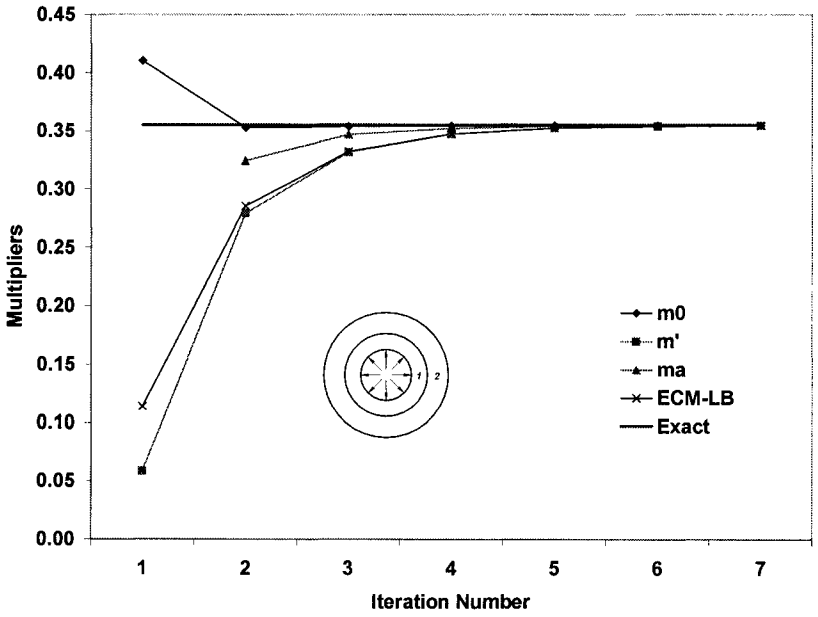

Figure 5.3 First geometric configuration (σ_{y1} = 70 MPa and σ_{y2} = 210 MPa, E_1 = 70 GPa and E_2 = 210 GPa)

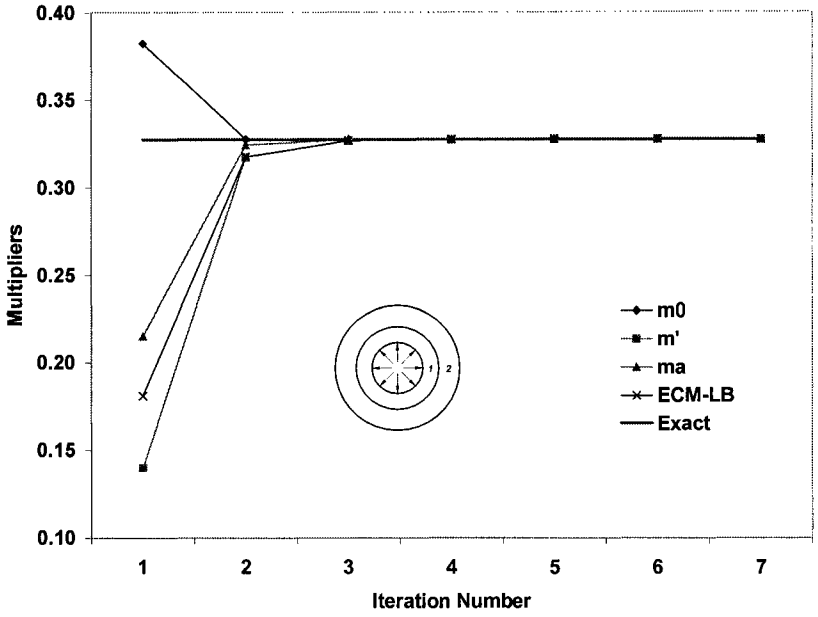

Figure 5.4 First geometric configuration (σ_{y1} = 210 MPa and σ_{y2} = 70 MPa, E_1 = 210 GPa and E_2 = 70 GPa)

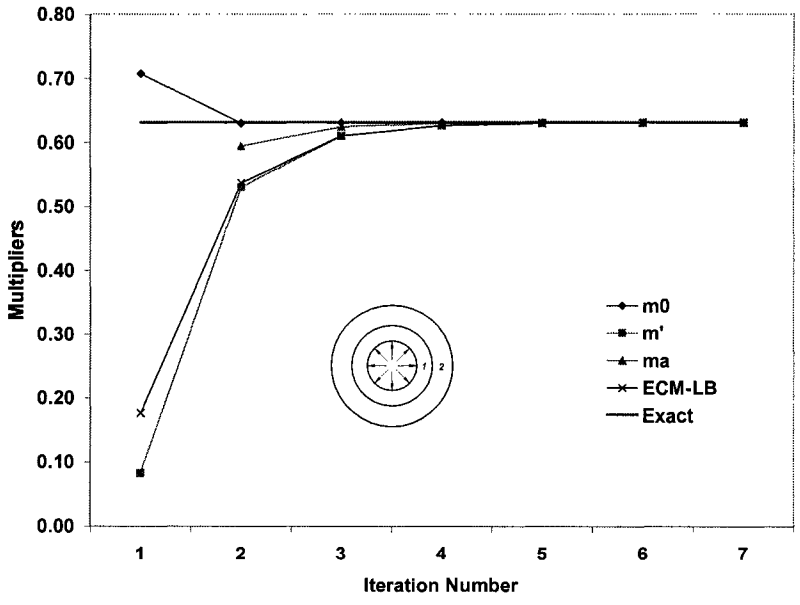

Figure 5.5 First geometric configuration (σ_{y1} = 70 MPa and σ_{y2} = 420 MPa, E_1 = 70 GPa and E_2 = 420 GPa)

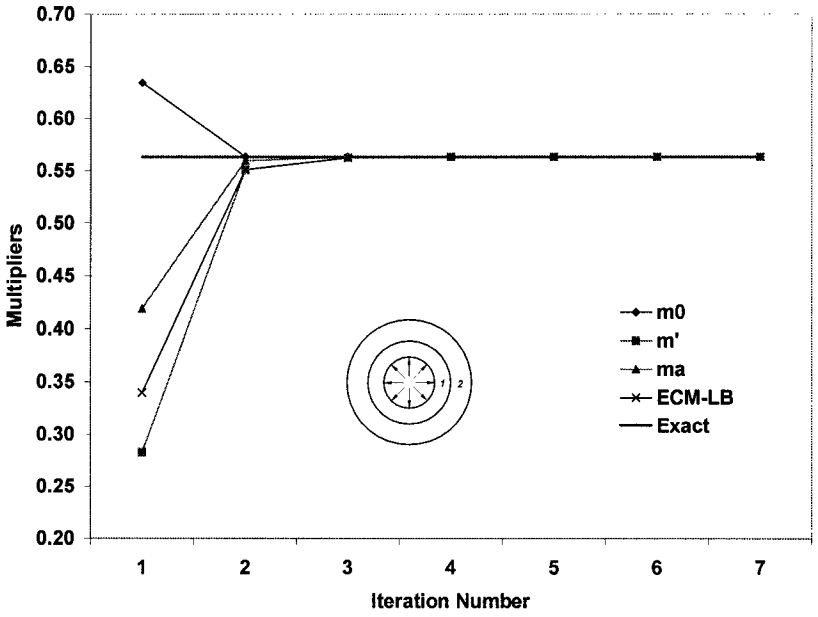

Figure 5.6 First geometric configuration (σ_{y1} = 420 MPa and σ_{y2} = 70 MPa, E_1 = 420 GPa and E_2 = 70 GPa)

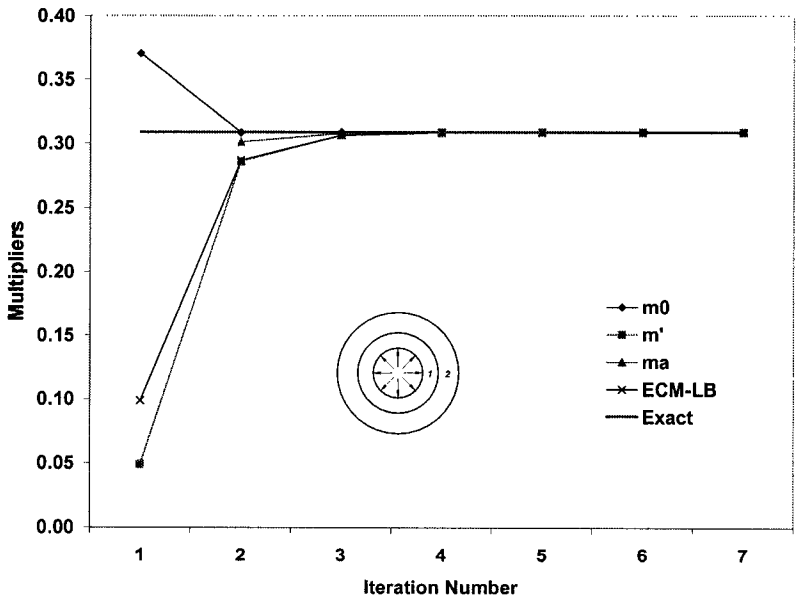

Figure 5.7 Second geometric configuration (σ_{y1} = 70 MPa and σ_{y2} = 210 MPa, E_1 = 70 GPa and E_2 = 210 GPa)

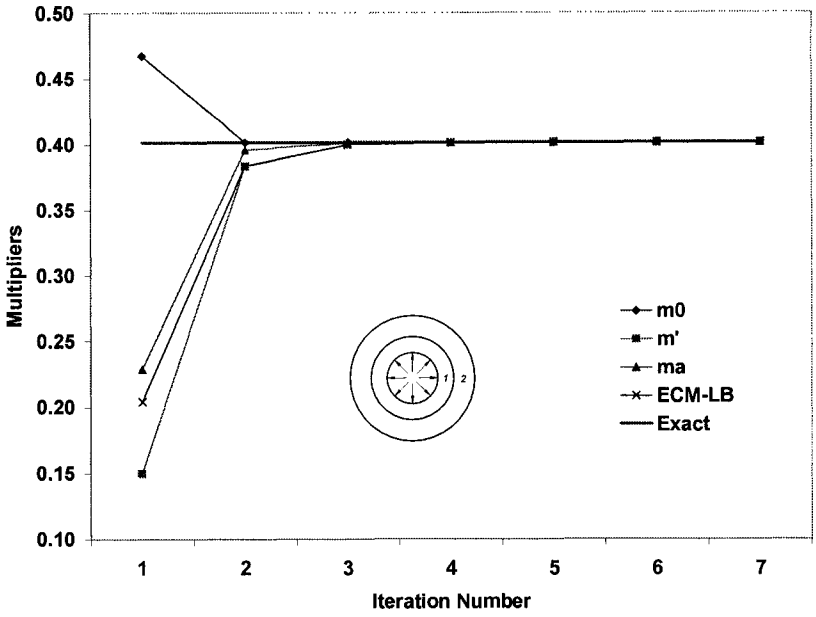

Figure 5.8 Second geometric configuration (σ_{y1} = 210 MPa and σ_{y2} = 70 MPa, E_1 = 210 GPa and E_2 = 70 GPa)

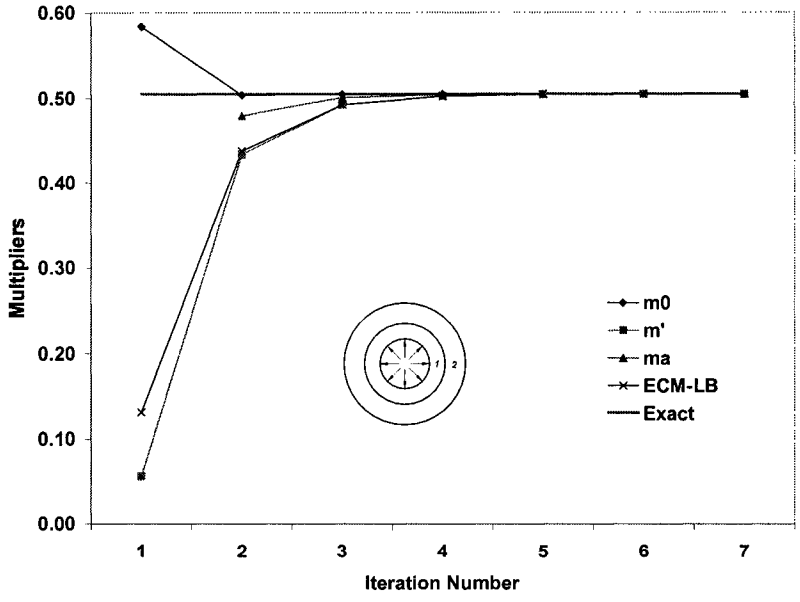

Figure 5.9 Second geometric configuration (σ_{y1} = 70 MPa and σ_{y2} = 420 MPa, E_1 = 70 GPa and E_2 = 420 GPa)

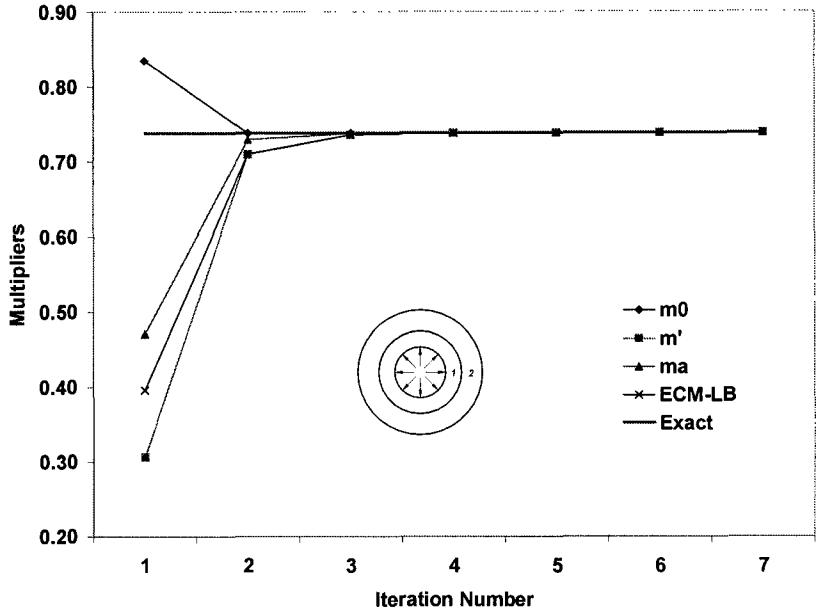

Figure 5.10 Second geometric configuration (σ_{y1} = 420 MPa and σ_{y2} = 70 MPa, E_1 = 420 GPa and E_2 = 70 GPa)

5.3.1.2 Two-Layered Beams under Uniformly Distributed Load

The two-layered beam is modeled under plane stress condition with one end clamped and the other simply-supported, while a uniformly distributed load is applied at top surface. The length of the beam is 500 mm and the height is 24 mm. Similar as in the case of the two-layered cylinder, two geometric configurations and four material combinations are used. Therefore, a total of eight cases have been analyzed.

In the first geometric configuration, the material interface is at half of the height, with both upper and lower layer of 12 mm high. In the second geometric configuration, the upper layered is 8 mm high and the lower layer is 16 mm high.

For the four material combinations, four yield stress ratios of β = 1/3, 3, 1/6, 6 are used, with material 1 for upper layer and material 2 for lower layer. The yield stress combinations are 70 MPa with 210 MPa, and 70 MPa with 420 MPa. The initial Young's modulus combinations are 70 GPa with 210 GPa, and 70 GPa with 420 GPa.

Poisson's ratios for both layers are 0.3, but a modified value of 0.47 is used for as the initial property. A uniformly distributed load of 1 MPa is applied for all the cases. The variation of multipliers predicted by various methods versus iteration for all the cases are plotted in Figure 5.12 to Figure 5.19. The best m_α values during iterations versus the exact multipliers for all the cases are listed in Table 5.1.

The exact multiplier m is obtained analytically as follows:

For the first geometric configuration of both layers of 12 mm with σ_{y1} = 70 MPa and σ_{y2} = 210 MPa, the stress distribution at a plastic hinge section is shown in Figure 5.11.

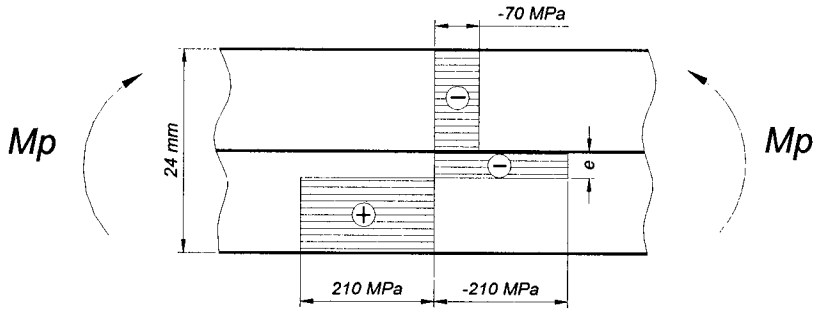

Figure 5.11 Stress distribution at plastic hinge for a two-layered beam

The section is under pure bending and the M_p is the plastic moment. Considering the equilibrium of forces at the hinge section, the height of compressive stress in the lower layer, e, is found to be 4 mm. Therefore the plastic moment is

$$M_p = (70 \times 12 \times 10) + (210 \times 4 \times 2) + (210 \times 8 \times 4) = 16800 \quad Nm/m \tag{5.27}$$

Using the classical solution of limit load for indeterminate beam (Mendelson, 1968),

$$q_{exact} = \frac{11.657 M_p}{L^2} \tag{5.28}$$

the exact limit load is

$$q_L = \frac{11.657 \times 16800}{0.5^2} = 783350 \quad Pa \tag{5.29}$$

Therefore, the exact multiplier is

$$m = \frac{0.783350 MPa}{1 MPa} = 0.78335 \tag{5.30}$$

For other cases, the exact multipliers can be evaluated in the same fashion.

Table 5.1 Best m_α value within iterations versus exact multiplier for two-layered beam

Geometric Configuration		Material Combination			
		σ_{y1} = 70 MPa σ_{y2} = 210 MPa	σ_{y1} = 210 MPa σ_{y2} = 70 MPa	σ_{y1} = 70 MPa σ_{y2} = 420 MPa	σ_{y1} = 420 MPa σ_{y2} = 70 MPa
Layer 1: 12 mm	m_α	0.76090	0.76553	1.15097	1.15421
Layer 2: 12 mm	Exact	0.78335	0.78335	1.15500	1.15500
Layer 1: 8 mm	m_α	0.91714	0.60358	1.53968	0.87726
Layer 2: 16 mm	Exact	0.92260	0.71372	1.55800	0.90520

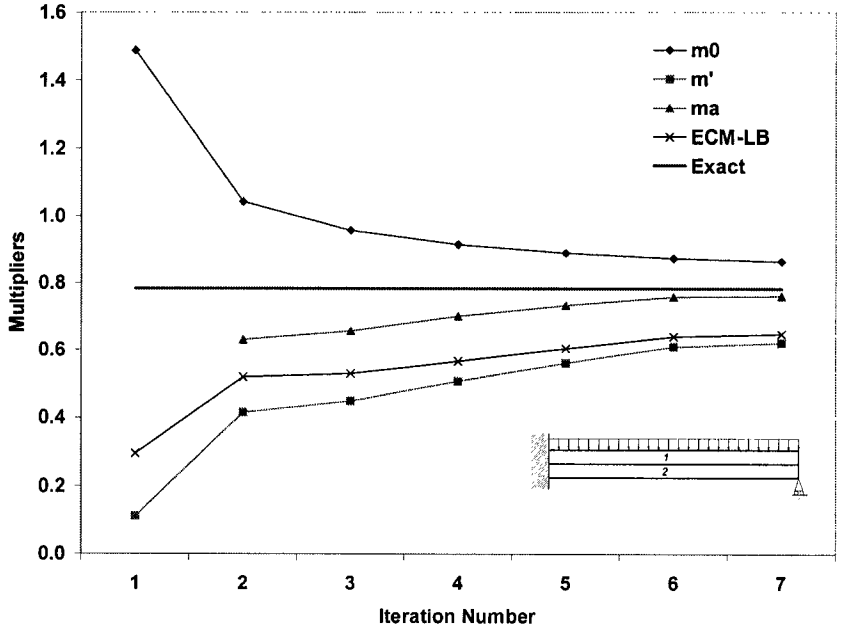

Figure 5.12 First geometric configuration (σ_{y1} = 70 MPa and σ_{y2} = 210 MPa, E_1 = 70 GPa and E_2 = 210 GPa)

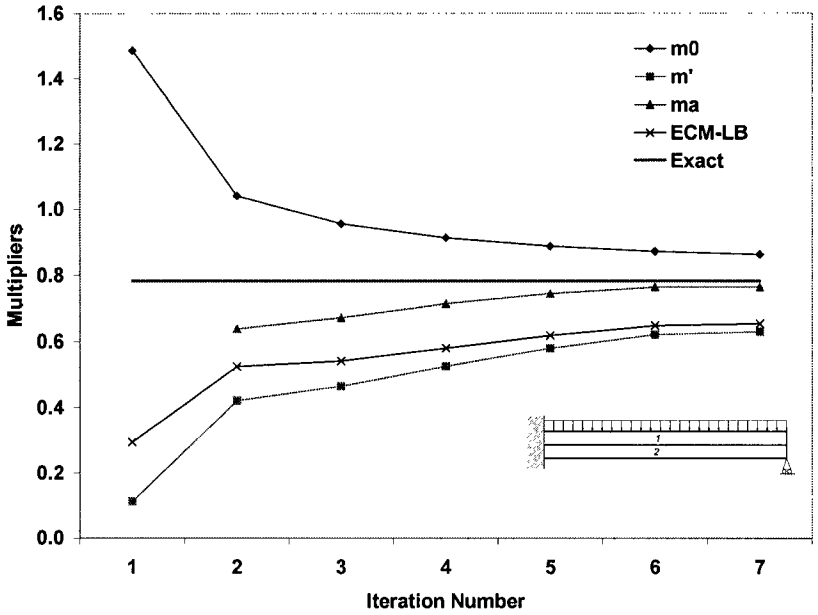

Figure 5.13 First geometric configuration (σ_{y1} = 210 MPa and σ_{y2} = 70 MPa, E_1 = 210 GPa and E_2 = 70 GPa)

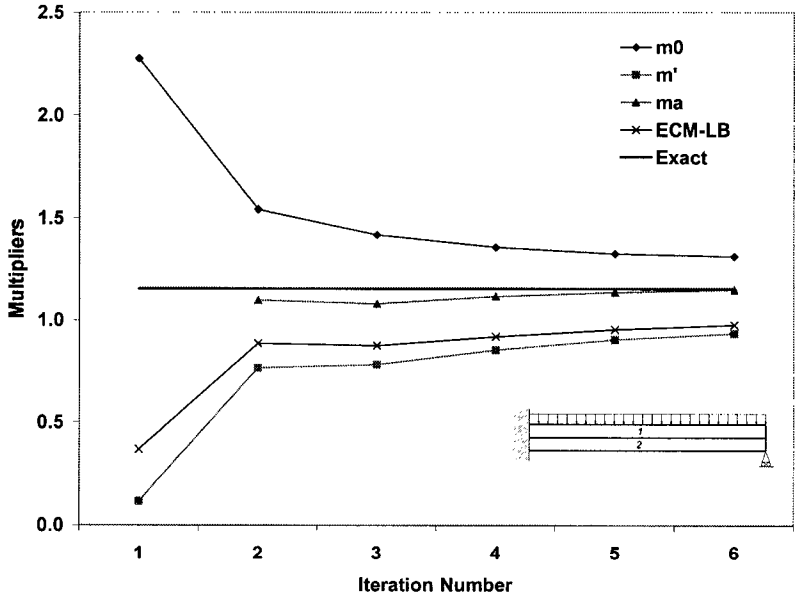

Figure 5.14 First geometric configuration (σ_{y1} = 70 MPa and σ_{y2} = 420 MPa, E_1 = 70 GPa and E_2 = 420 GPa)

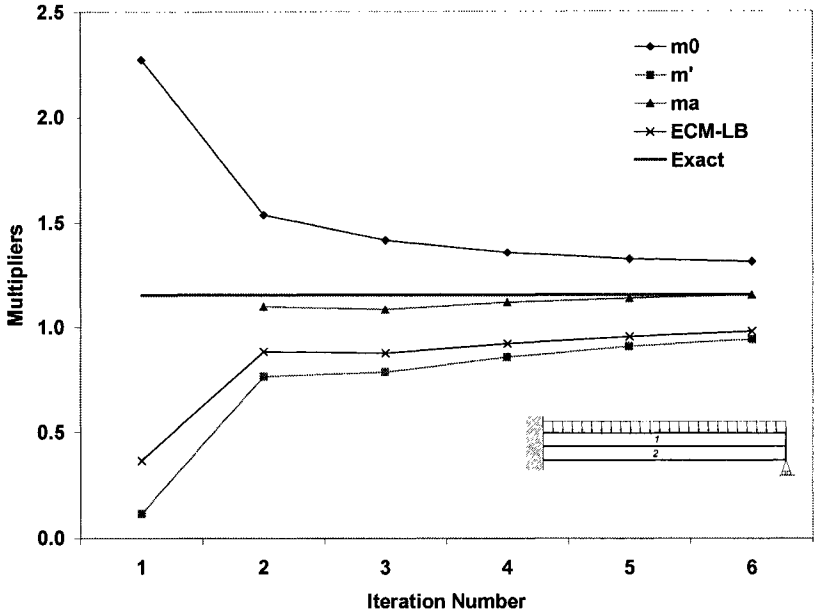

Figure 5.15 First geometric configuration (σ_{y1} = 420 MPa and σ_{y2} = 70 MPa, E_1 = 420 GPa and E_2 = 70 GPa)

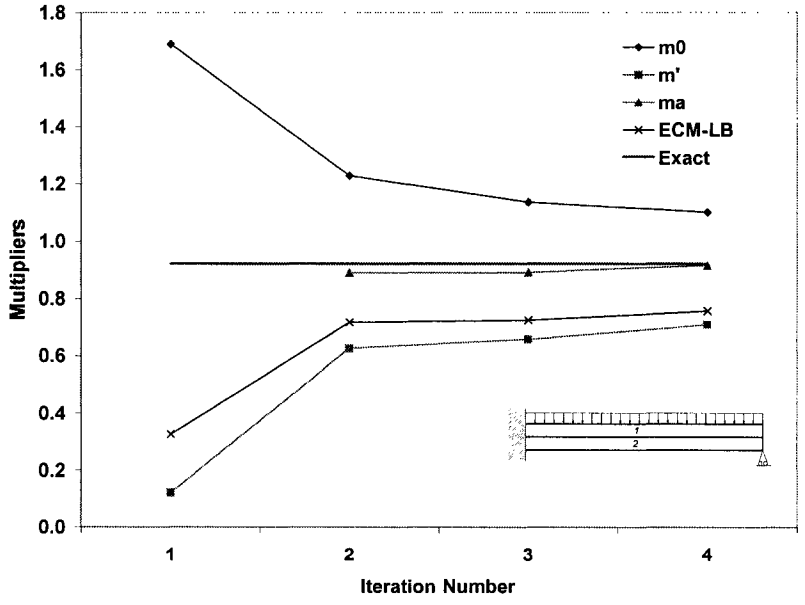

Figure 5.16 Second geometric configuration (σ_{y1} = 70 MPa and σ_{y2} = 210 MPa, E_1 = 70 GPa and E_2 = 210 GPa)

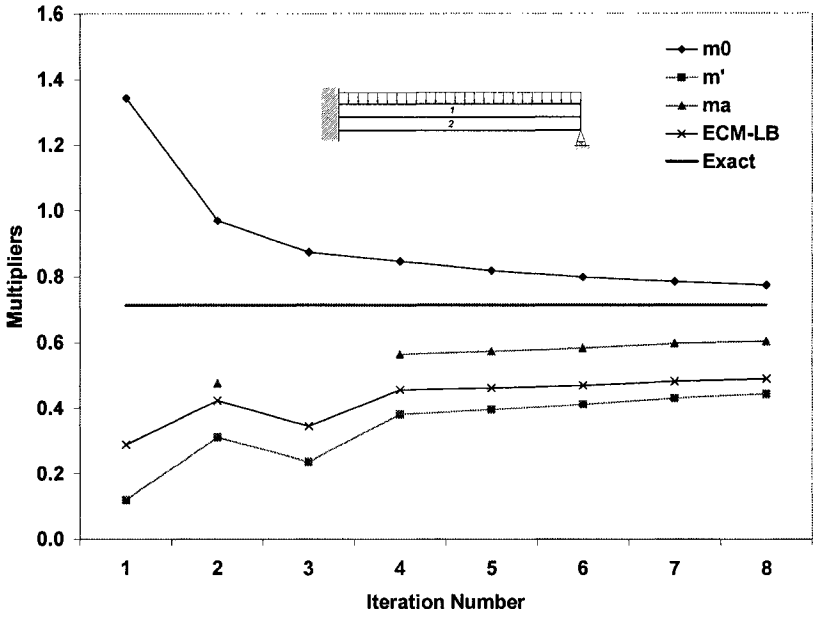

Figure 5.17 Second geometric configuration (σ_{y1} = 210 MPa and σ_{y2} = 70 MPa, E_1 = 210 GPa and E_2 = 70 GPa)

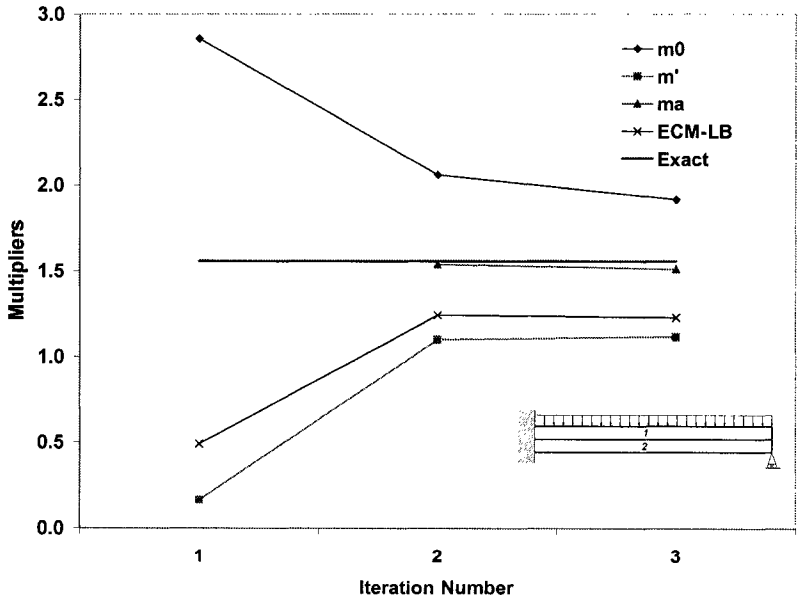

Figure 5.18 Second geometric configuration (σ_{y1} = 70 MPa and σ_{y2} = 420 MPa, E_1 = 70 GPa and E_2 = 420 GPa)

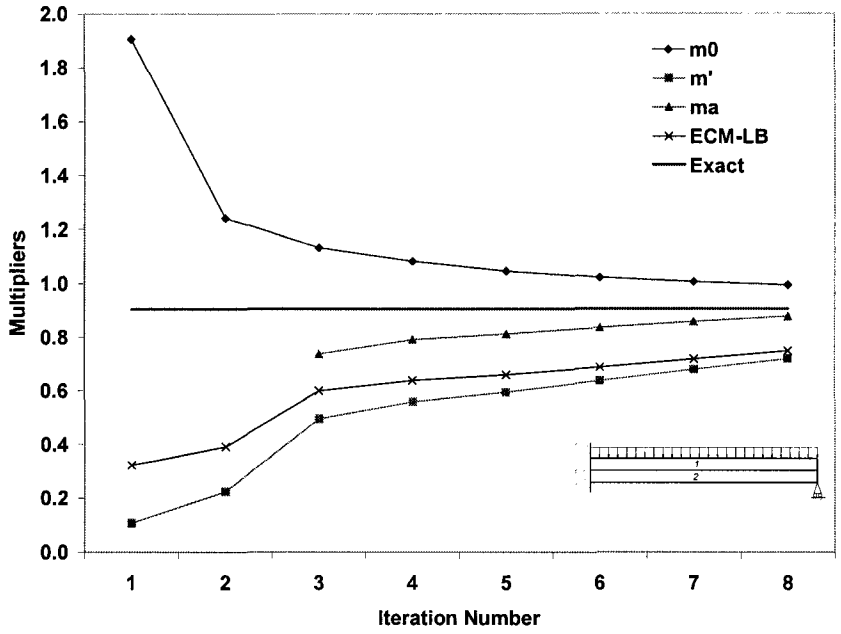

Figure 5.19 Second geometric configuration (σ_{y1} = 420 MPa and σ_{y2} = 70 MPa, E_1 = 420 GPa and E_2 = 70 GPa)

5.3.2 Three-Layered Structures

The examples for three-layered structures are three-layered cylinders under internal pressure and three-layered beams under uniformly distributed load (Figure 5.20).

The multipliers obtained by the modified m_α procedure are plotted in Figure 5.21 to Figure 5.24. The exact multipliers are obtained in the same fashion as those for two-layered structures.

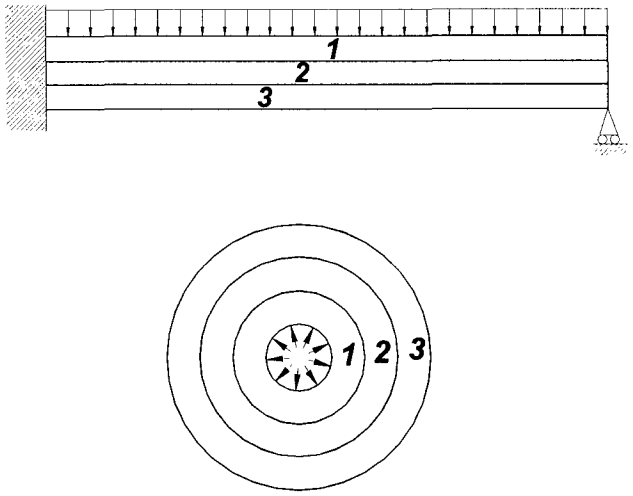

Figure 5.20 Three-layered beam and three-layered cylinder

5.3.2.1 Three-Layered Cylinders under Internal Pressure

The three-layered cylinder is modeled under axial plane strain condition with a uniform pressure applied at the inside surface. The inner radius is 80 mm, the outer radius is 320 mm, and the layer interface radii are 160 and 240 mm. Two cases have been studied. In the first case, the yield stresses from the inside layer to the outside layer are 210 MPa, 140 MPa and 70 MPa, respectively. In the second case, the yield stresses from the inside layer to the outside layer are 70 MPa, 140 MPa and 210 MPa, respectively. Poisson's ratio for all layers is 0.3, however, a modified value of 0.47 is specified initially. An internal pressure of 300 MPa is applied. The variations of multipliers predicted by various methods versus iteration are plotted in Figure 5.21 and Figure 5.22.

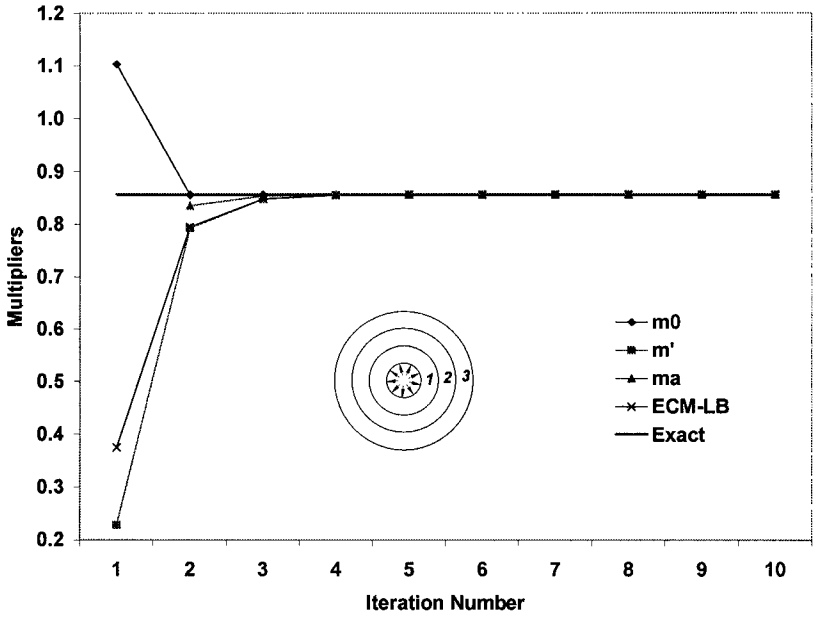

Figure 5.21 Three-layered cylinder (σ_{y1}, σ_{y2}, σ_{y3} = 210 MPa, 140 MPa, 70 MPa; E_1, E_2, E_3 = 210 GPa, 140 GPa, 70 GPa)

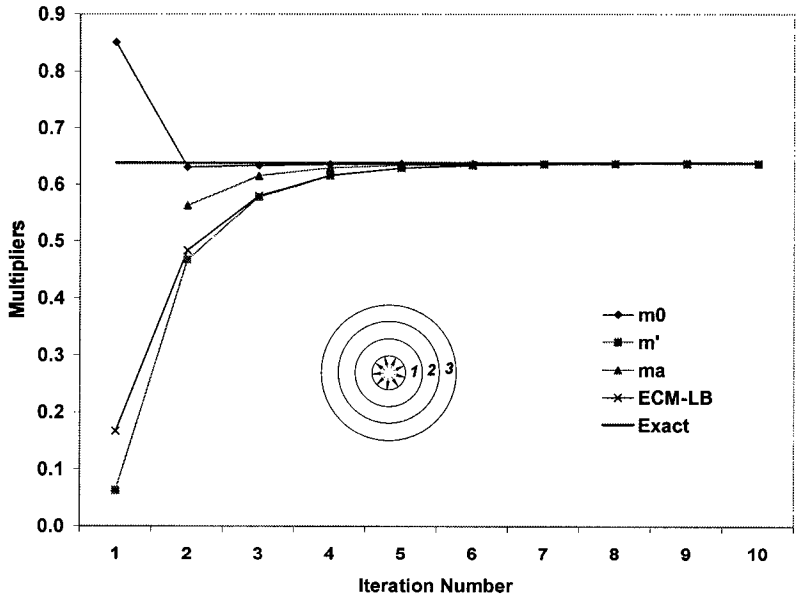

Figure 5.22 Three-layered cylinder (σ_{y1}, σ_{y2}, σ_{y3} = 70 MPa, 140 MPa, 210 MPa; E_1, E_2, E_3 = 70 GPa, 140 GPa, 210 GPa)

5.3.2.2 Three-Layered Beams under Uniformly Distributed Load

The three-layered beam is modeled under plane stress condition with one end clamped and the other simply-supported, while a uniformly distributed load of 1.0 MPa is applied to the top surface. The length is 500 mm and the height is 24 mm, with top, middle and bottom layer having an equal height of 8mm. Two cases have been studied. In the first case, the yield stresses from the top layer to the bottom layer are 210 MPa, 70 MPa and 210 MPa, respectively. In the second case, the yield stresses from the top layer to the bottom layer are 100 MPa, 50 MPa and 150 MPa, respectively. Poisson's ratio for all layers is 0.3, however, a modified value of 0.47 is specified initially. The variations of limit pressures predicted by various methods versus iteration are plotted in Figure 5.23 and Figure 5.24.

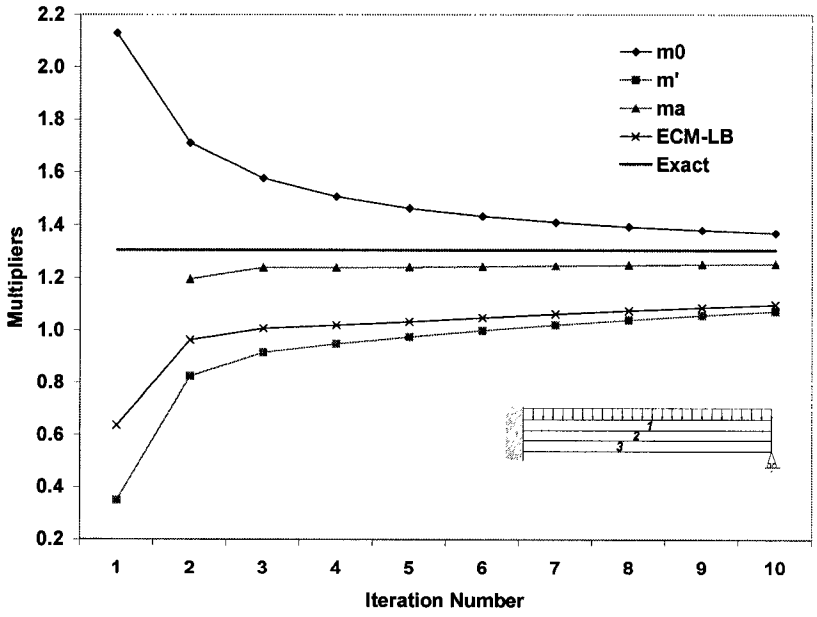

Figure 5.23 Three-layered beam (σ_{y1}, σ_{y2}, σ_{y3} = 210 MPa, 70 MPa, 210 MPa; E_1, E_2, E_3 = 210 GPa, 70 GPa, 210 GPa)

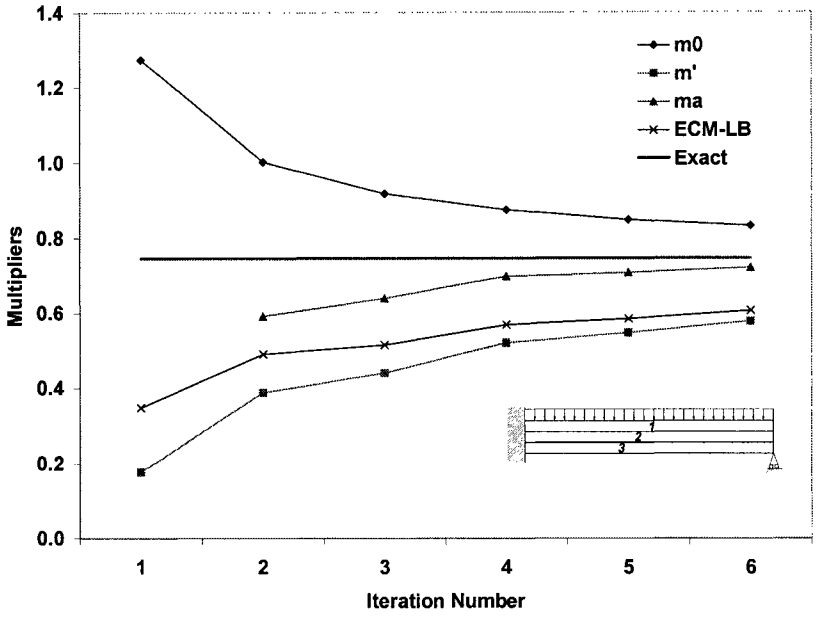

Figure 5.24 Three-layered beam (σ_{y1}, σ_{y2}, σ_{y3} = 100 MPa, 50 MPa, 150 MPa; E_1, E_2, E_3 = 100 GPa, 50 GPa, 150 GPa)

5.3.3 Observations and Discussions

In all the cases of two-layered and three-layered cylinders, the m_α procedure gives very good estimations. For cylinders with inner layer of higher yield strength, the multipliers converge to the exact value in the second and third iteration. For cylinders with inner layer of lower yield strength, the multipliers converge to the exact value in the third and fourth iteration. Since the inner layer usually takes more load initially, cylinders with weaker inner layer need more iterations for the load to redistribute.

For the first geometric configuration of two-layered beam, the m_α procedure gives very good estimations. Reasonable results are usually obtained in the second iteration. More iterations improve the estimation gradually. For the second geometric configuration of

two-layered beam, the m_α procedure yields good estimations. The reason for less iteration in Figure 5.16 and Figure 5.18 is that the m^0 value violates the theorem of nesting surfaces at later iterations.

The m_α procedure yields good results for the two cases of three-layered beams. The reason for less iteration in the second case is also due to the violation of the theorem of nesting surfaces of the m^0 multiplier at later iterations.

Generally speaking, the modified m_α - formulation gives good estimations of m^0 and m_α multipliers. The m_α estimations converge faster than the corresponding lower bound ECM values.

5.4 Conclusions

For layered structures, improved lower-bound limit loads can be obtained using the proposed procedure. A stress distribution close to limit state can be obtained by using a systematic modulus adjustment scheme. The notion of plastic flow parameter is introduced to give faster convergence of multipliers. The estimated limit loads are close to the analytical solutions.

Chapter 6 Collapse Load and Fracture Parameter Estimation for Cracked Components

6.1 Introduction

Cracks and flaws occur in many mechanical components and structures, and sometimes can lead to disastrous failures. Fracture mechanics methods are commonly used in the assessment of the integrity of structures containing defects. Collapse load information is of importance during this serviceability evaluation.

Knowing the collapse load is valuable because:

1. It is one of the important parameters in performing a two-criterion failure assessment of the R6 method (Milne et al, 1988), which limits the loading against both plastic collapse and fracture.

2. It can be used for estimation of fracture parameters, such as the J-integral by the reference stress approximation (Webster and Ainsworth, 1994), and the method of Seshadri and Wu (2001).

3. It may be used to calculate the creep crack growth parameter C* by the reference stress approximation. It is also of use in evaluation of continuum creep damage

using the relationship between the reference stress and the collapse load (Webster and Ainsworth, 1994).

Literature exists for the collapse loads of structures containing defects (Miller, 1988), but a limited range of components and loadings were covered. For components of general geometry and loading, the modified m_α - multiplier method is a simple and versatile approach.

In this chapter, collapse loads for a number of cracked components are estimated by the modified m_α - multiplier method. Then the J-integral estimation method by Seshadri and Wu (2001) is demonstrated by the analyses of two cracked components using the collapse loads obtained.

6.2 Numerical Considerations

6.2.1 Finite Element Modeling

Singular elements should be used to simulate the singular stress and strain distributions in the crack tip region. The use of singular elements allows a much coarser mesh than what would be possible with ordinary elements to capture the crack tip fields. At the crack tip, four-sided quadratic isoparametric elements (2D problem) are often degenerated to triangles, while quadratic isoparametric brick elements (3D problem) are degenerated to wedges.

For elastic problems, the nodes at the crack tip are normally tied, and the mid-side nodes are moved to the quarter points. Such modification leads to a $1/\sqrt{r}$ strain singularity

within the element as well as on the edge, with finite strain energy and stiffness at all points within the element (Barsoum, 1976 and 1977).

For elastic perfectly-plastic material properties, a $1 / r$ strain singularity exists at the crack tip (Rice and Rosengren, 1968). This can be accomplished by using degenerated triangular (or wedge) quarter-point elements with crack tip nodes untied (Barsoum, 1977).

In the present investigation, the ANSYS finite element package is used for the analysis. For 2D problems, the crack tip is modeled with 6-noded triangular PLANE2 elements or degenerated 8-noded PLANE82 elements. Degenerated 20-noded SOLID95 elements are used around the crack tip for 3D problems (Figure 6.1). For reasonable results, the first row of elements around the crack tip has a radial size of approximately $a / 8$ or smaller, where a is the crack length. In the circumferential direction, roughly one element every 30 or 40 degrees is recommended. These elements should take the shape of isosceles triangles (ANSYS, 1998). To obtain a good estimation of the collapse load and the J-integral, ten to twenty elements along the crack front are employed, and the mesh in the plastic region is refined to capture the deformation accurately.

The generation of singular elements for 2D problems is made easy by the use of the ANSYS command KSCON. For 3D problems, the singular element generation is considerably more involved.

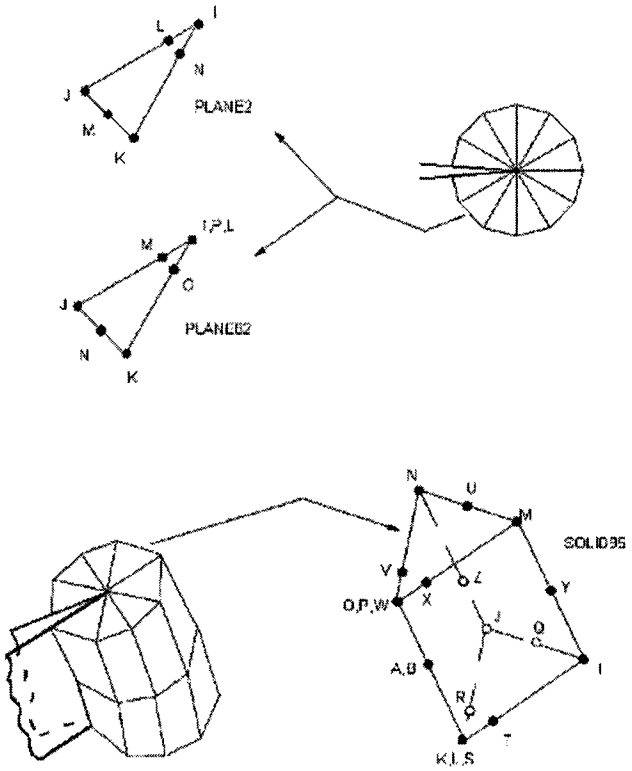

Figure 6.1 Singular elements for 2D and 3D models (ANSYS, 1998)

6.2.2 J-integral Evaluation

The elastic-plastic J-integral can be evaluated numerically by contour integration. An ANSYS macro is written in ANSYS APDL language to perform the operation automatically.

The J-integral for a 2D problem with the crack lying in the X-Y plane and X parallel to the crack (Figure 6.2) is given by

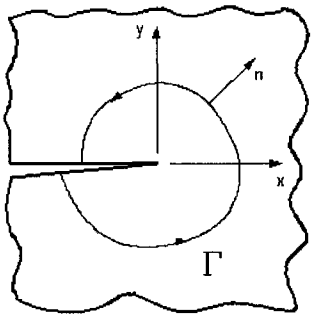

Figure 6.2 Arbitrary contour around the crack tip

$$J = \int_{\Gamma} W dy - \int_{\Gamma} (t_x \frac{\partial u_x}{\partial x} + t_y \frac{\partial u_y}{\partial x}) ds \qquad (6.1)$$

where Γ = any path surrounding the crack tip,

W = strain energy density,

t_x = traction vector along x axis, $t_x = \sigma_x n_x + \sigma_{xy} n_y$,

t_y = traction vector along y axis, $t_y = \sigma_y n_y + \sigma_{xy} n_x$,

σ = stress component,

n = unit outer normal vector to path Γ,

u = displacement vector,

s = distance along the path Γ.

In the finite element model, the variables W, t_x, and t_y in the integrand can be mapped onto the path Γ. The derivatives of the displacement vector in the second term can be obtained indirectly by shifting the path Γ a distance $\Delta x / 2$ and $-\Delta x / 2$ and calculating the gradient of u_x and u_y in the x direction. After all the variables are mapped onto the path, the J-integral can be found by integrating the variables numerically along the contour Γ (ANSYS, 1998).

An important characteristic of the J-integral is its independence of both the shape and size of the contour. The contour may lie within the plastic zone, or cross it, or lie outside it. In all these cases, the J-integral remains invariable, provided that the deformation theory of plasticity is used and unloading is not taken into account (Parton and Morozov, 1989; Gdoutos, 1990).

6.3 Collapse Load Evaluation

In this section, the modified m_α - multiplier method is applied to several cracked components, such as a center-cracked plate, a compact tension specimen, a single-edge-notched bend specimen, a plate with multiple cracks and a cylinder with semi-elliptical crack. The limit loads predicted by the modified m_α - multiplier method are compared with those obtained from the lower bound elastic compensation method and inelastic FEA.

6.3.1 Center-cracked Plate

A center-cracked plate (Figure 6.3) under tensile stress σ = 137.90 MPa (20,000 psi) is analyzed, with a width W = 254 mm (10 inch), thickness B = 3.175 mm (0.125 inch) and crack length $2a$ = 50.8 mm (2 inch). A symmetric quarter of the plate is modeled under plane stress condition with elastic perfectly-plastic material properties. Young's modulus E_0 is = 206.85 GPa (3×10^7 psi) and yield stress σ_y is 172.4 MPa (25,000 psi). Eight-noded PLANE82 elements are used, and eight singular elements cover the crack tip. The multipliers predicted by various methods versus iteration are plotted in Figure 6.4.

In Figure 6.4, the m^0 multiplier is much closer to inelastic FEA values than the m' multiplier in the first several iterations. The m_α estimation gives results after the second iteration. Since the convergence of m' multiplier is slower than m^0, good values of m_α are obtained only in the fifth and sixth iteration.

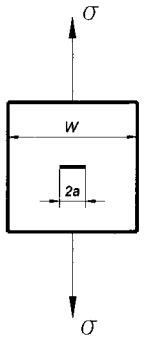

Figure 6.3 Center-cracked plate under tensile stress

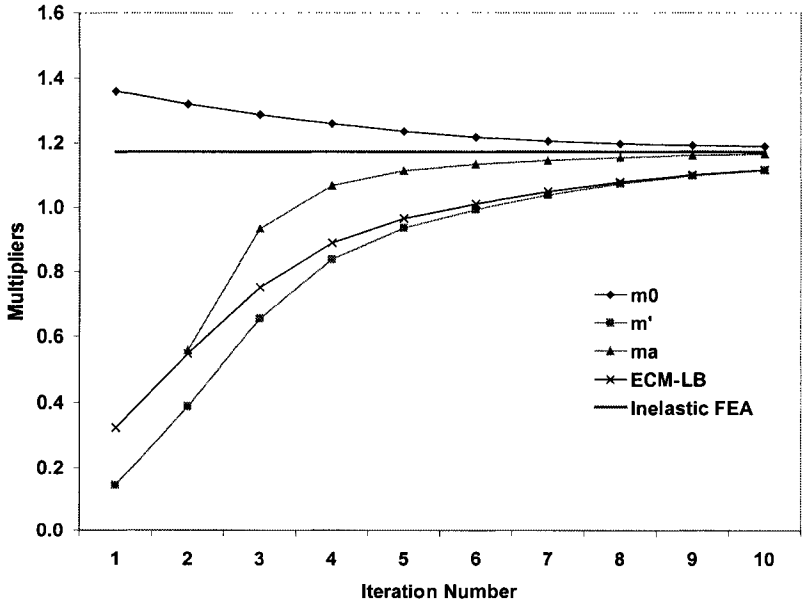

Figure 6.4 Multipliers versus iteration for center-cracked plate

6.3.2 Compact Tension Specimen

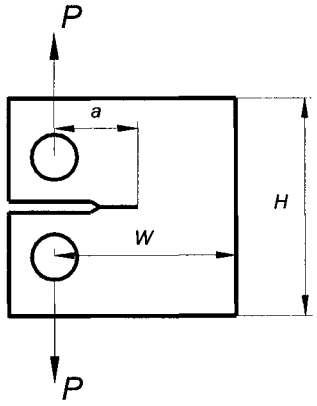

Figure 6.5 Compact tension specimen

A compact tension specimen with width $W = 100$ mm, height $H = 120$ mm, thickness $B = 3$ mm and crack length $a = 46$ mm (Figure 6.5) under a tensile load P of 20 kN is examined. The material is elastic perfectly-plastic. The Young's modulus is 211 GPa, and the yield stress is 488.43 MPa with Poisson's ratio 0.3. The component is modeled under plane stress condition. Nine singular elements (PLANE2) are used around the crack tip to allow a coarser mesh. The variation of multipliers predicted by various methods versus iteration is plotted in Figure 6.6.

From Figure 6.6, it can be seen that the third iteration gives excellent m_α value, while more iterations do not improve the result. This behavior suggests that the stress distribution reaches the near limit state in the third iteration while the m^0 is still improving. In later iterations, the convergence of m^0 even lowers the m_α values slightly.

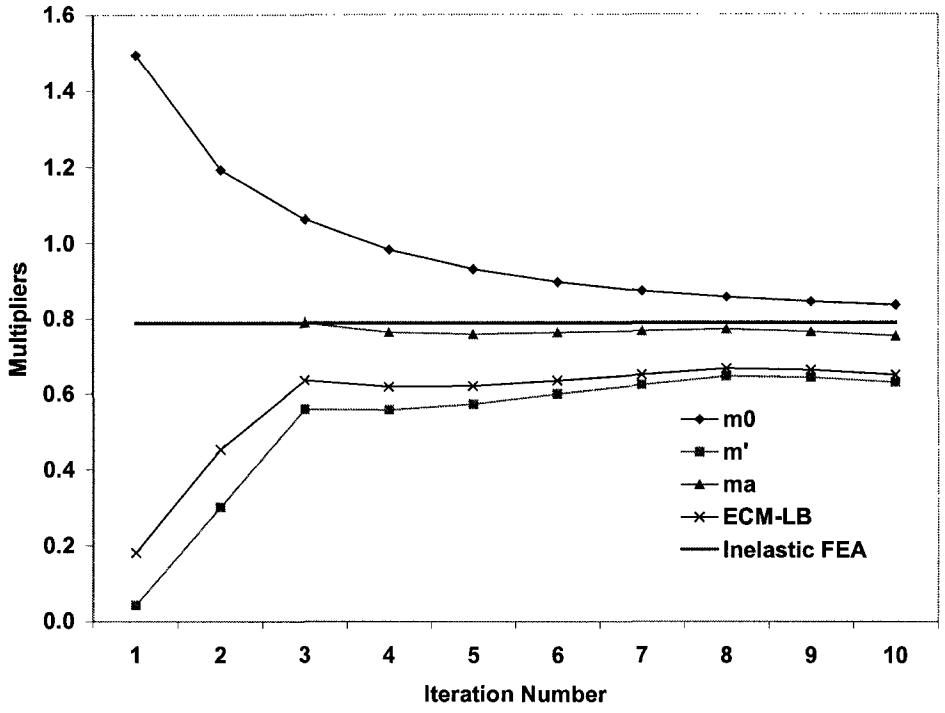

Figure 6.6 Multipliers versus iteration for compact tension specimen

6.3.3 Single-edge-notched Bend Specimen

A single-edge-notched bend specimen under load P = 6000 N (Figure 6.7) is modeled under plane stress condition. It has a span S = 400 mm, a width W = 100 mm and a crack length a = 50 mm. The material properties are the same as for the previous compact tension specimen. Half of the plate is analyzed due to symmetry, and the crack tip is covered by nine PLANE2 singular elements. Figure 6.8 gives the plot of the multipliers obtained by various methods versus iteration.

Figure 6.8 shows m' converges faster than m^0 in the beginning. Good m_α value is obtained at the fourth iteration, and more iterations improve the result slightly.

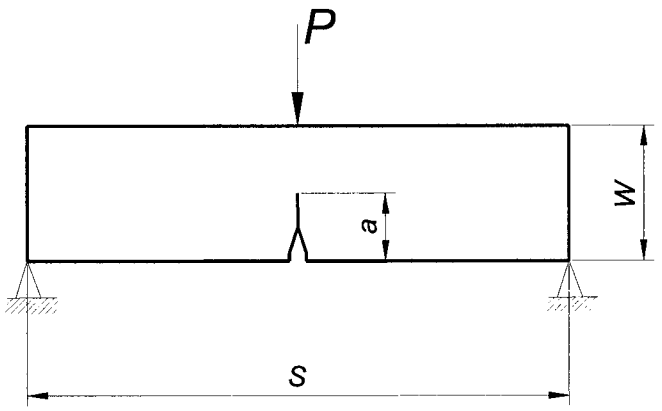

Figure 6.7 Single-edge-notched bend specimen

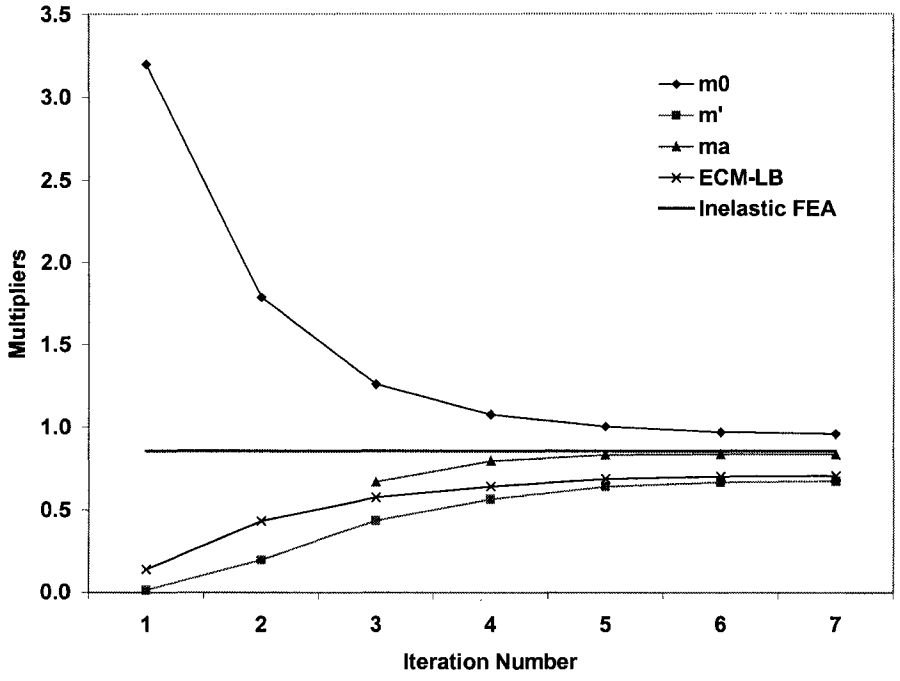

Figure 6.8 Multipliers versus iteration for notched bend specimen

6.3.4 Plate with Multiple Cracks

The collapse load is estimated for a plate with multiple cracks (Figure 6.9). Similar cases are common in the fracture analysis of interacting cracks. The plate has one horizontal crack (length $2a$ = 20 mm) at the center, and four 45° inclined cracks (length $2b$ = 21.2 mm) symmetrically located on both sides of the horizontal and vertical center lines. Their crack tips are 20 mm (dimension c) apart vertically and 40 mm (dimension d) apart horizontally. The plate has a width W = 100 mm and height H = 200 mm, and is loaded by a tensile stress of σ = 300 MPa at both ends. The material is elastic perfectly-plastic, with E_0 = 210 GPa, σ_y = 480 MPa and ν = 0.3.

Only one-quarter of the plate is modeled because of its symmetry. PLANE2 elements are used, and the crack tips are covered with 12 singular elements. The multipliers predicted by various methods versus iteration are plotted in Figure 6.10.

Figure 6.10 suggests that all the multipliers converge to the inelastic FEA value in general. The m_α values are very good in the fourth and sixth iteration, and the m_α multiplier shows a reducing oscillation with more iteration.

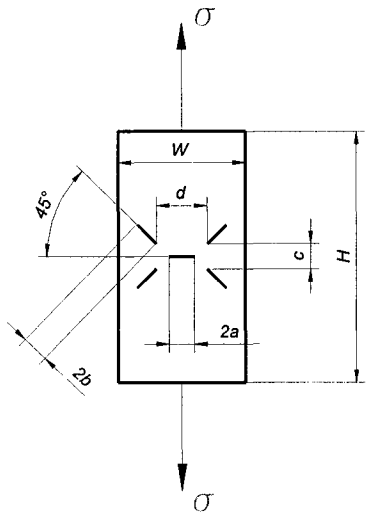

Figure 6.9 Plate with multiple cracks

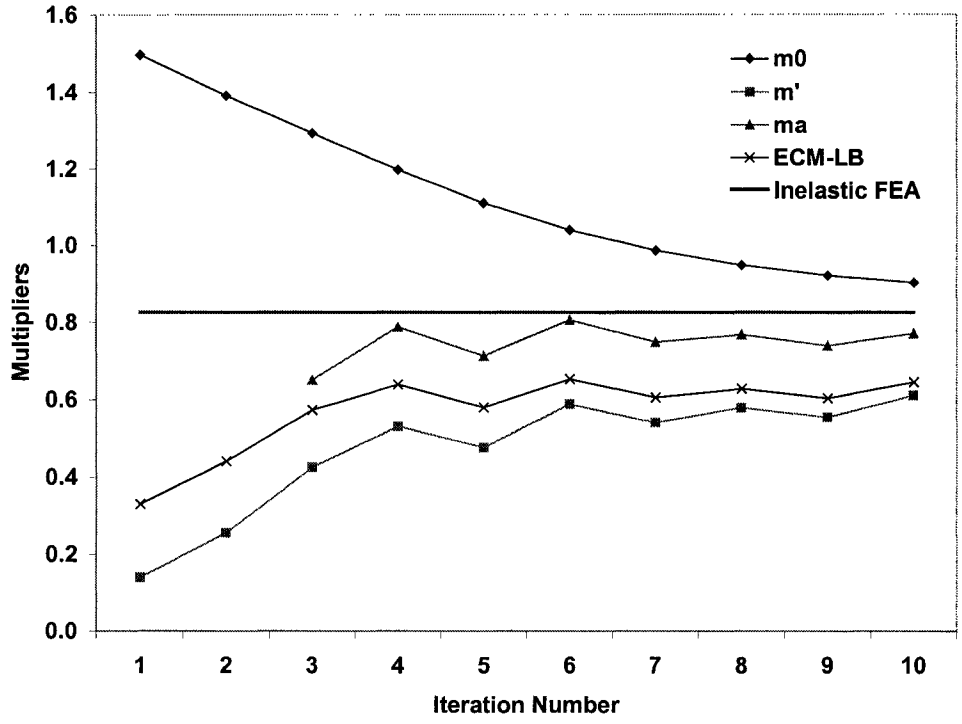

Figure 6.10 Multipliers versus iteration for plate with multiple cracks

6.3.5 Cylinder with Semi-elliptical Crack

The analysis of cylinder with semi-elliptical crack is of interest to many researchers (Newman Jr. and Raju, 1980; deLorenzi, 1982; Keeney and Bass, 1997). In the current investigation, a pressurized cylinder with semi-elliptical crack (Figure 6.11) is analyzed to obtain its collapse load. The cylinder has a length $2b$ = 3000 mm, internal radius R = 1400 mm and wall thickness t = 140 mm. The crack has the size of a = 80 mm and c = 240 mm. Therefore, the ratio of a / t = 0.57 and a / c = 0.33. The material is considered elastic perfectly-plastic with Young's modulus E_0 = 210 GPa, yield stress σ_y = 480 MPa and Poisson's ratio ν = 0.3. (ν = 0.47 is used for the modified m_α - multiplier method.) The cylinder is under a pressure p = 50 MPa, and no axial load is considered.

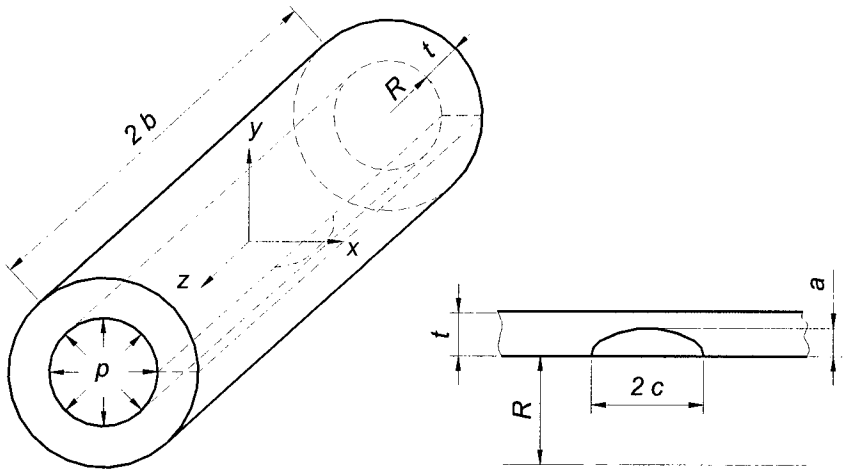

Figure 6.11 Cylinder with semi-elliptical crack under internal pressure

A quarter of the cylinder is modeled in 3D due to symmetry. The global coordinate system has its x-axis on the crack plane in the cylinder radial direction, y-axis in the direction of crack opening, and z-axis coinciding with the cylinder axis. Symmetry boundary conditions are applied on the $y = 0$ and $z = 0$ plane. The $z = b$ plane is free. The internal pressure is applied on both the cylinder inside surface and the crack surface.

Solid modeling is used to generate the crack region and the rest of the cylinder. Four wedge-shaped singular elements are used around the crack tip and a total of 40 singular elements are used along the crack front. The rest of the model is meshed with SOLID95 elements. The model has 3264 elements, 12953 nodes and 37516 degree of freedom (Figure 6.12).

The cylinder is examined by the modified m_α - multiplier method, lower bound ECM and inelastic FEA. The multipliers predicted by these methods are plotted in Figure 6.13.

In Figure 6.13, the m^0 multiplier gives very good estimation even in the first iteration. The m_α values are reasonable and converge to the inelastic FEA value in a vibrating manner. This may suggests a finer mesh is needed.

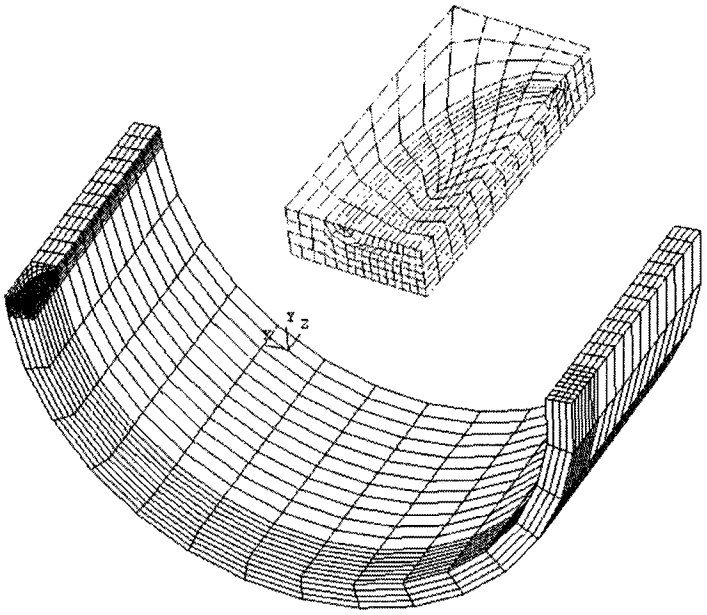

Figure 6.12 Finite element model with details of the crack region

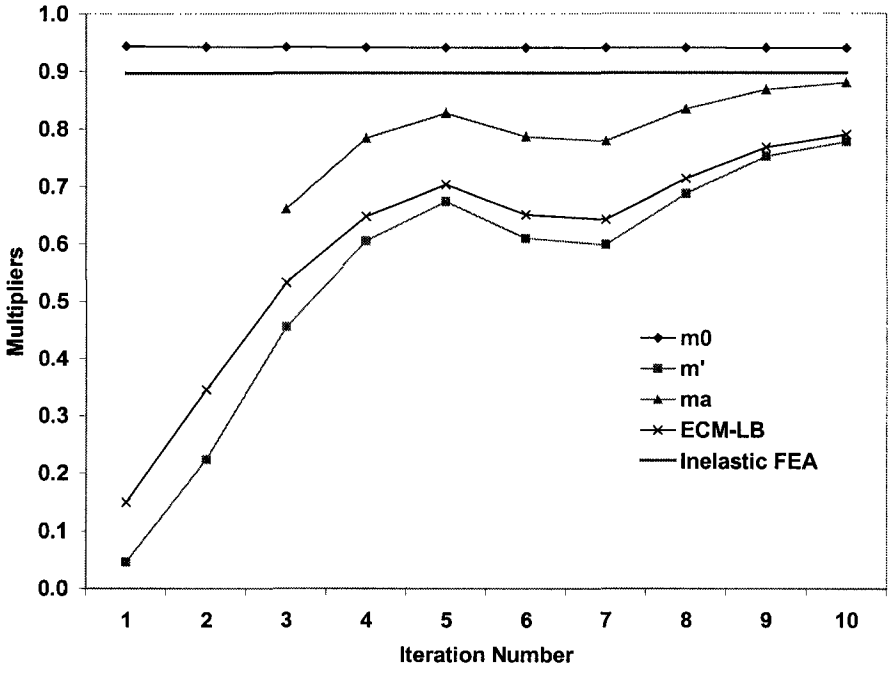

Figure 6.13 Multipliers versus iteration for cylinder with semi-elliptical crack

6.3.6 Conclusions

All five plots of multipliers versus iteration indicate that the modified m_α - multiplier method gives good estimations of the collapse load for cracked components. Due to the presence of a singularity in the elastic solution, real roots of m_α are usually only obtained after the third iteration.

The m^0 multiplier converges to the inelastic FEA value monotonically. The m', m_α and lower bound ECM value show convergence to the inelastic value, but sometimes in an oscillating manner. This is observed particularly for the plate with multiple cracks and the cylinder with semi-elliptical crack. This is due to the fluctuation of the maximum stress. As the general deformation pattern approaches the limit state, the maximum stress element may jump around locally when the load redistributes. Although the maximum stress oscillates between iterations, it decreases in the general sense.

As also observed in the previous two chapters, the m_α multiplier is closer to the inelastic FEA value than the lower bound ECM.

6.4 Fracture Parameter Estimation

6.4.1 J-integral Estimation Scheme

Seshadri and Wu (2001) suggested a simplified formulation for estimating the J-integral. This formulation relies on a knowledge of the linear elastic stress-intensity parameter and the plastic collapse load. An expression is provided in terms of the r-node strain, which

serves as an upper bound in the elastic-plastic regions for components subjected to mechanical loads.

The simple expression for the normalized J-integral is given by

$$\begin{aligned} \bar{J} &= \bar{\varepsilon}_n^2 \qquad \cdots 0 \le \bar{\varepsilon}_n \le 0.5 \\ \bar{J} &= 2\bar{\varepsilon}_n^3 \qquad \cdots 0.5 \le \bar{\varepsilon}_n \le 1.0 \end{aligned} \tag{6.2}$$

where the normalized J-integral is $\bar{J} = J / J_e(\varepsilon_y)$

and the normalized r-node strain is $\bar{\varepsilon}_n = \varepsilon_n / \varepsilon_y = P / P_L$.

In the above expressions, ε_n refers to the r-node strain for a component. As ε_n reaches ε_y (r-node strain at collapse), the applied load P reaches the collapse load P_L. The term J stands for the elastic-plastic J-integral, and J_e (ε_y) denotes the elastic J-integral at collapse load.

Based on the above information, Eq. (6.2) can be rewritten as

$$\begin{aligned} \bar{J} &= (P/P_L)^2 \qquad \cdots 0 \le P/P_L \le 0.5 \\ \bar{J} &= 2(P/P_L)^3 \qquad \cdots 0.5 \le P/P_L \le 1.0 \end{aligned} \tag{6.3}$$

Equation (6.3) enable us to estimate the normalized J-integral based on the collapse load information.

The value of elastic-plastic J-integral can be acquired if the elastic J-integral at the collapse load J_e (ε_y) is available. For simple components, the elastic J-integral can be acquired by its relationship with the stress intensity factor, such as

$$J_e = \frac{\beta K_I^2}{E_0} \qquad (6.4)$$

where β = 1 for plane stress and β = 1 - ν^2 for plane strain. For more complex components and loading, the elastic J-integral can be estimated by elastic FEA.

In the following two sections, the elastic-plastic J-integral is predicted for the center-cracked plate and the compact tension specimen by making use of Eq. (6.3), Eq. (6.4), and the collapse load calculated by the modified m_α method.

6.4.2 Center-cracked Plate

For the center-cracked plate in plane stress condition, the collapse load σ_{max} predicted by the modified m_α - multiplier method is 160.74 MPa (23,314 psi). The stress intensity factor for this component is

$$K_I = C\sigma\sqrt{\pi a} \qquad (6.5)$$

where $C = 1 + 0.256(\frac{a}{W}) - 1.152(\frac{a}{W})^2 + 12.200(\frac{a}{W})^3$.

Substituting Eq. (6.5) into (6.4) using the collapse load yields

$$J_e(\varepsilon_y) = \frac{K_{\mathrm{Im}ax}^2}{E_0} = \frac{C^2\sigma_{\max}^2\pi a}{E_0} = 10{,}498 \;\; N/m \;\; (59.95 \;\; lb/in) \qquad (6.6)$$

Then the elastic-plastic J-integral can be estimated using Eq. (6.3). The estimated J-integral (design curve) from Eq. (6.3), the linear elastic J-integral from Eq. (6.4) and the J-integral from inelastic FEA versus the applied load are plotted in Figure 6.14.

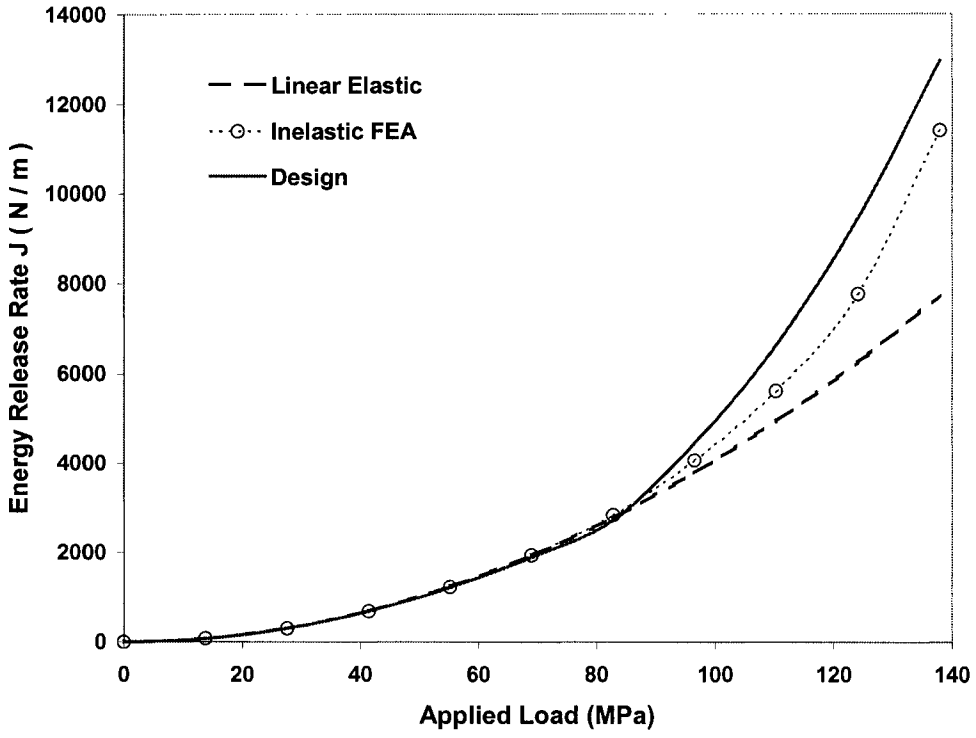

Figure 6.14 J-integral estimation versus applied load for center-cracked plate

6.4.3 Compact Tension Specimen

The stress intensity factor formula is given by (Anderson, 1995)

$$K_I = \frac{P}{B\sqrt{W}} f(\frac{a}{W}) \qquad (6.7)$$

where $f(\frac{a}{W}) = \frac{2+\frac{a}{W}}{\left(1-\frac{a}{W}\right)^{3/2}}\left[0.886+4.64\left(\frac{a}{W}\right)-13.32\left(\frac{a}{W}\right)^2+14.72\left(\frac{a}{W}\right)^3-5.60\left(\frac{a}{W}\right)^4\right]$.

15,774 N is the collapse load estimated for the compact tension specimen by the modified m_α - multiplier method. Therefore, the elastic J-integral at the collapse load is

$$J_e(\varepsilon_y) = \frac{K_{\mathrm{Im}ax}^2}{E_0} = \frac{P_L^2}{B^2 W E_0} f^2(\frac{a}{W}) = 96{,}445 \quad N/m \qquad (6.8)$$

Again, the elastic-plastic J-integral is estimated using Eq. (6.3). The estimated J-integral (design curve) versus applied load is plotted in Figure 6.15 along with the linear elastic J-integral and the J-integral predicted by inelastic FEA.

6.4.4 Observations and Conclusions

Collapse load information is important in the robust estimation of elastic-plastic J-integrals. The J-integral estimation scheme by Seshadri and Wu (2001) gives very good predictions.

As shown in Figure 6.14 and Figure 6.15, at the load below half collapse load, three curves (estimated J, elastic J and J from inelastic FEA) almost coincide. At loads above half of the collapse load, the estimated J-integral gives upper bound results. This is true for the center-cracked plate. For compact tension specimen, the inelastic FEA J-integral goes above the design curve at over 14,000 N, which is very close to the collapse load. At this load level, the failure mode is dominated by plastic collapse, not fracture. Hence,

the crossover of the curves would not undermine the conservativeness of this J-integral estimation scheme.

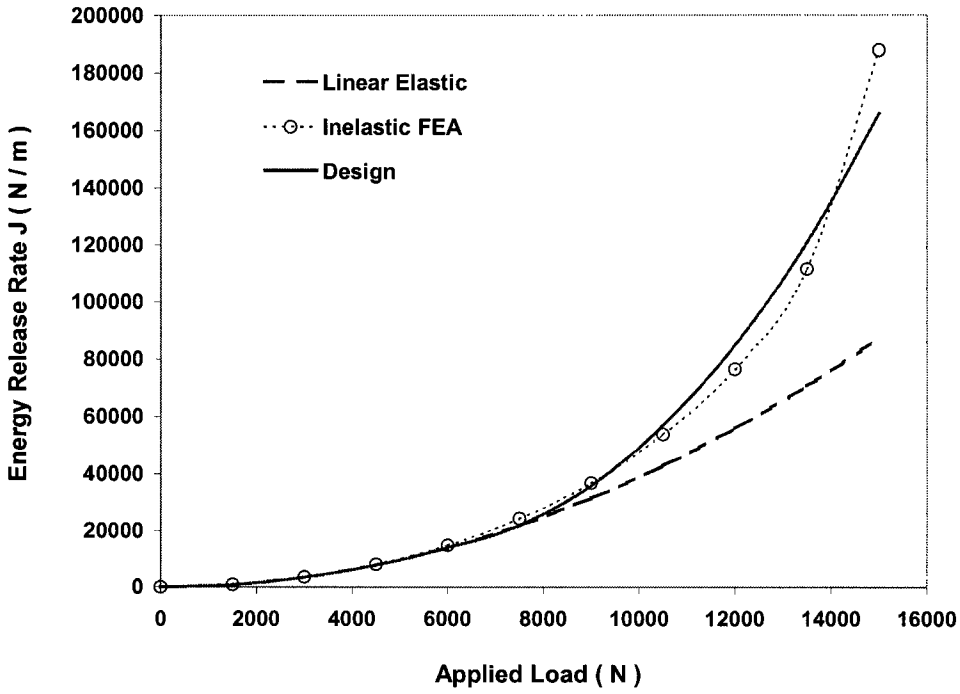

Figure 6.15 J-integral estimation versus applied load for compact tension specimen

Chapter 7 Collapse Load Estimation for Components and Structures Made of Anisotropic Materials

7.1 Introduction

Modern structural components are made not only of materials that can be considered as isotropic in design, but also of anisotropic materials. For the latter, the material properties show appreciable differences in different directions. Examples are rolled sheets in pressure vessels, composites, and directionally solidified superalloys in gas turbine blades. The knowledge of the limit load is useful in the design and sizing of components and structures made from these materials.

The following sections explain the theoretical background and procedures required for the extension of the m_α - method to anisotropic materials. In order to introduce variable plastic flow rates, a plastic flow parameter is introduced into the formulation. A method of modified initial elastic properties is adopted to ensure the repeated elastic FEA generate the stress distribution close to the anisotropic limit type.

The anisotropic material used in the current research is specified as orthotropic, which means it has three orthogonal planes of material property symmetry. It is further assumed that the material is homogeneous and perfectly plastic.

7.2 Anisotropic Constitutive Relationships

7.2.1 Elastic Stress-Strain Relationship

According to the generalized Hooke's Law, the stress tensor is linearly proportional to the strain tensor and can be expressed as

$$\sigma_{ij} = C_{ijkl}\varepsilon_{kl} \tag{7.1}$$

where σ_{ij} is the stress tensor, ε_{kl} is the strain tensor, and C_{ijkl} is a fourth order tensor of elastic constants which are independent of stress or strain.

Expressed in matrix form, Hooke's Law is given by

$$\{\sigma\} = [C]\{\varepsilon\} \tag{7.2}$$

If the structure of an anisotropic body has some form of symmetry, the number of independent constants in the stiffness matrix $[C]$ can be reduced: for a monoclinic material, there are 13; for an orthotropic material, 9; for a transversely isotropic material, 5; for a cubic symmetric material, 3 and for an isotropic material, 2 (Jones, 1975).

Another form of the generalized Hooke's law is

$$\{\varepsilon\} = [D]\{\sigma\} \tag{7.3}$$

in which $[D] = [C]^{-1}$, where $[D]$ is called the compliance matrix. The components of the compliance matrix are usually defined in a simpler form than those of the stiffness matrix, by making use of an analogy to isotropic elastic properties, such as the moduli of elasticity, Poisson's ratios, and shear moduli.

For an orthotropic material, the elastic constitutive relationship is (Jones, 1975)

$$\begin{Bmatrix} \varepsilon_x \\ \varepsilon_y \\ \varepsilon_z \\ \gamma_{xy} \\ \gamma_{yz} \\ \gamma_{zx} \end{Bmatrix} = \begin{bmatrix} \frac{1}{E_x} & -\frac{\nu_{yx}}{E_y} & -\frac{\nu_{zx}}{E_z} & 0 & 0 & 0 \\ -\frac{\nu_{xy}}{E_x} & \frac{1}{E_y} & -\frac{\nu_{zy}}{E_z} & 0 & 0 & 0 \\ -\frac{\nu_{xz}}{E_x} & -\frac{\nu_{yz}}{E_y} & \frac{1}{E_z} & 0 & 0 & 0 \\ 0 & 0 & 0 & \frac{1}{G_{xy}} & 0 & 0 \\ 0 & 0 & 0 & 0 & \frac{1}{G_{yz}} & 0 \\ 0 & 0 & 0 & 0 & 0 & \frac{1}{G_{zx}} \end{bmatrix} \begin{Bmatrix} \sigma_x \\ \sigma_y \\ \sigma_z \\ \sigma_{xy} \\ \sigma_{yz} \\ \sigma_{zx} \end{Bmatrix} \tag{7.4}$$

where E_x, E_y, E_z = Young's modulus in x, y and z direction, respectively; ν_{ij} = Poisson's ratio for transverse strain induced in the j-direction when loaded in the i-direction; G_{ij} = shear modulus in the i-j plane.

Since the compliance matrix is symmetric, we have

$$\frac{\nu_{ij}}{E_i} = \frac{\nu_{ji}}{E_j} \qquad (7.5)$$

Therefore, the compliance matrix for orthotropic materials has 9 independent constants.

7.2.2 Plastic Constitutive Relationship

7.2.2.1 Yield Criterion

The general yield criterion for anisotropic material can be expressed as (Shih and Lee, 1978)

$$f(\sigma_i, \beta_i, M_{ij}, k) = 0 \qquad (7.6)$$

or

$$3f = M_{ij}(\sigma_i - \beta_i)(\sigma_j - \beta_j) - k^2 = 0$$

where $i,j = 1\ldots6$. M_{ij} describes the effect of orientation on yield stresses, β_i describes the strength differential between tensile and compressive yield stresses and k determines the effective size of the yield surface.

In the absence of the strength differential, the yield criterion can be written as

$$3f = M_{ij}\sigma_i\sigma_j - k^2 = 0 \qquad (7.7)$$

There are 21 independent constants in M_{ij}. For an orthotropic material with incompressibility condition, the independent constants reduce to six. This is equivalent to

Hill's yield criterion for orthotropic materials (Hill, 1950), as given by the following equation

$$f' = F(\sigma_y - \sigma_z)^2 + G(\sigma_z - \sigma_x)^2 + H(\sigma_x - \sigma_y)^2 + 2L\tau_{yz}^2 + 2M\tau_{zx}^2 + 2N\tau_{xy}^2 = 1 \qquad (7.8)$$

In non-dimensional coefficient form, Hill's yield criterion can be written as (Valliappan et al, 1976)

$$f = \frac{\bar{\sigma}^2}{3} = \frac{1}{6}\left[\alpha_{12}(\sigma_x - \sigma_y)^2 + \alpha_{23}(\sigma_y - \sigma_z)^2 + \alpha_{31}(\sigma_z - \sigma_x)^2\right] +$$

$$(\alpha_{44}\tau_{xy}^2 + \alpha_{55}\tau_{yz}^2 + \alpha_{66}\tau_{zx}^2) - \frac{\bar{\sigma}_0^2}{3} = 0 \qquad (7.9)$$

In the above equation, the axes x, y, and z are taken to be the principal axes of anisotropy of the material. α_{ij} are dimensionless anisotropic parameters. $\bar{\sigma}_0$ is the reference yield stress adopted from one of the six yield stress values. $\bar{\sigma}$ is the reference effective stress and can be expressed as

$$\bar{\sigma} = \left\{\frac{1}{2}\left[\alpha_{12}(\sigma_x - \sigma_y)^2 + \alpha_{23}(\sigma_y - \sigma_z)^2 + \alpha_{31}(\sigma_z - \sigma_x)^2\right]\right.$$

$$\left. + 3\left[\alpha_{44}\tau_{xy}^2 + \alpha_{55}\tau_{yz}^2 + \alpha_{66}\tau_{zx}^2\right]\right\}^{1/2} \qquad (7.10)$$

The anisotropic parameters can be determined from yield stress in independent tests along various material principal axes. By successively letting all stress components in

Eq. (7.9) equal to zero except the one under consideration, these parameter can be derived as

$$\alpha_{12} = \bar{\sigma}_0^{\,2}\left(\frac{1}{\sigma_{0x}^2}+\frac{1}{\sigma_{0y}^2}-\frac{1}{\sigma_{0z}^2}\right)$$

$$\alpha_{23} = \bar{\sigma}_0^{\,2}\left(-\frac{1}{\sigma_{0x}^2}+\frac{1}{\sigma_{0y}^2}+\frac{1}{\sigma_{0z}^2}\right)$$

$$\alpha_{31} = \bar{\sigma}_0^{\,2}\left(\frac{1}{\sigma_{0x}^2}-\frac{1}{\sigma_{0y}^2}+\frac{1}{\sigma_{0z}^2}\right)$$

$$\alpha_{44} = \frac{1}{3}\left(\frac{\bar{\sigma}_0}{\tau_{0xy}}\right)^2,\ \alpha_{55} = \frac{1}{3}\left(\frac{\bar{\sigma}_0}{\tau_{0yz}}\right)^2,\ \alpha_{66} = \frac{1}{3}\left(\frac{\bar{\sigma}_0}{\tau_{0zx}}\right)^2 \qquad (7.11)$$

where σ_{0x}, σ_{0y}, σ_{0z} and τ_{0xy}, τ_{0yz} and τ_{0zx} are yield stresses obtained from three simple uniaxial tests in x, y and z direction and three shear test in xy, yz and zx plane. $\bar{\sigma}_0$ is the yield stress adopted from one of the above six test values.

7.2.2.2 Flow Rule

For associate flow rule, the plastic strain increments are given by

$$d\varepsilon_{ij}^{p} = d\lambda\frac{\partial f}{\partial \sigma_{ij}} \qquad (7.12)$$

where $i, j = 1, 2, 3$, and $d\lambda$ is a proportionality constant.

Using Eq. (7.9), Eq. (7.12) in expanded form gives

$$\left\{d\varepsilon_{ij}^{p}\right\}=\begin{Bmatrix} d\varepsilon_{x}^{p} \\ d\varepsilon_{y}^{p} \\ d\varepsilon_{z}^{p} \\ d\gamma_{xy}^{p} \\ d\gamma_{yz}^{p} \\ d\gamma_{zx}^{p} \end{Bmatrix}=\frac{d\lambda}{3}\begin{bmatrix} \alpha_{12}(\sigma_x-\sigma_y)+\alpha_{31}(\sigma_x-\sigma_z) \\ \alpha_{12}(\sigma_y-\sigma_x)+\alpha_{23}(\sigma_y-\sigma_z) \\ \alpha_{31}(\sigma_z-\sigma_x)+\alpha_{23}(\sigma_z-\sigma_y) \\ 6\alpha_{44}\tau_{xy} \\ 6\alpha_{55}\tau_{yz} \\ 6\alpha_{66}\tau_{zx} \end{bmatrix} \tag{7.13}$$

It can be shown that (Valliappan, 1972)

$$d\lambda=\frac{3d\bar{\varepsilon}_p}{2\bar{\sigma}} \tag{7.14}$$

where $\bar{\varepsilon_p}$ is the effective plastic strain.

For the uniaxial case

$$d\bar{\varepsilon}_p=\frac{d\bar{\sigma}}{E_p} \tag{7.15}$$

where E_p is the slope of the effective stress versus effective plastic strain curve.

From the equivalence of plastic work,

$$\sigma_{ij}d\varepsilon_{ij}^{p}=\bar{\sigma}d\bar{\varepsilon}_p \tag{7.16}$$

the effective plastic strain can be derived as

$$d\bar{\varepsilon}_p=\left\{\frac{2\left[\alpha_{12}(\alpha_{23}d\varepsilon_x^p-\alpha_{31}d\varepsilon_y^p)^2+\alpha_{23}(\alpha_{31}d\varepsilon_y^p-\alpha_{12}d\varepsilon_z^p)^2+\alpha_{31}(\alpha_{12}d\varepsilon_z^p-\alpha_{23}d\varepsilon_x^p)^2\right]}{(\alpha_{12}\alpha_{23}+\alpha_{23}\alpha_{31}+\alpha_{31}\alpha_{12})^2}\right.$$

$$+\frac{1}{3}\left(\frac{\left(d\gamma_{xy}^{p}\right)^2}{\alpha_{44}}+\frac{\left(d\gamma_{yz}^{p}\right)^2}{\alpha_{55}}+\frac{\left(d\gamma_{zx}^{p}\right)^2}{\alpha_{66}}\right)\Bigg\}^{1/2} \qquad (7.17)$$

7.2.2.3 Reference Stress-Strain Curve

The reference stress-strain curve is the effective stress versus effective strain curve. For anisotropic materials, the stress-strain curve is different along different principal axis. Usually the reference stress-strain curve is adopted from one of the stress-strain tests from the *x*, *y*, *z* direction or *xy*, *yz*, and *zx* plane (Valliappan et al, 1976). In the present investigation, the stress-strain curve along the *x* direction is taken as the reference stress-strain curve.

7.3 m_α Formulation for Anisotropic Materials

7.3.1 Mura's Variational Principle for Anisotropic Materials

Mura's variational principle for isotropic materials has been extended to anisotropic materials by Rimawi et al (1966) and Mura et al (1968). The integral mean of yield criterion is

$$\int_V \mu^0 \left\{ f(s_{ij}^0) + (\phi^0)^2 \right\} dV = 0 \qquad (7.18)$$

All the derivations are the same as for isotropic materials, except that the yield criterion is replaced by the anisotropic yield criterion as follows

$$f(s_{ij}) = \frac{1}{2} M_{ijkl} s_{ij} s_{kl} - 1 \qquad (7.19)$$

in which M_{ijkl} is the symmetric material tensor and s_{ij} is the deviatoric stress. In the current research, Eq. (7.9) is adopted as a special case of anisotropic yield criterion so that the generalized deviatoric stress tensor S_{ij} can be expressed as

$$S_{ij} = \frac{\partial f}{\partial \sigma_{ij}} = \frac{1}{3} \begin{bmatrix} \alpha_{12}(\sigma_x - \sigma_y) + \alpha_{31}(\sigma_x - \sigma_z) \\ \alpha_{12}(\sigma_y - \sigma_x) + \alpha_{23}(\sigma_y - \sigma_z) \\ \alpha_{31}(\sigma_z - \sigma_x) + \alpha_{23}(\sigma_z - \sigma_y) \\ 6\alpha_{44}\tau_{xy} \\ 6\alpha_{55}\tau_{yz} \\ 6\alpha_{66}\tau_{zx} \end{bmatrix} \qquad (7.20)$$

7.3.2 Plastic Flow Parameter Estimation

According to the deformation theory of plasticity, the stress-strain relationship is

$$\varepsilon_{ij}^{p} = \mu S_{ij} \qquad (7.21)$$

where μ is a positive scalar, ε_{ij}^{p} is the plastic strain components and S_{ij} is the generalized deviatoric stress.

By comparing the above equation with Hooke's law, a relationship can be established between the scalar μ and the secant modulus of a point in a component or structure. For example, the stress-strain equation of the deformation theory of plasticity in the x direction can be written as

$$\varepsilon_x = \frac{\mu}{3}(\alpha_{12} + \alpha_{31})\sigma_x - \frac{\mu}{3}\alpha_{12}\sigma_y - \frac{\mu}{3}\alpha_{31}\sigma_z \qquad (7.22)$$

The stress-strain equation of Hooke's law in terms of equivalent secant moduli is expressed as

$$\varepsilon_x = \frac{1}{E_{Sx}}\sigma_x - \frac{\nu_{yx}}{E_{Sy}}\sigma_y - \frac{\nu_{zx}}{E_{Sz}}\sigma_z \qquad (7.23)$$

where E_{Si} is the secant modulus in the i direction.

Equating the above two equations means that the coefficients of the same stress term between the two equations should be equal. Again, taking the x direction, we have

$$\frac{\mu}{3}(\alpha_{12} + \alpha_{31}) = \frac{1}{E_{Sx}} \qquad (7.24)$$

Using Eqs. (7.11), Eq. (7.24) can be rewritten as

$$\mu = \frac{3}{2E_{Sx}} \cdot \frac{\sigma_{0x}^2}{\bar{\sigma}_0^2} \qquad (7.25)$$

Therefore, if x is taken as the reference direction, μ can be defined in terms of secant modulus in x direction E_{Sx} as

$$\mu = \frac{3}{2E_{Sx}} = \frac{3\bar{\varepsilon}}{2\bar{\sigma}} \qquad (7.26)$$

where the effective stress $\bar{\sigma}$ and the effective strain $\bar{\varepsilon}$ are defined by Eqs. (7.10) and (7.17).

Repeated LEFEA are able to simulate the deformation field and stress field close to the limit type. Therefore, the distribution of μ^0 in LEFEA is close to the actual distribution μ at collapse state, as the simulation converges to limit type. Within each elastic iteration, it is postulated that the plastic flow parameter μ^0 can be considered as a function of the secant modulus of the reference direction (such as x direction) of each element in a LEFEA scheme, i.e.,

$$\mu^0 = \frac{C}{E_{Sx}} \tag{7.27}$$

where C is a constant whose value depends on the component geometry, loading and the arbitrary stress in the modulus adjustment equation.

Substituting Eq. (7.27) into the integral mean of yield criterion, Eq. (7.18), the upper bound multiplier m^0 can be obtained as

$$m^0 = \sigma_{0x}\left[\frac{\sum_{k=1}^{N} \Delta V_k / E_{Sxk}}{\sum_{k=1}^{N} \bar{\sigma}_k^2 \Delta V_k / E_{Sxk}}\right]^{1/2} \tag{7.28}$$

where N is the total number of finite elements of the structure; $\bar{\sigma}_k$, ΔV_k, E_{Sxk} are the effective stress, element volume and secant modulus in x direction of element k,

respectively. σ_{0x} is the yield stress in the reference direction x. The constant C cancels out of the equation.

The evaluation procedure of m' and m_α is the same as the isotropic material. The lower bound multiplier can be expressed as

$$m' = \frac{2m^0}{1+(m^0)^2(\bar{\sigma}_M^0)^2} \qquad (7.29)$$

where $\bar{\sigma}_M^0$ is the normalized maximum effective stress in a component or structure for a prescribed set of loads, and it is given by

$$\bar{\sigma}_M^0 = \frac{\bar{\sigma}_{\max}^0}{\sigma_{0x}} \qquad (7.30)$$

where $\bar{\sigma}_{\max}^0$ is the maximum effective stress in the finite element model.

7.3.3 Elastic Modulus Adjustment Scheme

The elastic modulus adjustment equation for orthotropic material is given as

$$(E_{jk})_i = \left[\frac{\sigma_{arb}}{\bar{\sigma}_{i-1}}\right]^q (E_{jk})_{i-1} \qquad (7.31)$$

where $(E_{jk})_i$ refers to Young's moduli and shear moduli along the anisotropic principal axes for the i-th iteration, σ_{arb} is the arbitrary stress, $\bar{\sigma}_{i-1}$ is the effective stress for the element of the previous iteration, q is a modulus adjustment index which is normally taken as one, and $(E_{jk})_{i-1}$ refers to the moduli for the previous iteration. Equation (7.31)

is applied to each element within the finite element model, and all the moduli for that element are modified.

But modifying the original material elastic properties with Eq. (7.31) may not lead to stress distributions close to the anisotropic limit type. A method of modified initial elastic properties (Reinhardt and Mangalaramanan, 1999) is adopted to overcome this problem.

Unlike an isotropic material with two elastic parameters, the deformation of an orthotropic material is controlled by nine parameters. Which of these dominates the collapse depends on both material properties and loading. Since all the moduli are adjusted by the same degree in Eq. (7.31), the initial values of these moduli must be chosen such that they can become compatible with the anisotropic plastic limit state. At collapse, it is expected that the stress and strain states in the significantly plastic regions of the structure are determined by the plastic flow rule. A realistic stress distribution at collapse should be obtained if the initial "elastic" parameters are chosen in such a proportion to each other as the plastic flow rule suggests. The objective is to allow, as much as possible, for the stress fields to follow the orthotropic yield surface (Reinhardt and Mangalaramanan, 1999).

The initial elastic moduli and Poisson's ratios are determined by comparing the "elastic" and plastic strains. The elastic stress-strain relationship has been given by Eq. (7.4). The plastic flow rule of deformation theory is expressed in similar form as

$$\begin{Bmatrix} \varepsilon_x^p \\ \varepsilon_y^p \\ \varepsilon_z^p \\ \gamma_{xy}^p \\ \gamma_{yz}^p \\ \gamma_{zx}^p \end{Bmatrix} = \frac{\mu}{3} \begin{bmatrix} \alpha_{12}+\alpha_{31} & -\alpha_{12} & -\alpha_{31} & 0 & 0 & 0 \\ -\alpha_{12} & \alpha_{12}+\alpha_{23} & -\alpha_{23} & 0 & 0 & 0 \\ -\alpha_{31} & -\alpha_{23} & \alpha_{31}+\alpha_{23} & 0 & 0 & 0 \\ 0 & 0 & 0 & 6\alpha_{44} & 0 & 0 \\ 0 & 0 & 0 & 0 & 6\alpha_{55} & 0 \\ 0 & 0 & 0 & 0 & 0 & 6\alpha_{66} \end{bmatrix} \begin{Bmatrix} \sigma_x \\ \sigma_y \\ \sigma_z \\ \sigma_{xy} \\ \sigma_{yz} \\ \sigma_{zx} \end{Bmatrix} \quad (7.32)$$

By relating Eq. (7.32) with Eq. (7.4), the expressions for the elastic properties can be obtained as

$$E_x = C\sigma_{0x}^2,\ E_y = C\sigma_{0y}^2,\ E_z = C\sigma_{0z}^2 \quad (7.33)$$

$$G_{xy} = C\tau_{0xy}^2,\ G_{yz} = C\tau_{0yz}^2,\ G_{zx} = C\tau_{0zx}^2$$

$$\nu_{yx} = \frac{\sigma_{0y}^2}{2}\left(\frac{1}{\sigma_{0x}^2} + \frac{1}{\sigma_{0y}^2} - \frac{1}{\sigma_{0z}^2}\right)$$

$$\nu_{zy} = \frac{\sigma_{0z}^2}{2}\left(-\frac{1}{\sigma_{0x}^2} + \frac{1}{\sigma_{0y}^2} + \frac{1}{\sigma_{0z}^2}\right)$$

$$\nu_{zx} = \frac{\sigma_{0z}^2}{2}\left(\frac{1}{\sigma_{0x}^2} - \frac{1}{\sigma_{0y}^2} + \frac{1}{\sigma_{0z}^2}\right)$$

where the variable $C = \dfrac{3}{2\mu\bar{\sigma}_0^2}$, and has a dimension of Pa^{-1}. Since the value of C would not affect the stress distribution of the components, it can take values such as 1 Pa^{-1}.

The elastic properties given in Eq. (7.33) are used as the initial elastic properties for the repeated elastic analyses, and are modified using Eq. (7.31) for each iteration. The Poisson's ratios' values in Eq. (7.33) are kept unchanged during the iterations. To ensure positive definiteness of the elastic matrix, the denominator 2 in the Poisson ratios' expressions is replaced by 2.13 in the current investigation.

7.3.4 Procedures for the Evaluation of Multipliers

The following is the procedure for performing the m_α method for components made of anisotropic materials:

1. Modified initial elastic properties derived from Eq. (7.33) are used as material input.

2. The first linear elastic finite element analysis is carried out for the model with the prescribed loading and boundary conditions.

3. Based on the stress distribution obtained, the elastic moduli of each element are modified using Eq. (7.31), while the Poisson's ratios are left unchanged.

4. The second elastic analysis is carried out with the modified material properties. The multipliers m^0 is evaluated using Eq. (7.28). m' and m_α are evaluated in the same fashion as isotropic materials.

5. Step 2 to 4 is repeated until the convergence of multipliers occurs, or the analysis is terminated after 10 iterations.

7.4 Applications

The m_α procedure for anisotropic materials is applied to two components to verify its robustness and validity. They are an orthotropic cylinder under internal pressure and a transversely isotropic Bridgman notch bar under tensile load. The multipliers m^0, m' and m_α obtained using the m_α procedure are compared with those obtained using lower bound elastic compensation method and inelastic finite element analysis.

The components are made of Zircalloy. The alloy is assumed to be perfectly-plastic and possesses orthotropic symmetry. A general three-dimensional orthotropic material has nine independent elastic constants and six plastic constants. For two-dimensional problems, the number of independent elastic and plastic constants required are seven and four, respectively.

In the present investigation, the following material properties are specified:

1. Original elastic properties are (for nonlinear finite element analysis)

   E_x = 100993 MPa ; E_y = 95793.6 MPa ; E_z = 100593 MPa ;

   G_{xy} = 36147.6 MPa ; ν_{yx} = 0.361 ; ν_{zy} = 0.345 ; ν_{zx} = 0.341

2. Yield stresses in the respective directions are given by

   σ_{0x} = 579.2 MPa ; σ_{0y} = 472.3 MPa ; σ_{0z} = 630.9 MPa; τ_{0xy} = 262.9 MPa

3. Modified initial elastic properties based on Eq. (7.33) are as follows:

$E_x = 335473$ MPa ; $E_y = 223067$ MPa ; $E_z = 398035$ MPa ;

$G_{xy} = 69116$ MPa ; $\nu_{yx} = 0.519$; $\nu_{zy} = 0.751$; $\nu_{zx} = 0.189$

7.4.1 Orthotropic Cylinder under Internal Pressure

A cylinder under internal pressure is analyzed axisymmetrically with axial plane strain condition. The material is orthotropic along the axial, radial and hoop direction. The inner radius of the cylinder is 30 mm, and the outer radius is 40 mm. An internal pressure of 250 MPa is applied. The material properties in the above section are used. The variation of the multipliers predicted by various methods versus iteration is plotted in Figure 7.1.

It can be seen that the multipliers rapidly converge to the inelastic FEA value in the second and third iterations. The m_α multiplier is closer to the inelastic value than the lower bound value from the elastic compensation method.

7.4.2 Transversely Isotropic Bridgman Notch Bar under Tensile Load

A Bridgman notch bar subjected to remote tensile load is modeled and analyzed axisymmetrically. It is assumed that the material is transversely isotropic, which means the material is isotropic in the *x-z* plane. The material properties are specified as follows:

1. Original elastic properties are (for nonlinear finite element analysis)

$E_x = E_z = 100993$ MPa ; $E_y = 95793.6$ MPa ;

$G_{xy} = 36147.6$ MPa ; $\nu_{yx} = \nu_{yz} = 0.361$; $\nu_{zx} = 0.341$

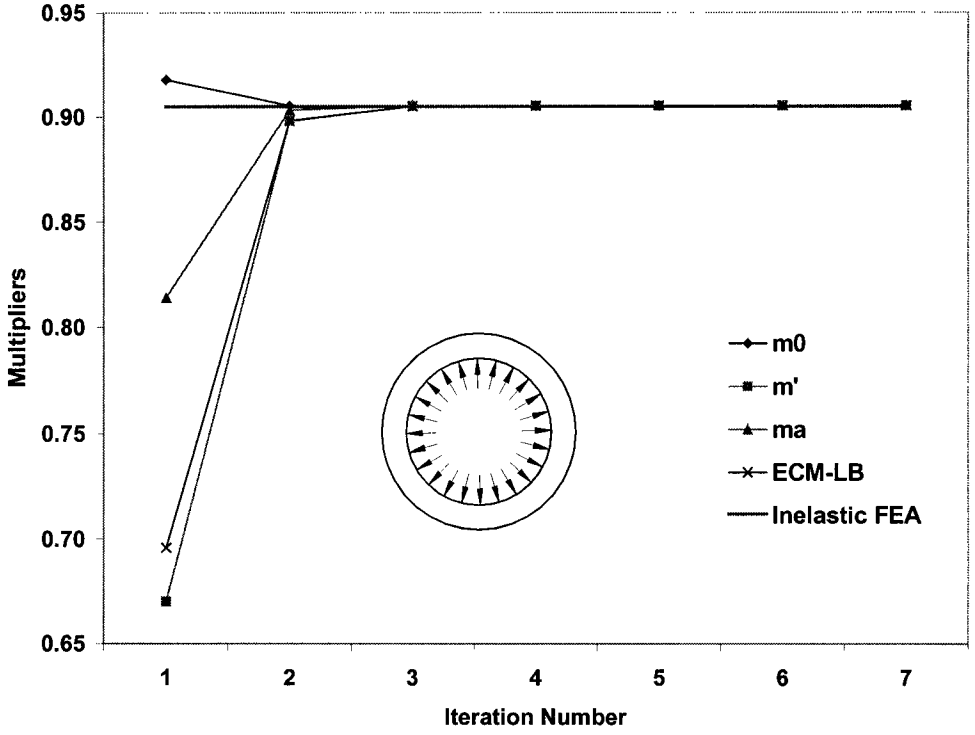

Figure 7.1 Variation of multipliers versus iteration for orthotropic cylinder under internal pressure

2. Yield stresses in the respective directions are given by

$\sigma_{0x} = \sigma_{0z} = 579.2$ MPa ; $\sigma_{0y} = 472.3$ MPa ; $\tau_{0xy} = 262.9$ MPa

3. Modified initial elastic properties based on Eq. (7.33) are as follows:

$E_x = E_z = 335473$ MPa ; $E_y = 223067$ MPa ;

$G_{xy} = 69116$ MPa ; $\nu_{yx} = \nu_{yz} = 0.470$; $\nu_{zx} = 0.233$

The notched bar has a maximum diameter of 26.416 mm, minimum diameter of 21.082 mm and notch radius of 6.858 mm. The remote tensile load is 500 MPa. The variation of the multipliers predicted by various methods versus iteration is plotted in Figure 7.2.

From the figure, the m_α multiplier converges to the inelastic value in the fourth iteration and its value is much better than the lower bound value from the elastic compensation method.

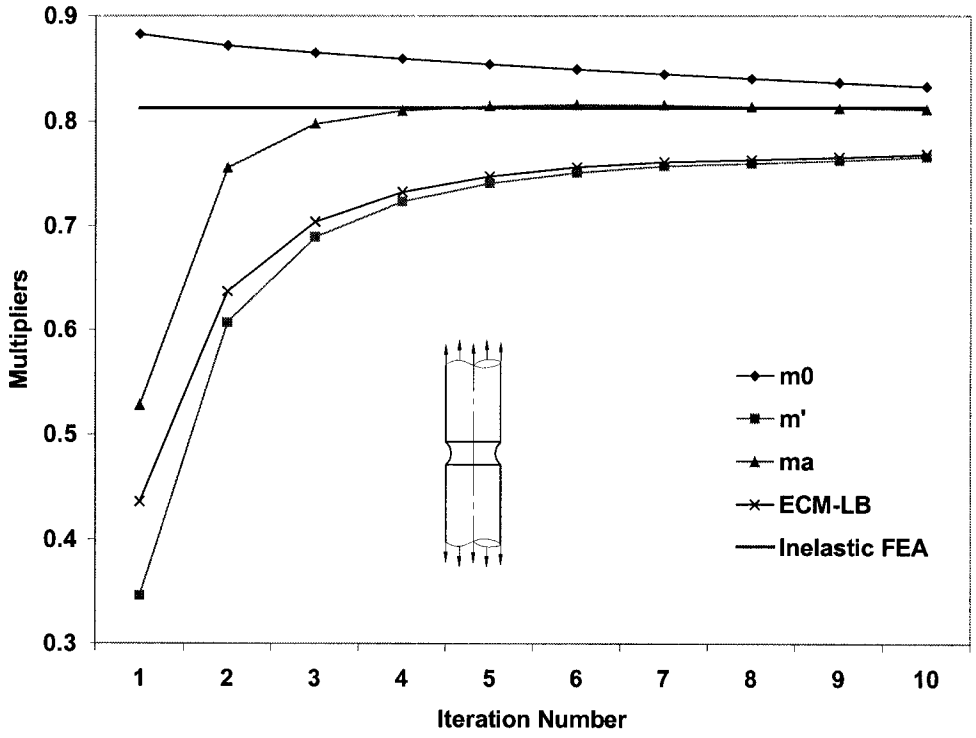

Figure 7.2 Variation of multipliers versus iteration for transversely isotropic Bridgman notch bar

7.5 Conclusions

A procedure is proposed to extend the m_α multiplier method to anisotropic materials. The secant modulus in the reference direction in the elastic analyses is used to estimate the plastic flow parameter for the anisotropic components. Modified initial elastic properties are adopted to ensure the "elastic" stress fields follow the anisotropic yield surface. This method gives improved limit loads compared with the elastic compensation method. It is robust and applicable to components and structures made of more general anisotropic materials.

Chapter 8 Conclusions and Recommendations

8.1 Conclusions

The concept of plastic flow parameter is introduced to the existing m_α procedures to formulate the modified m_α - multiplier method. The introduction of the plastic flow parameter is to account for the plastic flow variation in a component or structure at collapse. The secant modulus of every element in repeated linear elastic analyses is used to evaluate the plastic flow parameter. Numerical examples show that the multipliers m^0, m', and m_α predicted by the modified formulation give improved estimations of the limit load compared to the basic m_α multiplier method. The m_α predictions are usually a lower bound, and closer to inelastic FEA or analytical value compared to the lower bound estimates by elastic compensation method.

A study on the bounds of the multipliers has demonstrated that the multiplier m^0 is greater than the classical upper bound and m' is lower than the classical lower bound. The theoretical maximum possible overestimation of the m_α multiplier is 25%, and the worst practical example as found in the study gives 15%. However, the trend of overestimation can be often detected. In some cases, a refined finite element mesh is able to eliminate or reduce the overestimation.

The application of the modified m_α - multiplier method to several cracked components yields satisfactory estimation of limit loads. The limit load obtained is used to evaluate elastic-plastic J-integral of the corresponding cracked component by the method of Seshadri and Wu. The results are conservative and close to the inelastic FEA value.

The m_α - multiplier procedures for layered structures are formulated by extending Mura's variational principle to inhomogeneous bodies. The initial elastic modulus of each layer is adjusted according to its yield stress to represent its load-carrying capacity at collapse state. The formulation is tested using two- and three- layered beams and cylinders under various material combinations. The results are excellent for cylinders and very good for beams.

The m_α - multiplier procedures for components and structures made of anisotropic materials are also devised. The anisotropic plastic flow parameter is evaluated by utilizing the secant modulus of the discretized finite elements in the reference direction. A method of adjusting the initial anisotropic elastic parameters by using the anisotropic flow rule is adopted so that all moduli at a point can be adjusted in the same degree using the anisotropic equivalent stress. The application of this formulation to two anisotropic components gives very good results.

In summary, the modified m_α - multiplier method can be applied to a wide range of structures and components for simple and direct estimation of limit load. The introduction of plastic flow parameter facilitates the convergence of multipliers and improves the accuracy of estimations. The estimated m_α - multiplier is usually a lower

bound with limited chances and degree to give an upper bound value. This method is very useful in the assessment and design of mechanical components and structures.

8.2 Recommendations

The modified m_α - multiplier formulation for layered structures can be applied to welded structures to deal with the inhomogeneity of the components. This extension is easy to implement in principle.

The modified m_α - multiplier formulation for anisotropic materials can be extended to a more general class of yield criteria other than the current Hill's yield criteria for orthotropic materials. The load bearing capacity of soils can be an area of application.

Finally, more effort is needed to provide modeling guidelines for the modified m_α - multiplier formulation to obtain closer upper and lower bounds, especially to ensure the m_α multiplier a close lower bound. The finite element technique is an approximate method, and the displacement formulation generates a discontinuous stress field, which only satisfies the equilibrium equations at certain points within the element. Avoiding local stress errors to acquire accurate value of the maximum stress is important to a mainly lower bound technique. Hence, it is critical to have an appropriate mesh size, element type, stress extraction point and so on to prevent both over-conservatism and overestimation, especially for cracked and highly indeterminate structures. Guidelines and measures for appropriate modeling should be developed.

Publications and Presentations

1. L. Pan and R. Seshadri, 2002, "Limit Load Estimation Using Plastic Flow Parameter in Repeated Elastic Finite Element Analyses," Journal of Pressure Vessel Technology, Vol. 124, pp. 433-439.

2. L. Pan and R. Seshadri, 2002, "Limit Loads for Layered Structures Using Extended Variational Principles and Repeated Elastic Finite Element Analysis," Journal of Pressure Vessel Technology, Vol. 124, pp. 425-432.

3. L. Pan and R. Seshadri, 2002, "Limit Analysis for Anisotropic Solids using Variational Principle and Repeated Elastic Finite Element Analyses," Proceedings of ASME Pressure Vessels and Piping Conference, PVP-Vol. 442, pp. 149-155.

4. L. Pan and R. Seshadri, 2001, "Limit Load Estimation using Plastic Flow Parameter in Repeated Elastic Finite Element Analyses," Proceedings of ASME Pressure Vessels and Piping Conference, PVP-Vol. 430, pp. 145-150.

5. L. Pan and R. Seshadri, 2001, "Limit Loads for Layered Structures using Extended Variational Principles and Repeated Elastic Finite Element Analysis," Proceedings of ASME Pressure Vessels and Piping Conference, PVP-Vol. 430, pp. 151-154.

6. L. Pan and R. Seshadri, 2001, "Limit Load Estimation for Layered Structures," Proceedings of 18th Canadian Congress of Applied Mechanics, Vol.2, pp. 315-316.

7. L. Pan and R. Seshadri, 2001, "Limit Load Estimation using Secant Modulus in Repeated Elastic Finite Element Analyses," Proceedings of 18th Canadian Congress of Applied Mechanics, Vol. 2, pp. 323-324.

8. S. Babu, L. Pan and R. Seshadri, 2000, "Extended GLOSS method for determining inelastic effects in mechanical components and structures: anisotropic materials," Proceedings of ASME Pressure Vessels and Piping Conference, PVP-Vol. 401, pp. 109-113.

References

1. Anderson, T. L., 1995, Fracture Mechanics: Fundamentals and Applications, CRC Press, Boca Raton, Florida, USA.

2. ANSYS, 1998, ANSYS User's Manual for Revision 5.5, SAS IP, Inc.

3. ASME, 1992, Boiler and Pressure Vessel Code, Sections III and VIII. American Society of Mechanical Engineers, New York, USA.

4. Babu, S. and Iyer, P. K., 1998, "Inelastic Analysis of Components Using a Modulus Adjustment Scheme," Journal of Pressure Vessel Technology, Vol. 120, pp. 1-5.

5. Babu, S. and Iyer, P. K., 1999, "A Robust Method for Inelastic Analysis of Components Made of Anisotropic Material," Journal of Pressure Vessel Technology, Vol. 121, pp. 154-159.

6. Barsoum, R. S., 1976, "On the Use of Isoparametric Finite Elements in Linear Fracture Mechanics," International Journal for Numerical Methods in Engineering, Vol. 10, pp. 25-37.

7. Barsoum, R. S., 1977, "Triangular Quarter-point elements as Elastic and Perfectly-plastic Crack Tip Elements," International Journal for Numerical Methods in Engineering, Vol. 11, pp. 85-98.

8. Berak, E. G., and Gerdeen, J. C., 1990, "A Finite Element Technique for Limit Analysis of Structures," Journal of Pressure Vessel Technology, Vol. 112, pp. 138-144.

9. Boyle, J. T., 1982, "The Theorem of Nesting Surfaces in Steady Creep and Its Application to Generalized Models and Limit Reference Stress," Res Mechanica, Vol. 4, pp. 275-294.

10. Boyle, J. T., Hamilton, R., Shi, J. and Mackenzie, D., 1997, "A Simple Method of Calculating Lower-Bound Limit Loads for Axisymmetric Thin Shells," Journal of Pressure Vessel Technology, Vol. 119, pp. 236-242.

11. Calladine, C. R., 1969, Engineering Plasticity, Pergamon Press, Oxford, U.K.

12. Calladine, C. R. and Drucker, D. C., 1962, "Nesting Surfaces of Constant Rate of Energy Dissipation in Creep," Quarterly of Applied Mathematics, Vol. 20, No. 1, pp. 79-84.

13. Chen, H. and Ponter, A. R. S., 2001, "A Method for the Evaluation of a Ratchet Limit and the Amplitude of Plastic Strain for Bodies Subjected to Cyclic Loading," European Journal of Mechanics – A / Solids, Vol. 20, pp. 555-571.

14. Chen, H. F., and Shu, D. W., 1999, "A Numerical Method for Lower Bound Limit Analysis of 3-D Structures with Multi-loading Systems," International Journal of Pressure Vessels and Piping, Vol. 76, pp. 105-112.

15. Chen, H. F., and Shu, D. W., 2000, "Lower and Upper Bound Limit Analyses for Pipeline with multi-slots of Various Configurations," International Journal of Pressure Vessels and Piping, Vol. 77, pp. 17-25.

16. Chen, W. F. and Han, D. J., 1988, Plasticity for Structural Engineers, Springer-Verlag, New York, USA.

17. Dhalla, A. K., 1991, "Stress Classification for Elevated Temperature Service," Journal of Pressure Vessel Technology, Vol. 113, pp. 488-496.

18. Fowler, C. G., 1998, "Robust Estimation of Limit Loads for Cracked Components," M. Eng. Thesis, Faculty of Engineering and Applied Science, Memorial University of Newfoundland.

19. Gdoutos, E. E., 1990, Fracture Mechanics Criteria and Applications, Kluwer Academic Publishers, Dordrecht, The Netherlands.

20. Hill, R., 1950, "The Mathematical Theory of Plasticity," Oxford University Press, London.

21. Hoff, N. J., 1954, "Approximate Analysis of Structures in the Presence of Moderately Large Creep Deformations," Quarterly of Applied Mathematics, Vol. 12, No. 1, pp. 49-55.

22. Jones, G. L. and Dhalla, A. K., 1981, "Classification of Clamp Induced Stresses in Thin-Walled Pipe," ASME Paper 81-PVP-17, American Society of Mechanical Engineers, New York, USA.

23. Jones, R. M., 1975, "Mechanics of Composite Materials," Scripta Book Company, Washington, D. C.

24. Keeney, J. A. and Bass, B. R., "Fracture Analysis of the NESC-1 Spinning Cylinder Experiment," Journal of Pressure Vessel Technology, Vol. 119, pp. 52-56.

25. Kraus, H., 1980, Creep Analysis, Wiley-Interscience Publication, New York, USA.

26. deLorenzi, H. G., 1982, "Elastic-Plastic Analysis of the Maximum Postulated Flaw in the Beltline Region of a Reactor Vessel," Journal of Pressure Vessel Technology, Vol. 104, pp. 278-286.

27. Mackenzie, D. and Boyle, J. T., 1993a, "A Method of Estimating Limit Loads by Iterative Elastic Analysis. I – Simple Examples," International Journal of Pressure Vessels and Piping, Vol. 53, pp. 77-95.

28. Mackenzie, D. and Boyle, J. T., 1993b, "A Simple Method of Estimating Shakedown Loads for Complex Structures," Proceedings of ASME Pressure Vessels and Piping Conference, PVP-Vol. 265, pp. 89-94.

29. Mackenzie, D., Boyle, J. T. and Hamilton, R., 2000, "The Elastic Compensation Method for Limit and Shakedown Analysis: a Review," Journal of Strain Analysis, Vol. 35, No. 3, 171-188.

30. Mackenzie, D., Boyle, J. T., Hamilton, R., and Shi, J., 1995, "Secondary Stress and Shakedown in Axisymmetric Nozzles," Proceedings of ASME Pressure Vessels and Piping Conference, PVP-Vol. 313-1, pp. 409-413.

31. Mackenzie, D., Nadarajah, C., Shi, J. and Boyle, J. T., 1993, "Simple Bounds on Limit Loads by Elastic Finite Element Analysis," Journal of Pressure Vessel Technology, vol. 115, pp. 27-31.

32. Mackenzie, D., Shi, J. and Boyle, J. T., 1994, "Finite Element Modeling for Limit Analysis by the Elastic Compensation Method," Computers & Structures, Vol. 51, No. 4, pp. 403-410.

33. Maier, G., Grierson, D. E. and Best, M. J., 1977, "Mathematical Programming Methods for Deformation Analysis at Plastic Collapse," Computers & Structures, Vol. 7, pp. 599-612.

34. Mangalaramanan S. P., 1997a, "Conceptual Models for Understanding the Role of the R-Nodes in Plastic Collapse," Journal of Pressure Vessel Technology, Vol. 119, pp. 374-378.

35. Mangalaramanan S. P., 1997b, "Robust Limit Loads Using Elastic Modulus Adjustment Techniques," Ph. D. Thesis, Faculty of Engineering and Applied Science, Memorial University of Newfoundland.

36. Mangalaramanan, P. and Reinhardt, W., 2001, "On Relating Redistributed Elastic and Inelastic Stress Fields," International Journal of Pressure Vessels and Piping, Vol. 78, n. 4, pp. 283-293.

37. Mangalaramanan, S. P. and Seshadri, R., 1997, "Minimum Weight Design of Pressure Components Using R-Nodes," Journal of Pressure Vessel Technology, Vol. 119, pp. 224-231.

38. Mangalaramanan, S. P., Seshadri, R. and Reinhardt, W., 1999, "Limit Loads of Orthotropic Structures using the R-node Method," Proceedings of ASME Pressure Vessels and Piping Conference, PVP-Vol. 388, pp. 241-249.

39. Marriott, D. L., 1988, "Evaluation of Deformation or Load Control of Stresses Under Inelastic Conditions using Elastic Finite Element Stress Analysis," Proceedings of ASME Pressure Vessels and Piping Conference, Pittsburgh, PVP-Vol. 136, pp. 3-9.

40. Marriott D. L. and Leckie F. A., 1964, "Some Observations on the Deflections of Structures during Creep," Proceedings of the Institution of Mechanical Engineers, Vol. 178, Part 3L, pp. 115-125.

41. Mendelson, A., 1968, Plasticity: Theory and Application, The MacMillan Company, New York, USA.

42. Miller, A. G., 1988, "Review of Limit Loads of Structures Containing Defects," International Journal of Pressure Vessels and Piping, Vol. 32, pp. 197-327.

43. Milne, I., Ainsworth, R. A., Dowling, A. R., and Stewart, A. T., 1988, "Assessment of the Integrity of Structures Containing Defects," International Journal of Pressure Vessels and Piping, Vol. 32, pp. 3-104.

44. Mohamed, A. I., Megahed, M. M., Bayoumi, L. S. and Younan, M. Y. A., 1999, "Applications of Iterative Elastic Techniques for Elastic-Plastic Analysis of Pressure Vessels," Journal of Pressure Vessel Technology, Vol. 121, pp. 24-29.

45. Mura, T. and Koya, T., 1992, Variational Methods in Mechanics, Oxford University Press, New York, USA.

46. Mura, T. and Lee, S. L., 1963, "Application of Variational Principles to Limit Analysis," Quarterly of Applied Mathematics, Vol. 21, No. 3, pp. 243-248.

47. Mura, T., Lee, S. L. and Rimawi, W. H., 1968, "A Variational Method for Limit Analysis of Anisotropic and Nonhomogeneous Solids," Developments in Theoretical and Applied Mechanics. Volume 4 - Proceedings of the Fourth Southeastern Conference on Theoretical and Applied Mechanics, New Orleans, LA, USA, pp. 541-549.

48. Mura, T., Rimawi, W. H. and Lee, S. L., 1965, "Extended Theorems of Limit Analysis," Quarterly of Applied Mathematics, Vol. 23, No. 2, pp. 171-179.

49. Nadarajah, C., Mackenzie, D. and Boyle, J. T., 1993, "A Method of Estimating Limit Loads by Iterative Elastic Analysis. II – Nozzle Sphere Intersections with Internal Pressure and Radial Load," International Journal of Pressure Vessels and Piping, Vol. 53, pp. 97-119.

50. Newman Jr., J. C. and Raju, I. S., 1980, "Stress-Intensity Factors for Internal Surface Cracks in Cylindrical Pressure Vessels," Journal of Pressure Vessel Technology, Vol. 102, pp. 342-346.

51. Parton, V. Z. and Morozov, E. M., 1989, Mechanics of Elastic-Plastic Fracture, Hemisphere Publishing Corporation, Washington DC, USA.

52. Pastor, T. P. and Hechmer, J., 1997, "ASME Task Group Report on Primary Stress," Journal of Pressure Vessel Technology, Vol. 119, pp. 61-67.

53. Plancq, D. and Berton, M. N., 1998, "Limit Analysis Based on Elastic Compensation Method of Branch Pipe Tee Connection under Internal Pressure and Out-of-plane Moment Loading," International Journal of Pressure Vessels and Piping, Vol. 75, pp. 819-825.

54. Ponter, A. R. S. and Carter, K. F., 1997a, "Limit State Solutions, Based upon Linear Elastic Solutions with a Spatially Varying Elastic Modulus," Computer Methods in Applied Mechanics and Engineering, Vol. 140, pp. 237-258.

55. Ponter, A. R. S. and Carter, K. F., 1997b, "Shakedown State Simulation Techniques Based on Linear Elastic Solutions," Computer Methods in Applied Mechanics and Engineering, Vol. 140, pp. 259-279.

56. Ponter, A. R. S., and Chen, H., 2001, "A Minimum Theorem for Cyclic Load in Excess of Shakedown, with Application to the Evaluation of a Ratchet Limit," European Journal of Mechanics – A / Solids, Vol. 20, pp. 539-553.

57. Ponter, A. R. S., and Engelhardt, M., 2000, "Shakedown Limits for a General Yield Condition: Implementation and Application for a Von Mises Yield Condition," European Journal of Mechanics – A / Solids, Vol. 19, pp. 423-445.

58. Ponter, A. R. S., Fuschi, P. and Engelhardt, M., 2000, "Limit Analysis for a General Class of Yield Conditions," European Journal of Mechanics – A / Solids, Vol. 19, pp. 401-421.

59. Ralph, F. E., 2000, "Robust Methods of Finite Element Analysis: Evaluation of Non-linear, Lower Bound Limit Loads of Plated Structures and Stiffening Members," M. Eng. Thesis, Faculty of Engineering and Applied Science, Memorial University of Newfoundland.

60. Reinhardt, W. D. and Mangalaramanan, S. P., 1999, "Efficient Tubesheet Design Using Repeated Elastic Limit Analysis," Proceedings of ASME Pressure Vessels and Piping Conference, PVP-Vol. 385, pp. 141-149.

61. Reinhardt, W. D. and Mangalaramanan, S. P., 2000, "Plastic Limit Analysis of a Tubesheet Using an Elastic Modulus Modification Method," Proceedings of ASME Pressure Vessels and Piping Conference, PVP-Vol. 400, pp. 253-261.

62. Reinhardt, W. D., and Seshadri, R., 2003, "Limit Load Bounds for the m_α Multiplier," To be published in the Journal of Pressure Vessel Technology, Vol. 125, pp. 1-8.

63. Rice, J. R. and G. F. Rosengren, 1968, "Plane Strain Deformation near a Crack Tip in a Power-law Hardening Material," Journal of Mechanics and Physics of Solids, Vol. 16, pp. 1-12.

64. Rimawi, W. H., Mura, T. and Lee, S. L., 1966, "Extended Theorems of Limit Analysis of Anisotropic Solids," Developments in Theoretical and Applied Mechanics. Volume 3 - Proceedings of the Third Southeastern Conference on Theoretical and Applied Mechanics, Columbia, SC, USA, pp. 57-71.

65. Schulte, C. A., 1960, "Predicting Creep Deflections of Plastic Beams," Proceedings - American Society for Testing and Materials, Vol. 60, pp. 895-904.

66. Seshadri, R., 1991, "The Generalized Local Stress Strain (GLOSS) Analysis - Theory and Applications," Journal of Pressure Vessel Technology, Vol. 113, pp. 219-227.

67. Seshadri, R., 1996, "Robust Stress-Classification of Pressure Components Using the GLOSS and GLOSS R-Node Methods," Journal of Pressure Vessel Technology, Vol. 118, pp. 208-215.

68. Seshadri, R., 1997, "In Search of Redistribution Nodes," International Journal of Pressure Vessels and Piping, Vol. 73, pp. 69-76.

69. Seshadri, R., 2000, "Limit Loads Using Extended Variational Concepts in Plasticity," Journal of Pressure Vessel Technology, Vol. 122, pp. 379-385.

70. Seshadri, R. and Babu, S., 2000, "Extended GLOSS Method for Determining Inelastic Effects in Mechanical Components and Structures: Isotropic Materials," Journal of Pressure Vessel Technology, Vol. 122, pp. 413-420.

71. Seshadri, R. and Fernando, C. P. D., 1992, "Limit Loads of Mechanical Components and Structures Using the GLOSS R-Node Method," Journal of Pressure Vessel Technology, Vol. 114, pp. 201-208.

72. Seshadri, R. and Kizhatil, R. K., 1993, "Notch Root Inelastic Strain Estimates Using GLOSS Analysis," Advances in Multiaxial Fatigue, ASTM STP 1191, D. L. McDowell and R. Ellis, Eds., American Society for Testing and Materials, Philadelphia, pp. 397-411.

73. Seshadri, R. and Kizhatil, R. K., 1995, "Robust Approximate Methods for Estimating Inelastic Fracture Parameters," Journal of Pressure Vessel Technology, Vol. 117, pp. 115-123.

74. Seshadri, R. and Mangalaramanan, S. P., 1997, "Lower Bound Limit Loads Using Variational Concepts: the m_α-method," International Journal of Pressure Vessels and Piping, Vol. 71, pp. 93-106.

75. Seshadri, R. and Marriott, D. L., 1992, "On Relating the Reference Stress, Limit Load and the ASME Stress Classification Concepts," Proceedings of ASME Pressure Vessels and Piping Conference, PVP-Vol. 230, pp. 135-149.

76. Seshadri, R. and Wu, S., 2001, "Robust Estimation of Inelastic Fracture Energy Release Rate (J): A Design Approach," Journal of Pressure Vessel Technology, Vol. 123, pp. 214-219.

77. Shi, C. F. and Lee, D., 1978, "Further Developments in Anisotropic Plasticity," Journal of Engineering Materials and Technology, Vol. 100, pp. 294-302.

78. Shi, J., Mackenzie, D. and Boyle, J. T., 1993, "A Method of Estimating Limit Loads by Iterative Elastic Analysis. III – Torispherical Heads under Internal Pressure," International Journal of Pressure Vessels and Piping, Vol. 53, pp. 121-142.

79. Webster, G. A., and Ainsworth, R. A., 1994, High Temperature Component Life Assessment, Chapman & Hall, London, U.K.

80. Valliappan, S., 1972, "Elasto-plastic Analysis of Anisotropic Work-hardening Materials," Archives of Mechanics, Vol. 24, No. 3, pp. 465-481.

81. Valliappan, S., Boonlaulohr, P. and Lee, I. K., 1976, "Non-linear Analysis for Anisotropic Materials," International Journal for Numerical Methods in Engineering, Vol. 10, pp. 597-606.

82. Zhang, Yuan-Gao, and Lu, Ming-Wan, 1995, "An Algorithm for Plastic Limit Analysis," Computer Methods in Applied Mechanics and Engineering, Vol. 126, pp. 333-341.

Appendix A ANSYS Models for Major Components

The following lists sixteen ANSYS files for the major components analyzed using the m_α multiplier method. Five models (A.4–A.7, A.11) are adopted from the thesis by Mangalaramanan (1997b) and two (A.10 and A.12) are from the thesis by Fowler (1998) with modification. The model for cylinder with semi-elliptical crack is not included since it was created by using graphic user interface.

A. 1 Thick Cylinder under Internal Pressure

```
/BATCH

*SET,RI,3                       ! INNER RADIUS, INCH
*SET,RO,9                       ! OUTER RADIUS, INCH
*SET,DIV,30                     ! DIVISION NUMBER IN RADIAL DIRECTION
*SET,HI,(RO-RI)/DIV             ! LENGTH
*SET,PRSR,40000                 ! INTERNAL PRESSURE, PSI

*SET,YM,30E6                    ! YOUNG'S MODULUS
*SET,POIS,0.47                  ! POISSON'S RATIO
*SET,YS,30000                   ! YIELD STRESS, PSI

/PREP7

ET,1,42                         ! DEFINE ELEMENT TYPE AND BEHAVIOR
KEYOPT,1,3,1

MP,EX,1,YM                      ! DEFINE ELASTIC MATERIAL PROPERTY
MP,NUXY,1,POIS

K,1,RI,0                        ! DEFINE GEOMETRY
K,2,RO,0
K,3,RO,HI
K,4,RI,HI
L,1,2,DIV,1
L,2,3,1
L,3,4,DIV,1
```

```
L,4,1,1
A,1,2,3,4

AMESH,1

/SOLUTION

ANTYPE,0

D,ALL,UY,0                          ! APPLY BOUNDARY CONDITIONS

NSEL,S,LOC,X,RI
SF,ALL,PRES,PRSR
NSEL,ALL

SOLVE
SAVE
FINISH

/INPUT,ms,txt                       ! CALL MACRO TO CALCULATE MULTIPLIERS
```

A. 2 Thick Cylinder under Internal Pressure (Nonlinear Analysis)

```
/BATCH

*SET,RI,3                           ! INNER RADIUS, INCH
*SET,RO,9                           ! OUTER RADIUS, INCH
*SET,DIV,30                         ! DIVISION NUMBER IN RADIAL DIRECTION
*SET,HI,(RO-RI)/DIV                 ! LENGTH
*SET,PRSR,40000                     ! INTERNAL PRESSURE, PSI

*SET,YM,30E6                        ! YOUNG'S MODULUS
*SET,POIS,0.47                      ! POISSON'S RATIO
*SET,YS,30000                       ! YIELD STRESS, PSI

/PREP7

ET,1,42                             ! DEFINE ELEMENT TYPE AND BEHAVIOR
KEYOPT,1,3,1

MP,EX,1,YM                          ! DEFINE ELASTIC MATERIAL PROPERTY
MP,NUXY,1,POIS

TB,BKIN,1,1                         ! DEFINE PLASTIC MATERIAL PROPERTY
TBDATA,1,YS,0

K,1,RI,0                            ! DEFINE GEOMETRY
K,2,RO,0
K,3,RO,HI
K,4,RI,HI
L,1,2,DIV,1
L,2,3,1
```

```
L,3,4,DIV,1
L,4,1,1
A,1,2,3,4

AMESH,1

/SOLUTION

ANTYPE,0

TIME,1                          ! DEFINE NONLINEAR SOLUTION CONTROL
AUTOTS,1
KBC,0
NSUBST,100,500,20,0
NEQIT,40

OUTRES,ALL,ALL

D,ALL,UY,0                      ! APPLY BOUNDARY CONDITIONS

NSEL,S,LOC,X,RI
SF,ALL,PRES,PRSR
NSEL,ALL

SOLVE
SAVE
FINISH
```

A. 3 Indeterminate Beam

```
/BATCH

*SET,SPAN,20                    ! BEAM SPAN, INCH
*SET,HI,1                       ! BEAM HEIGHT, INCH
*SET,HI1,0.5
*SET,HI2,HI-HI1
*SET,PRSR,300                   ! UNIFORMLY DISTRIBUTED LOAD, PSI
*SET,DIVH,200                   ! DIVISION ALONG THE SPAN
*SET,DIVV,14                    ! DIVISION ALONG THE HEIGHT
*SET,RTH,3                      ! SPACING RATIO ALONG THE SPAN
*SET,RTV,-2                     ! SPACING RATIO ALONG THE HEIGHT

*SET,YM,30E6                    ! YOUNG'S MODULUS, PSI
*SET,POIS,0.47                  ! POISSON'S RATIO
*SET,YS,30E3                    ! YIELD STRESS, PSI

/PREP7

ET,1,42                         ! DEFINE ELEMENT TYPE AND BEHAVIOR
KEYOPT,1,3,0

MP,EX,1,YM                      ! DEFINE MATERIAL PROPERTY
```

```
MP,NUXY,1,POIS

K,1,0,-HI2                          ! DEFINE GEOMETRY
K,2,SPAN,-HI2
K,3,SPAN,HI1
K,4,0,HI1
L,1,2,DIVH,RTH
L,3,2,DIVV,RTV
L,3,4,DIVH,1/RTH
L,4,1,DIVV,RTV
A,1,2,3,4

AMAP,1,1,2,3,4
FINISH

/SOLU

ANTYPE,0

NSEL,S,LOC,X,0                      ! APPLY BOUNDARY CONDITION
D,ALL,UX,0

NSEL,R,LOC,Y,0
D,ALL,UY,0
NSEL,ALL

NSEL,S,LOC,X,1.005*SPAN
NSEL,R,LOC,Y,-HI2
D,ALL,UY,0
NSEL,ALL

NSEL,S,LOC,Y,HI1
SF,ALL,PRES,PRSR
NSEL,ALL

SAVE
SOLVE
FINISH

/INPUT,ms,txt                       ! CALL MACRO TO CALCULATE MULTIPLIERS
```

A. 4 Non-Symmetric Rectangular Plate

```
/BATCH

*SET,THIK,0.5                       ! THICKNESS OF PLATE, INCH
*SET,LENG,15                        ! LENGTH OF PLATE, INCH
*SET,WDTH,10                        ! WIDTH OF PLATE, INCH
*SET,LDIV,30                        ! DIVISIONS ALONG LENGTH
*SET,WDIV,21                        ! DIVISIONS ALONG WIDTH

*SET,PRSR,1000                      ! APPLIED PRESSURE, PSI
```

```
*SET,YM,30E06                    ! YOUNG'S MODULUS, PSI
*SET,YS,30E03                    ! YIELD STRESS, PSI
*SET,POIS,0.3                    ! POISSON'S RATIO

/PREP7

ET,1,45                          ! ELEMENT TYPE AND MATERIAL PROPERTY
MP,EX,1,YM
MP,NUXY,1,POIS

K,1,0,0,0                        ! DEFINE GEOMETRY
K,2,WDTH,0,0
K,3,WDTH,THIK,0
K,4,0,THIK,0
K,5,0,0,LENG
K,6,WDTH,0,LENG
K,7,WDTH,THIK,LENG
K,8,0,THIK,LENG

L,1,2,WDIV,-5
L,1,4,4
L,2,3,4
L,4,3,WDIV,-5
L,1,5,LDIV,-5
L,4,8,LDIV,-5
L,3,7,LDIV,-5
L,2,6,LDIV,-5
L,5,8,4
L,7,6,4
L,7,8,WDIV,-5
L,5,6,WDIV,-5

V,1,4,8,5,2,3,7,6
VMESH,ALL

FINISH

/SOLU

ANTYPE,0

NSEL,S,LOC,X,WDTH/3,2*WDTH/3    ! APPLY NON-SYMMETRIC BOUNDARY CONDITION
NSEL,R,LOC,Y,0
NSEL,R,LOC,Z,0
D,ALL,UY,0
NSEL,ALL

NSEL,S,LOC,X,WDTH
NSEL,R,LOC,Z,0,LENG/3
D,ALL,ALL,0
NSEL,ALL

NSEL,S,LOC,X,WDTH
NSEL,R,LOC,Z,2*LENG/3,LENG
```

```
D,ALL,ALL,0
NSEL,ALL

NSEL,S,LOC,X,0
NSEL,R,LOC,Z,LENG/3,2*LENG/3
D,ALL,ALL,0
NSEL,ALL

NSEL,S,LOC,X,0,WDTH/3
NSEL,R,LOC,Y,0
NSEL,R,LOC,Z,LENG
D,ALL,UY,0
NSEL,ALL

NSEL,S,LOC,X,2*WDTH/3,WDTH
NSEL,R,LOC,Y,0
NSEL,R,LOC,Z,LENG
D,ALL,UY,0
NSEL,ALL

NSEL,S,LOC,Y,THIK
SF,ALL,PRES,PRSR
NSEL,ALL

SAVE
SOLVE
FINISH

/INPUT,ms,txt                    ! CALL MACRO TO CALCULATE MULTIPLIERS
```

A. 5 Torispherical Head

```
/BATCH

!R/D=0.12

*SET,PI,3.1416
*SET,YM,206.85E06                ! YOUNG'S MODULUS, kPa
*SET,POIS,0.47                   ! POISSON'S RATIO
*SET,YS,206.85E03                ! YIELD STRESS, kPa
*SET,PRSR,1000                   ! APPLIED PRESSURE, kPa

*SET,T,2.54E-02                  ! THICKNESS OF VESSEL, m
*SET,LSBYD,0.8                   ! DEFINE DIMENSION RATIOS
*SET,RBYD,0.12
*SET,TBYD,1/300

*SET,PHITWO,ASIN((0.5-RBYD)/(LSBYD-RBYD))*180.0/PI   !DEFINE OTHER DIMENSIONS
*SET,PHI1,90.0-PHITWO
*SET,D,T/TBYD
*SET,RK,RBYD*D
*SET,RH,LSBYD*D
```

```
*SET,HH,RH-(RH-RK)*COS(PHITWO*PI/180.0)
*SET,A,D/2-RK
*SET,RI,D/2.0
*SET,RO,RI+T
*SET,H,1.2*5.0*SQRT(RO*T)

*SET,NDIV1,6                    ! DEFINE MESH SIZES
*SET,NDIV2,70
*SET,NDIV3,30
*SET,NDIV4,120

/PREP7

ET,1,42,0,0,1                   ! ELEMENT TYPE AND MATERIAL PROPERTIES
MP,EX,1,YM
MP,NUXY,1,POIS

K,1,RI                          ! DEFINE GEOMETRIES
K,2,RO
K,3,RI,H
K,4,RO,H

LOCAL,11,1,A,H

CSYS,11
K,5,RK,PHI1
K,6,RK+T,PHI1
CSYS,0

LOCAL,12,1,0,H+HH-RH

CSYS,12
K,7,RH,90
K,8,RH+T,90
CSYS,0

L,1,2,NDIV1
L,3,4,NDIV1
L,5,6,NDIV1
L,7,8,NDIV1

L,1,3,NDIV2
L,2,4,NDIV2

CSYS,11
L,3,5,NDIV3
L,4,6,NDIV3

CSYS,12
L,5,7,NDIV4
L,6,8,NDIV4
CSYS,0

A,1,2,4,3
```

```
AMESH,1

CSYS,11
A,3,4,6,5
AMESH,2

CSYS,12
A,5,6,8,7
AMESH,3

CSYS,0                          ! APPLY PRESSURE LOADING
SFL,5,PRES,PRSR

CSYS,11
SFL,7,PRES,PRSR
CSYS,0

CSYS,12
SFL,9,PRES,PRSR
CSYS,0

SFTRAN

NSEL,,LOC,X,0                   ! APPLY DISPLACEMENT BOUNDARY CONDITIONS
D,ALL,UX,0
NSEL,ALL

NSEL,,LOC,Y,0
D,ALL,UY,0
NSEL,ALL

FINISH

/SOLU

ANTYPE,0
SOLVE
SAVE
FINISH

/INPUT,ms,txt                   ! CALL MACRO TO CALCULATE MULTIPLIERS
```

A. 6 Sphere-Nozzle Junction

```
/BATCH

*SET,YM,200.0E6                 ! YOUNG'S MODULUS, kPa
*SET,YS,300.0E3                 ! YIELD STRESS, kPa
*SET,POIS,0.47
*SET,PRSR,150000                ! PRESSURE, kPa

*SET,RS,1.0                     ! DIMENSIONS, METER
```

```
*SET,TS,0.25
*SET,RN,0.20
*SET,TN,2.0*TS*RN/RS
*SET,H,1.2*5.0*SQRT(RN*TN)

*SET,NDIV1,50                    ! LINE DIVISIONS (MESH SIZE)
*SET,NDIV2,6
*SET,NDIV3,11
*SET,NDIV4,40
*SET,NDIV5,12
*SET,NDIV6,60

/PREP7

ET,1,42,0,0,1                    ! ELEMENT TYPE AND MATERIAL PROPERTIES
MP,EX,1,YM
MP,NUXY,1,POIS

RSI=RS-TS/2.0                    ! DEFINE COMPONENT GEOMETRIES
RSO=RS+TS/2.0
RNI=RN-TN/2.0
RNO=RN+TN/2.0

K,1,RSO
K,2,RNO,SQRT(RSO**2-RNO**2)
K,3,RNO,SQRT(RSO**2-RNO**2)+TN/2.0+H
K,4,RNI,SQRT(RSO**2-RNO**2)+TN/2.0+H
K,5,RNI,SQRT(RSO**2-RNO**2)+TN/2.0
K,6,RNI,SQRT(RSI**2-RNI**2)
K,7,RSI
K,12
K,15,,-RSI
K,16,,-RSO

CSYS,1
L,1,2
CSYS,0
L,2,3
L,3,4
L,4,5
L,5,6
CSYS,1
L,6,7
CSYS,0
L,7,1

LOCAL,11,1,RNO+TN/2.0,SQRT(RSO**2-RNO**2)+TN/2.0
CSYS,11
LFILLT,1,2,TN/2.0,10
CSYS,0
L,8,6
L,9,5

L,15,16
```

```
CSYS,1
L,15,7
L,16,1
CSYS,0

KDELE,10
KDELE,2
KDELE,12

LESIZE,1,,,NDIV6,2/5
LESIZE,2,,,NDIV4,2
LESIZE,3,,,NDIV5,2/3
LESIZE,4,,,NDIV4,1/2
LESIZE,5,,,NDIV3
LESIZE,6,,,NDIV6,2.5
LESIZE,7,,,NDIV5,1.5
LESIZE,8,,,NDIV3
LESIZE,9,,,NDIV5,2/3
LESIZE,10,,,NDIV5,2/3
LESIZE,11,,,NDIV5,1.5
LESIZE,12,,,NDIV1,-1.5
LESIZE,13,,,NDIV1,-1.5

CSYS,1
A,15,16,1,7
A,7,1,8,6
CSYS,0
A,6,8,9,5
A,5,9,3,4

ESHAPE,2
AMESH,ALL

FINISH

/SOLU

ANTYPE,0

SFL,4,PRES,PRSR                    ! APPLY PRESSURE LOADING
SFL,5,PRES,PRSR

CSYS,1
SFL,6,PRES,PRSR
SFL,12,PRES,PRSR

CSYS,0
SFTRAN

NSEL,,LOC,Y,SQRT(RSO**2-RNO**2)+TN/2.0+H   ! APPLY DISPLACEMENTS
D,ALL,UY,0
NSEL,ALL

NSEL,,LOC,X,0
```

```
D,ALL,UX,0
NSEL,ALL

SAVE
SOLVE
FINISH

/INPUT,ms,txt                    ! CALL MACRO TO CALCULATE MULTIPLIERS
```

A. 7 Pressure Vessel Support Skirt

```
/BATCH

*SET,PI,3.1415926536
*SET,DI,97.28                    ! DIMENSIONS, INCH
*SET,DO,101.28
*SET,LC,30.0
*SET,DSK,110.07
*SET,SKA,18.05

*SET,YM,30E06                    ! YOUNG'S MODULUS, PSI
*SET,YS,40E03                    ! YIELD STRESS, PSI
*SET,POIS,0.47
*SET,ENLD,40000                  ! END PRESSURE, PSI

*SET,NDIV1,12                    ! LINE DIVISIONS
*SET,NDIV2,28
*SET,NDIV3,23
*SET,NDIV4,5

RI=DI/2.0                        ! DIMENSIONS
RO=DO/2.0
RSK=DSK/2.0
T=RO-RI
THETA=PI/180.0*SKA
H1=(RSK-RO+T/COS(THETA))/TAN(THETA)

/PREP7

ET,1,42,0,0,1,0,0                ! ELEMENT TYPE AND MATERIAL PROPERTY
MP,EX,1,YM
MP,NUXY,1,POIS

K,1,RI                           ! DEFINE GEOMETRY
K,2,RO
K,3,RO,LC
K,4,RI,H1+LC+TAN(PI/2.0-THETA)*(RI-RSK)
K,5,RSK+T/COS(THETA),LC+H1
K,6,RSK,LC+H1

L,1,2
L,6,5
```

```
L,2,3
L,1,4
L,3,5
L,4,6

LOCAL,11,1,RO+T,LC-T
CSYS,11
LFILLT,3,5,T/2.0
LFILLT,4,6,3.0*T/2.0
CSYS,0

L,7,9
L,8,10

KDELE,3
KDELE,4

LDIV,3
LDIV,4
LDIV,5
LDIV,6

LESIZE,1,,,NDIV1
LESIZE,9,,,NDIV1
LESIZE,10,,,NDIV1
LESIZE,2,,,NDIV1

LESIZE,3,,,NDIV2,2
LESIZE,4,,,NDIV2,2
LESIZE,11,,,NDIV2,0.5
LESIZE,12,,,NDIV2,0.5

LESIZE,5,,,NDIV3,2
LESIZE,6,,,NDIV3,2
LESIZE,13,,,NDIV3,0.5
LESIZE,14,,,NDIV3,0.5

LESIZE,7,,,NDIV4
LESIZE,8,,,NDIV4

A,1,2,3,4
A,4,3,7,9
CSYS,11
A,9,7,8,10
CSYS,0
A,10,8,11,12
A,12,11,5,6

ESHAPE,2
AMESH,ALL

FINISH

/SOLU
```

```
NSEL,S,LOC,Y,H1+LC                ! APPLY BOUNDARY CONDITIONS
D,ALL,ALL,0
NSEL,ALL
SFL,1,PRES,ENLD
SFTRAN

SAVE
SOLVE
FINISH

/INPUT,ms,txt                     ! CALL MACRO TO CALCULATE MULTIPLIERS
```

A. 8 Two-Layered Cylinder

```
/BATCH

*SET,RI,80                        ! INNER RADIUS, MILLIMETER
*SET,RINT,130                     ! INTERFACE RADIUS
*SET,RO,230                       ! OUTER RADIUS
*SET,DIV,36                       ! RADIAL DIVISIONS
*SET,RAT,1                        ! RADIAL SPACE RATIO
*SET,HI,(RINT-RI)/DIV             ! LENGTH OF CYLINDER

*SET,PRSR,500                     ! APPLIED PRESSURE, MPa

*SET,YM1,70000                    ! YOUNG'S MODULUS, MPa
*SET,YM2,210000
*SET,POIS,0.47
*SET,YS1,70                       ! YIELD STRESS, MPa
*SET,YS2,210

/PREP7

ET,1,42                           ! DEFINE ELEMENT TYPE
KEYOPT,1,3,1

ET,2,42
KEYOPT,2,3,1

K,1,RI,0                          ! DEFINE GEOMETRY
K,2,RINT,0
K,3,RINT,HI
K,4,RI,HI
L,1,2,(RINT-RI)*DIV/(RO-RI),RAT
L,2,3,1,1
L,4,3,(RINT-RI)*DIV/(RO-RI),RAT
L,4,1,1,1
K,5,RO,0
K,6,RO,HI
L,2,5,(RO-RINT)*DIV/(RO-RI),RAT
L,5,6,1,1
```

```
L,3,6,(RO-RINT)*DIV/(RO-RI),RAT
A,1,2,3,4

MP,EX,1,YM1                    ! MATERIAL PROPERTY
MP,NUXY,1,POIS

TYPE,1
MAT,1
AMESH,1

A,2,5,6,3

MP,EX,2,YM2
MP,NUXY,2,POIS

TYPE,2
MAT,2
AMESH,2

/SOLU

ANTYPE,0
D,ALL,UY,0

NSEL,S,LOC,X,RI                ! APPLY INTERNAL PRESSURE
SF,ALL,PRES,PRSR
NSEL,ALL
SAVE
SOLVE

/INPUT,2ms,txt                 ! CALL MACRO TO CALCULATE MULTIPLIERS
```

A. 9 Two-Layered Beam

```
/BATCH

*SET,SPAN,500                  ! DIMENSION VALUES, MILLIMETER
*SET,HI,24
*SET,HI1,12
*SET,HI2,HI-HI1
*SET,PRSR,1                    ! PRESSURE VALUE, MPa
*SET,HDIV,200                  ! HORIZONTAL DIVISIONS
*SET,HRAT,1                    ! HORIZONTAL SPACE RATIO
*SET,VDIV,24                   ! VERTICAL DIVISIONS
*SET,VRAT,-2                   ! VERTICAL SPACE RATIO

*SET,YM1,70000                 ! YOUNG'S MODULUS, MPa
*SET,YM2,210000
*SET,POIS,0.47
*SET,YS1,70                    ! YIELD STRESS, MPa
*SET,YS2,210
```

```
/PREP7

ET,1,42                          ! ELEMENT TYPE
KEYOPT,1,3,0

ET,2,42
KEYOPT,2,3,0

K,1,0,0                          ! DEFINE GEOMETRY
K,2,SPAN,0
K,3,SPAN,HI1
K,4,0,HI1
L,1,2,HDIV,HRAT
L,3,2,VDIV*HI1/HI,VRAT
L,3,4,HDIV,HRAT
L,4,1,VDIV*HI1/HI,VRAT
K,5,SPAN,-HI2
K,6,0,-HI2
L,5,2,VDIV*HI2/HI,VRAT
L,5,6,HDIV,HRAT
L,6,1,VDIV*HI2/HI,VRAT
A,1,2,3,4

MP,EX,1,YM1                      ! MATERIAL PROPERTY AND MESH
MP,NUXY,1,POIS
TYPE,1
MAT,1
AMAP,1,1,2,3,4

A,1,2,5,6

MP,EX,2,YM2
MP,NUXY,2,POIS
TYPE,2
MAT,2
AMAP,2,1,2,5,6

FINISH

/SOLU

ANTYPE,0

NSEL,S,LOC,X,0                   ! DISPLACEMENT BOUNDARY CONDITION
D,ALL,UX,0
NSEL,R,LOC,Y,0
D,ALL,UY,0
NSEL,ALL

NSEL,S,LOC,X,1.005*SPAN
NSEL,R,LOC,Y,0
D,ALL,UY,0
NSEL,ALL
```

```
NSEL,S,LOC,Y,HI1                    ! PRESSURE LOADING
SF,ALL,PRES,PRSR
NSEL,ALL
SAVE

SOLVE

FINISH

/INPUT,2ms,txt                      ! CALL MACRO TO CALCULATE MULTIPLIERS
```

A. 10 Center-Cracked Plate

```
/BATCH


A=1                                 ! CRACK LENGTH, INCH
YM=30E6                             ! YOUNG'S MODULUS, PSI
YS=25E3                             ! YIELD STRESS, PSI
LOAD=20E3
POIS=0.3
LEN=1                               ! PLATE LENGTH, INCH

/PREP7

ET,1,PLANE82,,,2                    ! ELEMENT TYPE

MP,EX,1,YM                          ! MATERIAL PROPERTY
MP,NUXY,1,POIS

K,1                                 ! DEFINE GEOMETRY
K,2,4
K,3,4,5
K,4,-1,5
K,5,-1
L,1,2
L,2,3
LESIZE,2,,,4
L,3,4
LESIZE,3,,,4
L,4,5,
LESIZE,4,,,6,.2
L,5,1
ESIZE,,5
KSCON,1,.15,1,8                     ! DEFINE CRACK TIP ELEMENT LAYOUT
AL,1,2,3,4,5

DL,1,1,SYMM                         ! BOUNDARY CONDITIONS
DL,4,1,SYMM
SFL,3,PRES,-LOAD

AMESH,1
```

```
OUTPR,ALL
FINISH

/SOLU

ANTYPE,0

SOLVE
SAVE
FINISH

/INPUT,ms,txt                    ! CALL MACRO TO CALCULATE MULTIPLIERS
```

A. 11 Compact Tension Specimen

```
/BATCH

A=0.046                          ! DIMENSION VALUE, METER
B=0.003
W=0.1
W1=0.125
H=0.06
R=0.0125
E=0.0275
S=0.003
D1=0.08
D2=0.075

YM=211E09                        ! YOUNG'S MODULUS, Pa
YS=488.43E06                     ! YIELD STRESS, Pa
POIS=0.3

LOAD=20000/5

/PREP7

MP,EX,1,YM
MP,NUXY,1,POIS

K,1,A                            ! DEFINE GEOMETRY
K,2,W
K,3,W,H
K,4,,H
K,5,W-W1,H
K,6,W-W1,S
K,7,,S
K,8,W-D1,S
K,9,W-D2
K,10,,E
K,11,,E,E
CIRCLE,10,R,11,4,,8
```

```
L,1,2
*REPEAT,8,1,1
L,9,1
L,4,12
L,16,7
KSEL,S,LOC,X,-1E-6,1
LSLK,S,1
AL,ALL
KSEL,S,LOC,X,-1,1E-6
LSLK,S,1
AL,ALL
KSEL,ALL
LSEL,ALL

ET,1,PLANE2,,,3
R,1,B
ESIZE,A/8
LESIZE,9,,,20
KSCON,1,A/16,1,9                ! DEFINE CRACK TIP ELEMENT LAYOUT
AMESH,ALL

FINISH

/SOLU

ANTYPE,0
ERESX,NO

NSEL,S,LOC,Y                    ! APPLY DISPLACEMENT BOUNDARY CONDITIONS
NSEL,R,LOC,X,A,W
D,ALL,UY,0
NSEL,R,LOC,X,A
D,ALL,UX,0
NSEL,ALL

FK,12,FY,LOAD                   ! APPLY LOAD
FK,13,FY,LOAD
FK,14,FY,LOAD
FK,18,FY,LOAD
FK,19,FY,LOAD

SAVE
SOLVE
FINISH

/INPUT,ms,txt                   ! CALL MACRO TO CALCULATE MULTIPLIERS
```

A. 12 Single-Edge-Notched Bend Specimen

```
/BATCH

*SET,YS,488.43E6                ! YIELD STRESS, Pa
```

```
*SET,YM,211E9                    ! YOUNG'S MODULUS, Pa
*SET,POIS,0.3

*SET,LOAD,-6000                  ! LOAD, NEWTON

/PREP7

ET,1,PLANE2,,,3                  ! ELEMENT TYPE AND MATERIAL PROPERTY
MP,EX,1,YS
MP,NUXY,,POIS

K,1,0,0                          ! DEFINE GEOMETRY, METER
K,2,0.19375,0
K,3,0.19375,0.00625
K,4,0.2,0.025
K,5,0.2,0.05
K,6,0.2,0.1
K,7,0,0.1

L,1,2
L,2,3
L,3,4
L,4,5
L,5,6
L,6,7
L,7,1

R,1,0.003
KSCON,5,0.001,0.5,9              ! DEFINE CRACK TIP ELEMENT LAYOUT

LESIZE,ALL,0.015
LESIZE,5,,,10

AL,ALL

REAL,1

AMESH,1
FINISH

/SOLU

ANTYPE,0

NSEL,S,LOC,X,0                   ! APPLY BOUNDARY CONDITIONS
NSEL,R,LOC,Y,0
D,ALL,UY,0
NSEL,ALL

LSEL,S,LINE,,5
NSLL,S,1
D,ALL,UX,0
LSEL,ALL
NSEL,ALL
```

```
NSEL,S,LOC,X,0.2
NSEL,R,LOC,Y,0.1
F,ALL,FY,LOAD
NSEL,ALL

SOLVE
SAVE
FINISH

/INPUT,ms,txt                    ! CALL MACRO TO CALCULATE MULTIPLIERS
```

A. 13 Plate with Multiple Cracks

```
/BATCH

YM=210000                        ! YOUNG'S MODULUS, MPa
YS=480                           ! YIELD STRESS, MPa
POIS=0.3

LOAD=-300                        ! TENSILE STRESS, MPa

/PREP7

ET,1,PLANE2

MP,EX,1,YM
MP,NUXY,1,POIS

K,1                              ! DEFINE GEOMETRY, MILLIMETER
K,2,10
K,3,15
K,4,25
K,5,32.5
K,6,40
K,7,50
K,8,0,5
K,9,15,5
K,10,27.5,5
K,11,32.5,5
K,12,50,5
K,13,20,10
K,14,27.5,17.5
K,15,35,25
K,16,27.5,17.5
K,17,0,50
K,18,27.5,50
K,19,50,40
K,20,50,50
K,21,50,100
K,22,0,100
```

```
A,1,2,3,9,8
A,3,4,5,11,10,9
A,5,6,7,12,11
A,8,9,13,14,18,17
A,9,10,16,13
A,10,11,12,19,15,16
A,14,15,19,20,18
A,17,18,20,21,22

KSCON,2,2,1,12                    ! DEFINE CRACK TIP ELEMENT LAYOUT
KSCON,13,2,1,6
KSCON,15,2,1,6

ESIZE,2
LESIZE,2,,,8
AMESH,1,2

ESIZE,4
LESIZE,15,,,10
LESIZE,23,,,15
LESIZE,16,,,12
LESIZE,21,,,12
LESIZE,24,,,12
LESIZE,25,,,12
AMESH,3
AMESH,4,5
AMESH,6,7

ESIZE,10
AMESH,8

FINI

/SOLU

ANTYPE,0

NSEL,S,LOC,X,0                    ! DEFINE BOUNDARY CONDITIONS
D,ALL,UX,0
NSEL,ALL

NSEL,S,LOC,Y,0
NSEL,R,LOC,X,10,50
D,ALL,UY,0
NSEL,ALL

NSEL,S,LOC,Y,100
SF,ALL,PRES,LOAD
NSEL,ALL

SOLVE
SAVE

FINISH
```

```
/INPUT,ms,txt                          ! CALL MACRO TO CALCULATE MULTIPLIERS
```

A. 14 Orthotropic Cylinder under Internal Pressure

```
/BATCH

*SET,RI,30                             ! DIMENSION VALUES, MILLIMETER
*SET,RO,40
*SET,DIV,30                            ! RADIAL DIVISION
*SET,HI,(RO-RI)/DIV
*SET,PRSR,250                          ! PRESSURE VALUE, MPa

*SET,XX,579.2                          ! YIELD STRESSES, MPa
*SET,YY,472.3
*SET,ZZ,630.9
*SET,RR,262.9
*SET,SS,262.9
*SET,TT,262.9

*SET,YMX,XX**2                         ! MODIFIED INITIAL ELASTIC PROPERTIES
*SET,YMY,YY**2
*SET,YMZ,ZZ**2
*SET,SMXY,RR**2
*SET,SMYZ,SS**2
*SET,SMXZ,TT**2
*SET,PXY,0.47*YY**2*(1/XX**2+1/YY**2-1/ZZ**2)
*SET,PYZ,0.47*ZZ**2*(-1/XX**2+1/YY**2+1/ZZ**2)
*SET,PXZ,0.47*ZZ**2*(1/XX**2-1/YY**2+1/ZZ**2)

/PREP7

ET,1,42                                ! ELEMENT TYPE
KEYOPT,1,3,1

UIMP,1,EX,EY,EZ,YMX,YMY,YMZ            ! MATERIAL PROPERTIES
UIMP,1,NUXY,NUYZ,NUXZ,PXY,PYZ,PXZ
UIMP,1,GXY,GYZ,GXZ,SMXY,SMYZ,SMXZ

K,1,RI,0                               ! DEFINE GEOMETRY
K,2,RO,0
K,3,RO,HI
K,4,RI,HI
L,1,2,DIV,1
L,2,3,1
L,3,4,DIV,1
L,4,1,1
A,1,2,3,4

AMESH,1

FINISH
```

```
/SOLU

ANTYPE,0

D,ALL,UY,0                          ! APPLY BOUNDARY CONDITIONS

NSEL,S,LOC,X,RI
SF,ALL,PRES,PRSR
NSEL,ALL
SOLVE
SAVE

FINISH

/INPUT,ams,txt                      ! CALL MACRO TO CALCULATE MULTIPLIERS
```

A. 15 Orthotropic Cylinder under Internal Pressure (Nonlinear Analysis)

```
/BATCH

*SET,RI,30                          ! DIMENSIONS, MILLIMETER
*SET,RO,40
*SET,DIV,30
*SET,HI,(RO-RI)/DIV
*SET,PRSR,250                       ! PRESSURE VALUE, MPa

*SET,XX,579.2                       ! YIELD STRESSES, MPa
*SET,YY,472.3
*SET,ZZ,630.9
*SET,RR,262.9
*SET,SS,262.9
*SET,TT,262.9

*SET,YMX,100993                     ! YOUNG'S MODULI, MPa
*SET,YMY,95793.6
*SET,YMZ,100593
*SET,SMXY,36147.6                   ! SHEAR MODULUS, MPa
*SET,PXY,0.3610                     ! POISSON'S RATIOS
*SET,PYZ,0.3450
*SET,PXZ,0.3406

/PREP7

ET,1,42                             ! ELEMENT TYPE
KEYOPT,1,3,1

UIMP,1,EX,EY,EZ,YMX,YMY,YMZ         ! DEFINE ELASTIC PROPERTIES
UIMP,1,NUXY,NUYZ,NUXZ,PXY,PYZ,PXZ
UIMP,1,GXY,GYZ,GXZ,SMXY,SMYZ,SMXZ

TB,ANISO,1                          ! DEFINE PLASTIC PROPERTIES
```

```
TBMODIF,1,1,XX
TBMODIF,1,2,YY
TBMODIF,1,3,ZZ
TBMODIF,3,1,XX
TBMODIF,3,2,YY
TBMODIF,3,3,ZZ
TBMODIF,5,1,RR
TBMODIF,5,2,SS
TBMODIF,5,3,TT

K,1,RI,0                          ! DEFINE GEOMETRY
K,2,RO,0
K,3,RO,HI
K,4,RI,HI
L,1,2,DIV,1
L,2,3,1
L,3,4,DIV,1
L,4,1,1
A,1,2,3,4

AMESH,1

FINISH

/SOLU

ANTYPE,0

TIME,1                            ! SOLUTION CONTROL
AUTOTS,1
KBC,0
NSUBST,100,500,20
NEQIT,40

OUTRES,ALL,ALL

D,ALL,UY,0                        ! DEFINE DISPLACEMENT BOUNDARY CONDITION

NSEL,S,LOC,X,RI                   ! APPLY PRESSURE LOAD
SF,ALL,PRES,PRSR
NSEL,ALL
SOLVE
SAVE

FINISH                            ! CALL MACRO TO CALCULATE MULTIPLIERS
```

A. 16 Transversely Isotropic Bridgman Notch Bar

```
/BATCH

*SET,LOAD,500                     ! TENSILE PRESSURE, MPa
```

```
*SET,D1,26.416                    ! DIMENSIONS, MILLIMETER
*SET,D2,21.082
*SET,R,6.858
*SET,H,30

*SET,XX,579.2                     ! YIELD STRESSES, MPa
*SET,YY,472.3
*SET,ZZ,579.2
*SET,RR,262.9
*SET,SS,262.9
*SET,TT,366.6

*SET,YMX,XX**2                    ! MODIFIED INITIAL ELASTIC PROPERTIES
*SET,YMY,YY**2
*SET,YMZ,ZZ**2
*SET,SMXY,RR**2
*SET,SMYZ,SS**2
*SET,SMXZ,TT**2
*SET,PXY,0.47*YY**2*(1/XX**2+1/YY**2-1/ZZ**2)
*SET,PYZ,0.47*ZZ**2*(-1/XX**2+1/YY**2+1/ZZ**2)
*SET,PXZ,0.47*ZZ**2*(1/XX**2-1/YY**2+1/ZZ**2)

/PREP7

ET,1,PLANE182                     ! DEFINE ELEMENT
KEYOPT,1,3,1

UIMP,1,EX,EY,EZ,YMX,YMY,YMZ,      ! DEFINE MATERIAL PROPERTY
UIMP,1,NUXY,NUYZ,NUXZ,PXY,PYZ,PXZ
UIMP,1,GXY,GYZ,GXZ,SMXY,SMYZ,SMXZ

BLC4,0,0,D1/2,H                   ! DEFINE GEOMETRY
CYL4,D2/2+R,0,R
ASBA,1,2

K,10,0,H/2,,
K,11,D1/2+1,H/2,,
KBET,7,9,0,RATI,0.5,
L,10,11
L,2,10
ASBL,3,1
ASBL,2,2
LESIZE,4, , ,20,10,
LESIZE,12, , ,20,0.1,
LESIZE,9, , ,20,0.1,
LESIZE,1, , ,12,1,
LESIZE,3, , ,12,1,
LESIZE,5, , ,12,1,
LESIZE,6, , ,12,1,
LESIZE,7, , ,12,1,
LESIZE,8, , ,12,1,
LESIZE,10, , ,12,1,
ASEL,ALL
AMESH,ALL
```

```
CSYS,0                          ! DISPLACEMENT BOUNDARY CONDITIONS
NSEL,S,LOC,Y,0
D,ALL,UY,0
NALL

NSEL,S,LOC,X,0
D,ALL,UX,0
NALL

SAVE

FINISH
/SOLU

ANTYPE,0

NSEL,S,LOC,Y,H                  ! APPLIED LOAD
SF,ALL,PRES,-LOAD
NSEL,ALL

SOLVE
SAVE

FINISH

/INPUT,ams,txt                  ! CALL MACRO TO CALCULATE MULTIPLIERS
```

Appendix B ANSYS Macros for Multiplier Evaluations

B. 1 For Components Made of Isotropic Materials (ms.txt)

```
*DO,I,1,10                          ! TEN ITERATIONS

/POST1

SET,1

ETABLE,SEQV,S,EQV
ETABLE,VOL,VOLU
*GET,K,ELEM,0,COUNT

SOM1=0                              ! SET INITIAL VALUES
SOM2=0
EQ=0
VT=0
S=0

*DO,J,1,K                           ! PERFORM SUMMATION FOR ALL ELEMENTS
*IF,ESEL(J),EQ,1,THEN
*GET,SS,ELEM,J,ETAB,SEQV
*GET,VL,ELEM,J,ETAB,VOL
*GET,NN,ELEM,J,ATTR,MAT
*GET,MOD,EX,NN
SOM1=SOM1+VL/MOD
SOM2=SOM2+SS**2*VL/MOD
EQ=EQ+SS**2*VL
VT=VT+VL
*IF,SS,GT,S,THEN
S=SS
*ENDIF
*ENDIF
*ENDDO

YSS=S/YS                            ! NORMALIZED YIELD STRESS
ECM=1/YSS                           ! ECM LOWER BOUND VALUE
M0=YS*(SOM1/SOM2)**0.5              ! NEW M0 VALUE
MML=2*M0*YS**2/(YS**2+(M0*S)**2)    ! NEW M' VALUE
AA=(M0*YSS)**4+4*(M0*YSS)**2-1
BB=-8*(M0)**3*(YSS)**2
CC=4*(M0)**3*YSS
DD=BB*BB-4*AA*CC
*IF,DD,LT,0,THEN
```

```
MA=0
*ELSE
MA=(-BB+SQRT(DD))/(2*AA)              ! NEW M-ALPHA VALUE
*ENDIF

MM0=YS*(VT/EQ)**0.5                   ! BASIC M0 VALUE
MMML=2*MM0*YS**2/(YS**2+(MM0*S)**2)   ! BASIC M' VALUE
AA=(MM0*YSS)**4+4*(MM0*YSS)**2-1
BB=-8*(MM0)**3*(YSS)**2
CC=4*(MM0)**3*YSS
DD=BB*BB-4*AA*CC
*IF,DD,LT,0,THEN
MMA=0
*ELSE
MMA=(-BB+SQRT(DD))/(2*AA)             ! BASIC M-ALPHA VALUE
*ENDIF

*CFOPEN,multi,txt,,APPEND             ! EXPORT MULTIPLIERS
*VWRITE,M0,MML,MA,MM0,MMML,MMA,ECM
(E15.8,3X,E15.8,3X,E15.8,3X,E15.8,3X,E15.8,3X,E15.8,3X,E15.8)
*CFCLOS

*CFOPEN,chgmod                        ! WRITE MODULUS ADJUSTMENT FILE
MN=2
*DO,J,1,K
*IF,ESEL(J),EQ,1,THEN
*GET,SS,ELEM,J,ETAB,SEQV
*GET,NN,ELEM,J,ATTR,MAT
*GET,YMN,EX,NN
ES=(YS/SS)*YMN
*CFWRITE,MP,EX,MN,ES
*CFWRITE,MP,NUXY,MN,POIS
*CFWRITE,MAT,MN
*CFWRITE,EMODIF,J,MAT,MN
MN=MN+1
*ENDIF
*ENDDO
*CFCLOS

FINISH

/PREP7

RESUME

MP,EX,1,YM
MP,NUXY,1,POIS

*USE,chgmod                           ! PERFORM MODULUS ADJUSTMENT

FINISH

/SOLU
```

```
SOLVE
SAVE
FINISH

*ENDDO

FINISH
```

B. 2 For Two-Layered Structures (2ms.txt)

```
*DO,I,1,10                              ! TEN ITERATIONS

/POST1

SET,1

ETABLE,SEQV,S,EQV
ETABLE,VOL,VOLU
*GET,K,ELEM,0,COUNT

SU1=0                                   ! SET INITIAL VALUES
SL1=0
S1=0
SU2=0
SL2=0
S2=0
EQ1=0
EQ2=0
VT1=0
VT2=0

*DO,J,1,K                               ! PERFORM SUMMATION FOR ALL ELEMENTS
*GET,SS,ELEM,J,ETAB,SEQV
*GET,VL,ELEM,J,ETAB,VOL
*GET,ELTP,ELEM,J,ATTR,TYPE
*GET,NN,ELEM,J,ATTR,MAT
*GET,MOD,EX,NN
*IF,ELTP,EQ,1,THEN
SU1=SU1+YS1**2*VL/MOD
SL1=SL1+SS**2*VL/MOD
EQ1=EQ1+SS**2*VL
VT1=VT1+VL
*IF,SS,GT,S1,THEN
S1=SS
*ENDIF
*ELSE
SU2=SU2+YS2**2*VL/MOD
SL2=SL2+SS**2*VL/MOD
EQ2=EQ2+SS**2*VL
VT2=VT2+VL
*IF,SS,GT,S2,THEN
S2=SS
```

```
*ENDIF
*ENDIF
*ENDDO

ARB1=(EQ1/VT1)**0.5                    ! REFERENCE STRESS OF LAYER ONE
ARB2=(EQ2/VT2)**0.5                    ! REFERENCE STRESS OF LAYER TWO
YSS1=S1/YS1
YSS2=S2/YS2

*IF,YSS1,GT,YSS2,THEN                 ! OBTAIN LARGER NORMALIZED MAX STRESS
YSS=YSS1
*ELSE
YSS=YSS2
*ENDIF

ECM=1/YSS                              ! ECM LOWER BOUND VALUE
M0=SQRT((SU1+SU2)/(SL1+SL2))           ! M0 VALUE
MML=2*M0/(1+(M0*YSS)**2)               ! M' VALUE
AA=(M0*YSS)**4+4*(M0*YSS)**2-1
BB=-8*(M0)**3*(YSS)**2
CC=4*(M0)**3*YSS
DD=BB*BB-4*AA*CC
*IF,DD,LT,0,THEN
MA=0
*ELSE
MA=(-BB+SQRT(DD))/(2*AA)               ! M-ALPHA VALUE
*ENDIF

*CFOPEN,multi,txt,,APPEND              ! EXPORT MULTIPLIERS
*VWRITE,M0,MML,MA,ECM,ARB1,ARB2
(E15.8,3X,E15.8,3X,E15.8,3X,E15.8,3X,E15.8,3X,E15.8)
*CFCLOS

*CFOPEN,chgmod                         ! WRITE MODULUS ADJUSTMENT FILE
MN=3
*DO,J,1,K
*GET,SS,ELEM,J,ETAB,SEQV
*GET,ELTP,ELEM,J,ATTR,TYPE
*GET,N1,ELEM,J,ATTR,MAT
*GET,YMM,EX,N1
*IF,ELTP,EQ,1,THEN
ES=(YS1/SS)*YMM
*ELSE
ES=(YS2/SS)*YMM
*ENDIF
*CFWRITE,MP,EX,MN,ES
*CFWRITE,MP,NUXY,MN,POIS
*CFWRITE,TYPE,ELTP
*CFWRITE,MAT,MN
*CFWRITE,EMODIF,J
MN=MN+1
*ENDDO
*CFCLOS
```

```
FINISH

/PREP7

RESUME

MP,EX,1,YM1
MP,NUXY,1,POIS
MP,EX,2,YM2
MP,NUXY,2,POIS

*USE,chgmod                          ! PERFORM MODULUS ADJUSTMENT

FINISH

/SOLU

SAVE
SOLVE
FINISH

*ENDDO

FINISH
```

B. 3 For Components Made of Anisotropic Materials (ams.txt)

```
*DO,I,1,10                           ! TEN ITERATIONS

A12=XX**2*(1/XX**2+1/YY**2-1/ZZ**2)  ! CALCULATE ANISOTROPIC PARAMETERS
A23=XX**2*(-1/XX**2+1/YY**2+1/ZZ**2)
A31=XX**2*(1/XX**2-1/YY**2+1/ZZ**2)
A44=(XX/RR)**2/3
A55=(XX/SS)**2/3
A66=(XX/TT)**2/3
YS=XX                                ! REFERENCE YIELD STRESS

/POST1

SET,1

ETABLE,SX,S,X                        ! OBTAIN STRESS COMPONENTS
ETABLE,SY,S,Y
ETABLE,SZ,S,Z
ETABLE,SXY,S,XY
ETABLE,SYZ,S,YZ
ETABLE,SXZ,S,XZ
ETABLE,VOL,VOLU
*GET,K,ELEM,0,COUNT

SOM1=0                               ! SET INITIAL VALUES
SOM2=0
```

```
EQ=0
VT=0
S=0

*DO,J,1,K                              ! PERFORM SUMMATION FOR ELEMENTS
*GET,S1,ELEM,J,ETAB,SX
*GET,S2,ELEM,J,ETAB,SY
*GET,S3,ELEM,J,ETAB,SZ
*GET,S4,ELEM,J,ETAB,SXY
*GET,S5,ELEM,J,ETAB,SYZ
*GET,S6,ELEM,J,ETAB,SXZ
*GET,VL,ELEM,J,ETAB,VOL
*GET,NN,ELEM,J,ATTR,MAT
*GET,MOD,EX,NN
T1=0.5*(A12*(S1-S2)**2+A23*(S2-S3)**2+A31*(S3-S1)**2)
T2=3*(A44*S4**2+A55*S5**2+A66*S6**2)
SS=(T1+T2)**0.5                        !EFFECTIVE STRESS
SOM1=SOM1+VL/MOD
SOM2=SOM2+SS**2*VL/MOD
EQ=EQ+SS**2*VL
VT=VT+VL
*IF,SS,GT,S,THEN
S=SS
*ENDIF
*ENDDO

YSS=S/YS
ECM=1/YSS                              ! ECM LOWER BOUND VALUE
M0=YS*(SOM1/SOM2)**0.5                 ! M0 VALUE
MML=2*M0*YS**2/(YS**2+(M0*S)**2)       ! M' VALUE
AA=(M0*YSS)**4+4*(M0*YSS)**2-1
BB=-8*(M0)**3*(YSS)**2
CC=4*(M0)**3*YSS
DD=BB*BB-4*AA*CC
*IF,DD,LT,0,THEN
MA=0
*ELSE
MA=(-BB+SQRT(DD))/(2*AA)
*ENDIF

*CFOPEN,multi,txt,,APPEND              ! EXPORT MULTIPLIERS
*VWRITE,M0,MML,MA,ECM
(E15.8,3X,E15.8,3X,E15.8,3X,E15.8)
*CFCLOS

*CFOPEN,chgmod                         ! WRITE MODULUS ADJUSTMENT FILE
MN=2
*DO,J,1,K
*GET,S1,ELEM,J,ETAB,SX
*GET,S2,ELEM,J,ETAB,SY
*GET,S3,ELEM,J,ETAB,SZ
*GET,S4,ELEM,J,ETAB,SXY
*GET,S5,ELEM,J,ETAB,SYZ
*GET,S6,ELEM,J,ETAB,SXZ
```

```
*GET,NN,ELEM,J,ATTR,MAT
*GET,MX,EX,NN
*GET,MY,EY,NN
*GET,MZ,EZ,NN
*GET,MXY,GXY,NN
*GET,MYZ,GYZ,NN
*GET,MXZ,GXZ,NN
T1=0.5*(A12*(S1-S2)**2+A23*(S2-S3)**2+A31*(S3-S1)**2)
T2=3*(A44*S4**2+A55*S5**2+A66*S6**2)
SS=(T1+T2)**0.5                          ! EFFECTIVE STRESS
ESX=(YS/SS)*MX
ESY=(YS/SS)*MY
ESZ=(YS/SS)*MZ
ESXY=(YS/SS)*MXY
ESYZ=(YS/SS)*MYZ
ESXZ=(YS/SS)*MXZ
*CFWRITE,UIMP,MN,EX,EY,EZ,ESX,ESY,ESZ,
*CFWRITE,UIMP,MN,NUXY,NUYZ,NUXZ,PXY,PYZ,PXZ
*CFWRITE,UIMP,MN,GXY,GYZ,GXZ,ESXY,ESYZ,ESXZ
*CFWRITE,MAT,MN
*CFWRITE,EMODIF,J
MN=MN+1
*ENDDO
*CFCLOS

FINISH

/PREP7

RESUME

UIMP,1,EX,EY,EZ,YMX,YMY,YMZ
UIMP,1,NUXY,NUYZ,NUXZ,PXY,PYZ,PXZ
UIMP,1,GXY,GYZ,GXZ,SMXY,SMYZ,SMXZ

*USE,chgmod                              ! PERFORM MODULUS ADJUSTMENT

FINISH

/SOLU

SOLVE
SAVE
FINISH

*ENDDO

FINISH
```